Methane Exchanges between Terrestrial Ecosystems and the Atmosphere in Response to Multiple Environmental Changes -A Process-Based Modeling Study

by

Bowen Zhang

A dissertation submitted to the Graduate Faculty of
Auburn University
in partial fulfillment of the
requirements for the Degree of
Doctor of Philosophy

Auburn, Alabama
August 6, 2016

Keywords: Global Changes, Wetland, Rice, Fire
Terrestrial ecosystem, process-based model, Methane

Approved by

Hanqin Tian, Chair, Solon Dixon Professor of School of Forestry and Wildlife Sciences
Lisa Samuelson, Dwain G. Luce Professor of School of Forestry and Wildlife Sciences
Xing Fang, Arthur H. Feagin Chair Professor of Civil Engineering
Christopher J. Anderson, Associate Professor, School of Forestry and Wildlife Sciences
Xiaofeng Xu, Assistant Professor, Ecology Biology Department, San Diego State University

Abstract

Methane (CH_4), the most abundant non-carbon dioxide (CO_2) greenhouse gas, has a relatively shorter lifetime (approx. 9 years) and higher global warming potential (approx. 28 times) than CO_2 at a 100-year time horizon. The changes in CH_4 fluxes have immediate feedback on the climate system. Since the early 1990s, the rate of increment in atmospheric CH_4 concentration experienced a temporary slowdown, pause, and resumption; however, the reasons for those significant changes are still unclear. Variation of the CH_4 fluxes from biogenic and pyrogenic sources and sinks were proposed to explain those changes in the atmospheric CH_4 growth rate. In this study, we applied a data-model integration approach to comprehensively quantify the CH_4 fluxes from wetlands, rice field, ruminants, biomass burning and upland soil. Our results showed that the global CH_4 flux from wetlands, rice fields, ruminants, biomass burning and upland soil was 163.9±6.4 Tg C/yr (Avg. ± 1 std. dev.), and exhibited substantial inter-annual variation during 1993-2014. Among all the CH_4 sources, wetlands contributed almost half (~49.2%) of the global total CH_4 emission, followed by ruminants (~36.8%), rice fields (~7.5%) and biomass burning (~6.5%). The upland soil offset ~13.2% of the total emitted CH_4 from wetlands, ruminants, rice fields and biomass burning. Regionally, tropics accounted for the largest portion of the estimated net CH_4 fluxes, followed by the northern middle latitude region, northern high latitude region and southern middle latitude region. The results further revealed that CH_4 emission from wetlands dominated the atmospheric CH_4 variation during 1993-2014. In addition, the contribution of ruminants to CH_4 emission became increasingly

important after 2006. Likewise, biomass burning played a critical role on CH_4 emissions only during years of large peatland fires. By adopting different water management practices in the rice field, the estimated CH_4 emissions could be reduced by 50.6% under intermittent irrigation when compared to continuous flooding from global rice field. Over the past 110 years, global CH_4 emissions from rice cultivation increased by 85%. The expansion of rice fields was the dominant factor for the increasing trends of CH_4 emissions, followed by elevated CO_2 concentration, and nitrogen fertilizer use. Under the future scenarios, the magnitude of CH_4 emission from wetlands in the arctic and boreal region is projected to increase by 2%~65%, when compared with the contemporary level (2001-2010). Seasonal analyses indicated that the change of CH_4 fluxes exhibits great spatial variability over time throughout the 21st century. The projected CH_4 fluxes in summer accounted for the largest portion of annual emission and showed the largest increasing trend during the 21st century. By feeding different wetland datasets into the dynamic land ecosystem model (DLEM), the results further suggested that tropical regions accounted for the largest portion (~72 ± 7%) of the estimated CH_4 emission from wetlands and also exhibited the largest uncertainty. To reduce the uncertainty in estimating CH_4 emission from global wetlands, it is urgent to develop robust datasets delineating dynamic wetland extent and the inter-annual and intra-annual variation of inundation patterns, particularly in the tropical region. It can be anticipated that the future atmospheric CH_4 variation will be determined by the increasing demand for food production with the climate sensitive natural emissions.

Acknowledgments

This study has been supported by NASA Interdisciplinary Science Program (NNX10AU06G, NNX11AD47G, NNG04GM39C), NASA Land Cover/Land Use Change Program (NNX08AL73G; NNX14AD94G), NASA Carbon Monitoring System Program (NNX14AO73G), National Science Foundation (1243232, 1243220) and NASA terrestrial ecology program.

My sincere appreciation goes to my supervisor, Dr. Hanqin Tian. I am deeply grateful to have him as my advisor for the Ph.D. study in Auburn. His insightful comments and constructive suggestions were thought-provoking at different stages of my study and will always inspire me to fulfill my dream to become a great scientist. Completion of this dissertation would be impossible without his extraordinary support, inspiring guidance, great patience and constant encouragement throughout my study. I am deeply thankful for my research committees: Dr. Lisa Samuelson, Dr. Xing Fang, Dr. Xiaofeng Xu, and Dr. Christopher Anderson for their invaluable comments and suggestions, continuous assistant, and generous encouragement.

I would like to thank Dr. Susan Pan for her continuous help on both the school life and research. I am also grateful to the former EDGE members: Mingliang Liu, Guangsheng Chen, Chaoqun Lu, Wei Ren, Bo Tao, Kamaljit Banger, Qichun Yang, Xia Li, for their pioneer contributions to the development of the Dynamic Land Ecosystem Model and various forms of support during my graduate study, and current EDGE members: Jia Yang, Shree Dangal, Yuanzhi Yao, Tina Xu, Zhuonan Wang, Jingwei Wu for their valuable discussions and technical

supports. I would like to express my appreciation to Dr. John Kush, Ms. Patti Staudenmaier, Ms. Audrey Grindle, Ms. Paula Davis, James Fukai, and all the faculty and staff members in the School of Forestry and Wildlife Sciences.

Most importantly, I would express my deepest appreciation and gratitude to my parents Zhang, Quan and Lan, Suping and my parents-in-law Xue, Chuitang and Sun, Jianhua, my college, friend and husband Jia Xue, and my lovely daughter Olivia Xue to whom I dedicate this work. None of this would have been possible without their endless love and unconditional support.

Table of Contents

List of Tables

List of Illustrations

Chapter 1

1.1 Introduction

Global abundance of atmospheric methane (CH_4) increased from 700 ppb in pre-industrial times to 1840 ppb in 2016 (WMO, 2015, NOAA, 2016) and reached an unprecedentedly high level since the past 800,000 years (Montzka *et al.*, 2011). Methane has relative shorter lifetime (approx. 9 years) and higher global warming potential than carbon dioxide (CO_2), indicating the change of CH_4 fluxes has an immediate feedback on the climate system (Ciais *et al.*, 2014, Tian *et al.*, 2016). Human-induced biogenic CH_4 fluxes alone could fully offset the global land CO_2 sink by 1.3 and 4 times based on GWP100 and GWP20 metrics during the 2000s, respectively (Tian *et al.*, 2016).

Since the early 1990s, the atmospheric CH_4 concentration experienced a temporary slowdown, pause and resumption; however, the reasons for those significant changes are still not fully understood (Dlugokencky *et al.*, 2009, Nisbet *et al.*, 2014, Schaefer *et al.*, 2016). Increasing lines of evidence with the findings from top-down (TD) approaches (e.g., atmospheric inversion model), bottom-up (BU) approaches (e.g., inventory study and process-based model) and isotopic measurements showed that biogenic and pyrogenic CH_4 sources and sinks play a critical role in determining the global atmospheric CH_4 anomalies in the recent two decades. Previous studies indicated that TD approaches and isotopic measurements could provide additional restrictions to assess the CH_4 fluxes from different sources and sinks but were hard to disentangle their relative contributions to the atmospheric CH_4 anomalies (Schaefer *et al.*, 2016,

Tian *et al.*, 2016). Top-down approaches were difficult to unravel the CH_4 sources with similar distribution and isotopic measurements failed to separate the CH_4 fluxes with similar isotopic signatures (Schaefer *et al*., 2016).

The magnitude of CH_4 fluxes from the terrestrial ecosystems are influenced by multiple environmental factors and anthropogenic perturbations, such as climate variability, atmospheric composition (e.g., elevated CO_2 and tropospheric ozone concentrations, nitrogen deposition, etc.), and land use and land management practices (e.g., irrigation, rotation, nitrogen fertilizer use, etc.) (Banger *et al.*, 2012, Bridgham *et al.*, 2013, Paudel *et al.*, 2016, Xu *et al.*, 2010). More specifically, a warming climate could enhance microbial activities, which could potentially accelerate the release and uptake of CH_4 from the terrestrial ecosystems (Paudel *et al.*, 2016). The variation in precipitation regulates water availability in the ecosystems, which could ultimately affect CH_4 producing and oxidizing processes. In addition, changes in climate will indirectly affect CH_4 sinks and sources by influencing plant and root growth (Dijkstra *et al.*, 2012, van Groenigen *et al.*, 2011), which is the source of carbon substrate for microbial activities. Similarly, elevated atmospheric CO_2 concentration tends to increase plant productivity, carbon input and water availability (Dijkstra *et al.*, 2012, Hungate *et al.*, 2009, Kimball *et al.*, 2002), which could enhance the release of CH_4 from the terrestrial ecosystems. The response of CH_4 fluxes to nitrogen addition may vary in magnitude and direction based on local environmental conditions and ecosystem types (Liu & Greaver, 2009). Land conversion from wetland to dryland tends to reduce CH_4 emission from global wetlands, while an increase in rice producing area could enhance CH_4 emission (FAOSTAT, 2014, Paudel *et al.*, 2016). Land management practices, such as irrigation and fertilizer use, also regulate CH_4 fluxes from crop fields (Banger *et al.*, 2012, Bouman *et al.*, 2007).

Despite only covering ~20% of the global land surface area, arctic and boreal regions are the home for over one-third of the world's wetlands and more than 50% of the global carbon storage (Lehner & Döll, 2004, Schuur *et al.*, 2015, Tian *et al.*, 2015). The vast portion of soil organic carbon stored in this region is susceptible and vulnerable to future environmental changes (Hugelius *et al.*, 2014, Koven *et al.*, 2011, Schneider von Deimling *et al.*, 2015). The annual average temperature in the arctic and boreal region has risen two times faster than the global average (O'Shea *et al.*, 2014, Stocker *et al.*, 2013), and is further projected to increase based on different climatic scenarios. It is important to have a robust estimation of the magnitude and timing of the projected CH_4 fluxes to the atmosphere in response to multiple environmental factors.

The lack of accurate knowledge on the spatial and temporal variations of wetland extent from different datasets have impeded the understanding of related biogeochemical processes, especially CH_4 fluxes (Mitra *et al.*, 2005) and the feedbacks between CH_4 fluxes and future climate change (Zhu *et al.*, 2013). These knowledge gaps likely resulted in significant uncertainties and errors in large-scale estimation of CH_4 emission (Bridgham *et al.*, 2013). Thus, to what extent different wetland data could explain the modeling divergence in the global CH_4 estimation needs to be identified.

To answer the above questions, I conducted the following studies (**Fig. 1.1**) to comprehensively quantify CH_4 fluxes from different sectors. In Chapter 2, I examined the spatial and temporal distribution of CH_4 fluxes from wetlands, rice fields, ruminants, biomass burning and upland soil during 1993-2014 through a data-model integration. In addition to environmental driver inputs including climate change, atmospheric composition, land use and land management practices, I have included dynamic wetland data developed from the Global Inundation Extent

from Multi-Satellites during 1993-2007 (GIEMS, Prigent *et al*., 2012), and burned area derived from Global Fire Emission Data version 4 (GFED4) during 1996-2014 (Giglio *et al.*, 2010, Giglio *et al.*, 2013) and reconstructed burned history before 1996 (Yang *et al.*, 2014) to drive a process-based biogeochemical model, the Dynamic Land Ecosystem Model version 2.0 (DLEM v2.0) to quantify terrestrial CH_4 sinks and sources (**Fig. 1.2**). In Chapter 3, I quantified the effects of multiple environmental factors on the magnitude and spatio-temporal variation of CH_4 emissions from global rice fields during 1901-2010. In Chapter 4, I examined the magnitude and spatio-temporal variation of CH_4 emissions from global wetlands and identified the impacts of precipitation and temperature on wetland extent change over time. In Chapter 5, I further quantified the projected CH_4 exchange between terrestrial ecosystem and the atmosphere in the arctic and boreal region in response to future scenarios. Finally, in Chapter 6, I assessed the uncertainties of global and regional-scale estimations of CH_4 emission associated with wetland datasets.

1.2 References

Banger K, Tian HQ, Lu CQ (2012) Do nitrogen fertilizers stimulate or inhibit methane emissions from rice fields? Global Change Biology, **18**, 3259-3267.

Bouman BaM, Lampayan RM, Tuong TP (2007) *Water management in irrigated rice: coping with water scarcity*, Int. Rice Res. Inst.

Bridgham SD, Cadillo-Quiroz H, Keller JK, Zhuang QL (2013) Methane emissions from wetlands: biogeochemical, microbial, and modeling perspectives from local to global scales. Global Change Biology, **19**, 1325-1346.

Ciais P, Sabine C, Bala G *et al.* (2014) Carbon and other biogeochemical cycles. In: *Climate Change 2013: The Physical Science Basis. Contribution of Working Group I to the Fifth Assessment Report of the Intergovernmental Panel on Climate Change.* pp Page., Cambridge University Press.

Dijkstra FA, Prior SA, Runion GB, Torbert HA, Tian H, Lu C, Venterea RT (2012) Effects of elevated carbon dioxide and increased temperature on methane and nitrous oxide fluxes: evidence from field experiments. Frontiers in Ecology and the Environment, **10**, 520-527.

Dlugokencky EJ, Bruhwiler L, White JWC *et al.* (2009) Observational constraints on recent increases in the atmospheric CH4 burden. Geophysical Research Letters, **36**.

Faostat (2014) FOOD AND AGRICULTURE ORGANIZATION OF THE UNITED NATIONS STATISTICS DIVISION.

Giglio L, Randerson J, Van Der Werf G, Kasibhatla P, Collatz G, Morton D, Defries R (2010) Assessing variability and long-term trends in burned area by merging multiple satellite fire products. Biogeosciences, **7**.

Giglio L, Randerson JT, Werf GR (2013) Analysis of daily, monthly, and annual burned area using the fourth-generation global fire emissions database (GFED4). Journal of Geophysical Research: Biogeosciences, **118**, 317-328.

Hugelius G, Strauss J, Zubrzycki S *et al.* (2014) Estimated stocks of circumpolar permafrost carbon with quantified uncertainty ranges and identified data gaps. Biogeosciences, **11**, 6573-6593.

Hungate BA, Van Groenigen KJ, Six J *et al.* (2009) Assessing the effect of elevated carbon dioxide on soil carbon: a comparison of four meta-analyses. Global Change Biology, **15**, 2020-2034.

Kimball B, Kobayashi K, Bindi M (2002) Responses of agricultural crops to free-air CO 2 enrichment. Advances in Agronomy, **77**, 293-368.

Koven CD, Ringeval B, Friedlingstein P *et al.* (2011) Permafrost carbon-climate feedbacks accelerate global warming. Proceedings of the National Academy of Sciences, **108**, 14769-14774.

Lehner B, Döll P (2004) Development and validation of a global database of lakes, reservoirs and wetlands. Journal of Hydrology, **296**, 1-22.

Liu L, Greaver TL (2009) A review of nitrogen enrichment effects on three biogenic GHGs: the CO2 sink may be largely offset by stimulated N2O and CH4 emission. Ecology Letters, **12**, 1103-1117.

Mitra S, Wassmann R, Vlek PL (2005) An appraisal of global wetland area and its organic carbon stock. Current Science, **88**, 25.

Montzka SA, Dlugokencky EJ, Butler JH (2011) Non-CO2 greenhouse gases and climate change. Nature, **476(7358)**, 43-50.

Nisbet EG, Dlugokencky EJ, Bousquet P (2014) Methane on the Rise-Again. Science, **343**, 493-495.

O'shea S, Allen G, Gallagher M *et al.* (2014) Methane and carbon dioxide fluxes and their regional scalability for the European Arctic wetlands during the MAMM project in summer 2012. Atmospheric Chemistry and Physics, **14**, 13159-13174.

Paudel R, Mahowald NM, Hess PG, Meng L, Riley WJ (2016) Attribution of changes in global wetland methane emissions from pre-industrial to present using CLM4. 5-BGC. Environmental Research Letters, **11**, 034020.

Schaefer H, Fletcher SEM, Veidt C *et al.* (2016) A 21st-century shift from fossil-fuel to biogenic methane emissions indicated by 13CH4. Science, **352**, 80-84.

Schneider Von Deimling T, Grosse G, Strauss J *et al.* (2015) Observation-based modelling of permafrost carbon fluxes with accounting for deep carbon deposits and thermokarst activity. Biogeosciences, **12**, 3469-3488.

Schuur E, Mcguire A, Schädel C *et al.* (2015) Climate change and the permafrost carbon feedback. Nature, **520**, 171-179.

Stocker TF, Qin D, Plattner GK *et al.* (2013) IPCC, 2013: climate change 2013: the physical science basis. Contribution of working group I to the fifth assessment report of the intergovernmental panel on climate change.

Tian H, Lu C, Ciais P *et al.* (2016) The terrestrial biosphere as a net source of greenhouse gases to the atmosphere. Nature, **531**, 225-228.

Tian HQ, Lu CQ, Yang J *et al.* (2015) Global patterns and controls of soil organic carbon dynamics as simulated by multiple terrestrial biosphere models: Current status and future directions. Global Biogeochemical Cycles, **29**, 775-792.

Van Groenigen KJ, Osenberg CW, Hungate BA (2011) Increased soil emissions of potent greenhouse gases under increased atmospheric CO2. Nature, **475**, 214-U121.

Wmo (2015) World Meteorlogical Organization Greenhouse Gas Bulletin. pp Page, Citeseer.

Xu XF, Tian HQ, Zhang C *et al.* (2010) Attribution of spatial and temporal variations in terrestrial methane flux over North America. Biogeosciences, **7**, 3637-3655.

Yang J, Tian H, Tao B, Ren W, Kush J, Liu Y, Wang Y (2014) Spatial and temporal patterns of global burned area in response to anthropogenic and environmental factors: Reconstructing global fire history for the 20th and early 21st centuries. Journal of Geophysical Research: Biogeosciences, **119**, 249-263.

Zhu X, Zhuang Q, Gao X, Sokolov A, Schlosser CA (2013) Pan-Arctic land–atmospheric fluxes of methane and carbon dioxide in response to climate change over the 21st century. Environmental Research Letters, **8**, 045003.

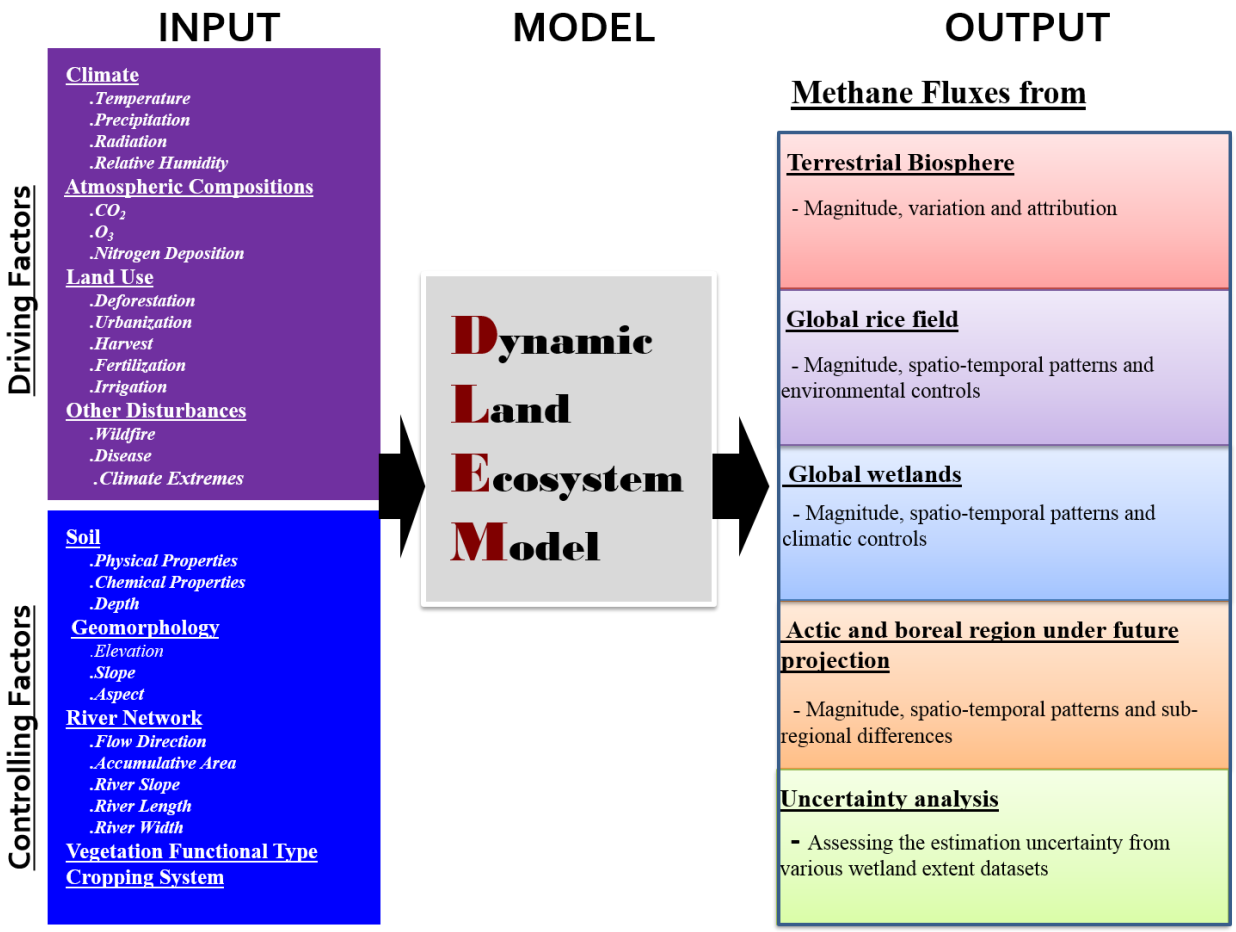

Figure 1.1 Major driving and controlling factors and key outputs associated with CH_4 fluxes from the Dynamic Land Ecosystem Model (DLEM)

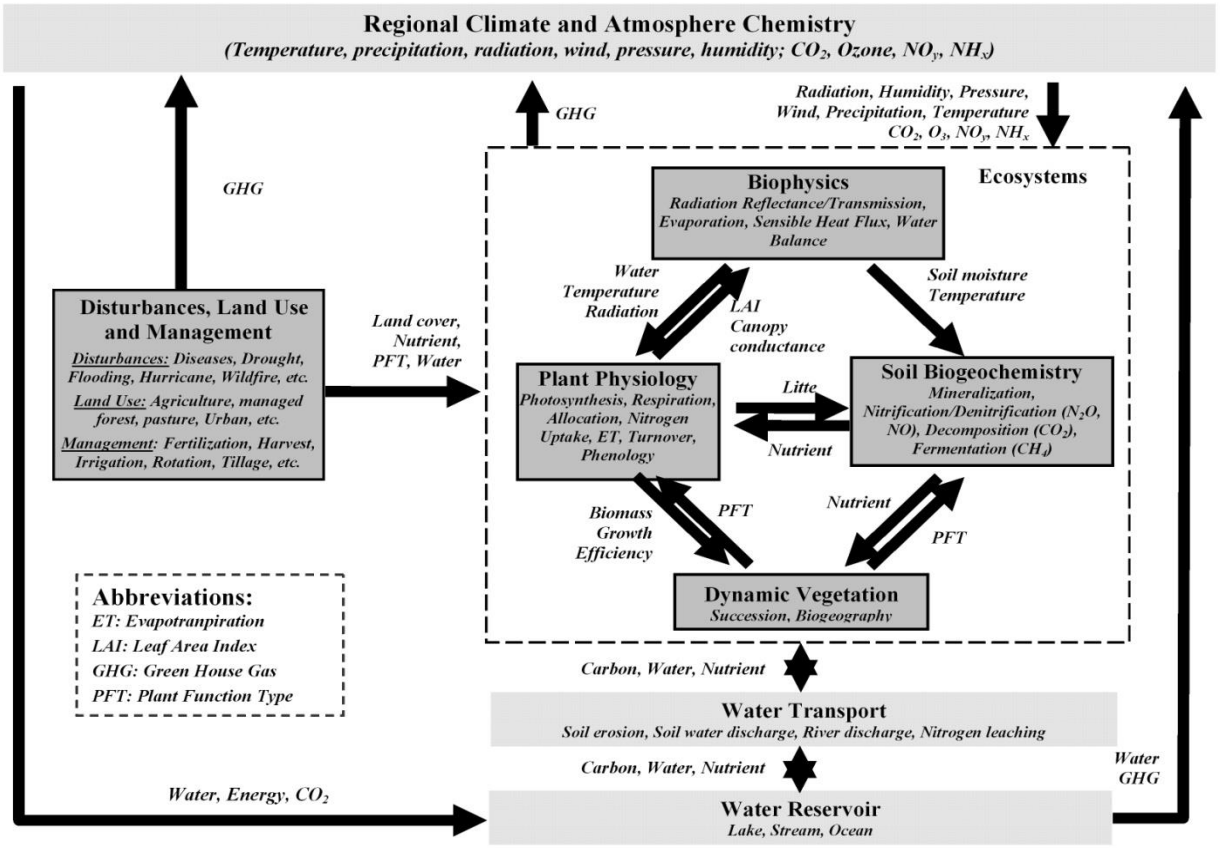

Figure 1.2 Framework of the Dynamic Land Ecosystem Model: major components and processes

Chapter 2

Methane Emissions from Terrestrial Biosphere: Magnitude, Variation, and Attribution

2.1 Abstract

Methane, a potent greenhouse gas, has a relative shorter lifetime (approx. 9 years) and higher global warming potential than carbon dioxide (CO_2), with immediate feedback on the climate system. Since the early 1990s, the rate of increment in atmospheric CH_4 concentration experienced the temporary slowdown, pause, and resumption; however, the reasons for those significant changes are still unclear. Different biogenic and pyrogenic sources were suggested to explain those changes in the atmospheric CH_4 growth rate. It is important to have a comprehensive quantification of the CH_4 fluxes from different sectors to explain the changes in atmospheric CH_4 concentration since the early 1990s. Here, we examined the spatial and temporal distribution of CH_4 flux from wetlands, rice fields, ruminants, biomass burning and upland soil during 1993 -2014 by using a process-based biogeochemical model, Dynamic Land Ecosystem Model (DLEM) and an inventory approach. Our results showed that the global CH_4 flux from wetlands, rice field, ruminants, biomass burning and upland soil was 163.9±6.4 Tg C/yr and exhibited the strong inter-annual variation. Among all the CH_4 sources, wetlands contributed almost half (~49.2%) of the global total CH_4 emission, followed by ruminants (~36.8%), rice fields (~7.5%) and biomass burning (~6.5%). The upland soil consumed 25.0±0.5 Tg C/yr CH_4, offsetting ~13.2% of the total emitted CH_4 from those four sources. The tropical region accounted for the largest portion of the estimated net CH_4 fluxes. Wetlands were found to

be the major contributor of the net CH_4 fluxes in the 30°N-30°S and 60°-90° N, while ruminant shared the largest portion of the net CH_4 fluxes in the 30°-60°S and N. Among six continents, Asia accounted for over one-third (~38.4%) of the global net CH_4 fluxes, associated with large emission from rice fields and high ruminant density. Our results suggested that CH_4 emission from wetlands dominated the atmospheric CH_4 variation during 1993-2014 and the contribution of CH_4 emission from ruminants became increasingly important, especially after 2006. Methane emissions from biomass burning played a critical role in years with huge peatland fires. It can be anticipated that the future atmospheric CH_4 variation will be determined by the increasing demand for food production with the climate sensitive natural emissions.

2.2 Introduction

Global abundance of atmospheric methane (CH_4) increased from 700 ppb in pre-industrial times to 1833 ppb at present (WMO, 2015), accounting for around one-fifth of anthropogenic caused radiative forcing increase (Nisbet *et al.*, 2014). Compared with carbon dioxide (CO_2), methane has relative shorter lifetime (approx. 9 years) and higher global warming potential (GWP, integrative radiative forcing of 1g CH_4 is equivalent to 28 times that of 1 g CO_2 on a 100-year time horizon), which has immediate feedback on the climate system (Ciais *et al.*, 2014, Dlugokencky *et al.*, 2011). A recent synthesis study indicated that human-induced biogenic CH_4 fluxes alone could offset the global land CO_2 sink by 1.3 and 1.4 times when using estimates from top-down (TD) and bottom-up (BU) approaches based on GWP100 metric during the 2000s, respectively (Tian *et al.*, 2016). On a 20-year time horizon, the relative importance of CH_4 was further enhanced owing to much greater GWP (84 times higher GWP compared with CO_2), and human-induced biogenic CH_4 source overwhelmed global land CO_2 sink by about 4 times (Tian *et al.*, 2016).

Since the early 1990s, the continuous increase of atmospheric CH_4 concentration was interrupted by a near-zero growth period during 1999-2006 and the rate of increment in global CH_4 concentration experienced a temporary slowdown, pause, and resumption; however, the reasons for those significant changes are still not fully understood (Dlugokencky *et al.*, 2009, Nisbet *et al.*, 2014, Schaefer *et al.*, 2016). The fluctuation of atmospheric CH_4 concentration growth rate is associated with shifting the net balance of CH_4 fluxes from different sinks and sources (Walter *et al.*, 2001). The major pathways in CH_4 removal include the destruction of CH_4 by the hydroxyl radical (OH) and CH_4 oxidation by the methanotrophic bacteria, in which the OH contributes around 90% of the atmospheric CH_4 removal and the methanotroph consumed

another 4% of CH_4 (Bousquet *et al.*, 2006, Kirschke *et al.*, 2013). However, little change in OH concentration was found in previous studies (Bousquet *et al.*, 2006, Kai *et al.*, 2011, Montzka *et al.*, 2011) and CH_4 oxidation through methanotroph lacked the magnitude to trigger the abrupt change in the CH_4 budget (Schaefer *et al.*, 2016, Tian *et al.*, 2016). Methane emission from different sources has been proposed to explain the changes in CH_4 growth rate since the early 1990s. Isotopic measurements, TD and BU approaches were used to attribute the change in CH_4 source strength to the atmospheric CH_4 variability but still failed to reach consistent conclusions. Isotopic measurements indicated a slowdown in fossil fuel emission since the late 1980s (Bousquet *et al.*, 2006, Schaefer *et al.*, 2016), and identified the dominant contribution of biogenic emissions in the Northern Hemisphere (NH) for the slowdown of CH_4 growth rate since the early 1990s (Kai *et al.*, 2011) and for the increase in the post-2006 [CH_4]-growth (Schaefer *et al.*, 2016). Isotopic measurements are suitable to assess the relative contribution of the CH_4 sources with distinctive isotope signatures (e.g., biogenic, pyrogenic and thermogenic sources), but failed to disentangle the CH_4 sources with similar isotope signatures (e.g., microbial oriented CH_4 fluxes with isotopically depleted signatures: wetland ~ -52 to -60‰, ruminants ~-60‰ to -74‰, and rice field ~ -59 to -65‰) (Kai *et al.*, 2011, Schaefer *et al.*, 2016). Reduced CH_4 emission from rice fields in the NH was suggested to explain the decline of atmospheric CH_4 growth rate, partly owing to no significant change in the total wetland area and total CH_4 emission from wetlands before 1999 (Kai *et al.*, 2011). However, multi-satellite observations revealed that the global inundation extent decreased at the rate of 67700 km^2/yr in the 1990s (Prigent *et al.*, 2012, Prigent *et al.*, 2007). Hence, variations in CH_4 emission from wetlands could be a potential driver of the recent CH_4 anomalies (Bousquet *et al.*, 2006, Bousquet *et al.*, 2011, Pison *et al.*, 2013). Increasing lines of evidence with the findings from TD approaches

(e.g., atmospheric inversion model) showed wetland CH_4 emissions played a critical role in determining the global CH_4 anomalies in the last two decades. For example, it has been suggested that CH_4 emissions from wetlands were affected by the eruption of Mount Pinatubo through sulfur deposition and temperature perturbation in the early 1990s (Bândă *et al.*, 2013). A significant reduction in CH_4 emissions from wetlands was found in the northern regions during the largest El Nino year (1997), followed by an increase in the southern regions in 1998 due to drier and wetter climate conditions (Bousquet *et al.*, 2006). Pison *et al.* (2013) suggested that wetlands in South America dominated atmospheric CH_4 anomalies between 2000 and 2006. In addition, fire-induced CH_4 emissions, owing to extensive drought or intensive human disturbance (e.g., tropical peat fire), have been recognized as another important contributor, dominating the atmospheric CH_4 anomalies in specific year, such as 1997 and 1998 (van der Werf *et al.*, 2004, van der Werf *et al.*, 2010).

However, our understanding on how the terrestrial biosphere contributed to atmospheric CH_4 anomalies is limited by a lack of comprehensive quantification of the CH_4 fluxes from different sectors. Here, we examined the spatial and temporal distribution of CH_4 fluxes from wetlands, rice fields, ruminants, biomass burning and upland soil during 1993-2014 through a data-model integration. In addition to environmental driver inputs, such as climate change, atmospheric composition, land use and land management practices, we have included dynamic wetland data developed from the Global Inundation Extent from Multi-Satellites during 1993-2007 (GIEMS, Prigent *et al*., 2012), and burned area derived from Global Fire Emission Data version 4 (GFED4) during 1996-2014 (Giglio *et al.*, 2010, Giglio *et al.*, 2013) and reconstructed burned history before 1996 (Yang *et al.*, 2014) to drive a process-based biogeochemical model, the Dynamic Land Ecosystem Model (DLEM), to quantify terrestrial CH_4 sink and sources. We

chose the study period from 1993 to 2014, which covered the major change interval for atmospheric CH_4 variation.

2.3 Methodology

2.3.1 Dynamic Land Ecosystem Model

The DLEM version 2.0 is a highly integrated process-based ecosystem model, which includes five major components (biophysics, plant physiology, soil biogeochemistry, vegetation dynamics, as well as disturbance and land use/land management practices). In general, the biophysics component simulates the water and energy fluxes within the terrestrial ecosystems and their interactions with the environments. The plant physiology component simulates the key physiological processes, such as photosynthesis, respiration, allocation, and evapotranspiration. The soil biogeochemistry component simulates the processes of decomposition, nitrogen mineralization/immobilization, nitrification/denitrification, fermentation and some other major biogeochemical processes in soil, such as CH_4 production/oxidation and related processes. The land use, disturbance, and land management component simulates the impact of natural and human disturbance on the water and nutrient fluxes and storages in the land ecosystems. The DLEM is able to simulate the hydrological and biogeochemical cycles (e.g., carbon and nitrogen cycles) over the terrestrial ecosystem at daily time-step. The DLEM-estimated carbon and nutrient fluxes and storages have been validated against field measurements, eddy covariance observations and the estimate from other approaches (e.g., inventory approaches, TD and BU estimation) (Lu & Tian, 2013, Pan *et al.*, 2014, Ren *et al.*, 2012, Tian *et al.*, 2010a, Tian *et al.*, 2015, Tian *et al.*, 2010b).

2.3.2 Description of the CH_4 Module in the DLEM

The biogenic CH_4 fluxes in the DLEM include CH_4 emission from wetlands and rice fields as well as CH_4 uptake from soil sinks, are determined by CH_4 production, consumption and transportation through ebullition, diffusion and plant transport (Tian *et al.*, 2010b), and are assumed to occur in the top 50-cm soil layer. The net CH_4 flux between the atmosphere and soil is calculated as follow:

$$F_{CH_4} = F_P - F_O + \Delta[CH_4]$$

where F_{CH_4} is the flux of CH_4 between soil and the atmosphere (g C m^{-2} d^{-1}); F_P is the CH_4 production from inundated soil (g C m^{-2} d^{-1}); F_O is the CH_4 oxidation (g C m^{-2} d^{-1}); $\Delta[CH_4]$ is the net CH_4 fluxes changed within the soil column. Dissolved organic carbon (DOC) is assumed to be the only substrate for CH_4 production, which comes from the decomposition of litter and soil organic matter, as well as allocation of gross primary production (GPP) **(Fig. 2.1)**. Methane oxidation is assumed to occur in the atmosphere, soil pore water and during the plant-mediated transport. Both CH_4 production and oxidation are a function of environmental factors including soil pH, temperature and soil moisture content. Methane is assumed to be transported from soil pore water to the atmosphere via ebullition, diffusion, and plant-mediated transport. The CH_4 modules in the DLEM were originally described in Tian *et al.* (2010a), and further improved by introducing the mechanism of freeze-thaw process, and considering the impact of inter-annual and intra-annual variation of wetland extent on CH_4 flux. More specifically, the changing state of water during freezing and thawing is considered according to energy excess/deficit. We assume that CH_4 production and oxidation only occur when soil water is in liquid phase. The process of freezing and thawing also influences the CH_4 transportation through ebullition and diffusion. Once ice is formed at the top soil layer, the produced CH_4 will be stored within the soil profile and further released when ice melts. We introduced the seasonal variation of wetland extent by

incorporating the dynamic inundation extent from multi-satellite observations (Prigent *et al.*, 2012).

The pyrogenic CH_4 flux is produced owing to the incompletion combustion of organic matter (Houweling, 2000). In the DLEM, the pyrogenic CH_4 emission M (g C m^{-2}) is assumed only from biomass burning and is computed as

$$C_{bt} = \sum_{ipft=1}^{4} \sum_{ifuel=1}^{5} (C_{ipft,ifuel}\, CC_{ipft,ifuel}\, BF_{ipft} f_{ipft}\, EF) + f_{peatfire} Depth_{fire} Dens_{peat} EF_{peat}$$

in which, $ipft$ is the index of natural vegetation types within one model grid (DLEM allows a maximum of four natural vegetation types coexisting in one grid); $ifuel$ is the index of fuel types (1-leaf, 2-stem, 3-root, 4-litter, and 5-coarse woody debris); $BF_{ipft}$is the monthly burned fraction of each natural vegetation type (%), which is assumed to be equal to burned fraction at grid level; f_{ipft} is the fraction of biome in the grid (%); $C_{ipft,ifuel}$ is the DLEM-simulated fuel loading of each fuel type (g C m^{-2}); $CC_{ipft,ifuel}$ is the combustion completeness (%); and EF indicates the CH_4 emission factor (g C/kg). The details of parameters were described in Yang *et al.* (2015) and van der Werf *et al.* (2010).

2.3.3 Input Data

A series of geo-referenced and time series input data are needed to drive the DLEM model, which include (1) climate data (maximum, minimum and mean air temperature, precipitation, and shortwave solar radiation); (2) atmospheric chemical components (atmospheric CO_2 concentration, AOT40 O_3 index and nitrogen deposition); (3) soil properties (soil texture, soil pH, and soil bulk density); (4) topographic data (slope, aspect, and elevation); (5) river network; (6) land use data with cohort structure and land management practices (irrigation, fertilization, rotation, etc.). In this study, daily climate variables during 1901-2014 were derived

from CRUNCEP_v6 6-hourly climate datasets (http://dods.extra.cea.fr/store/p529viov/cruncep/). Atmospheric CO_2 concentration data were obtained from a spline fit of the Law Dome and DE08-2 ice cores before 1959 (http://cdiac.ornl.gov/ftp/trends/co2/lawdome.smoothed.yr20), and from NOAA (http://www.esrl.noaa.gov/gmd/ccgg/trends/global.html) during 1959-2014. Atmospheric ozone concentration was represented by AOT40 index, which was a measure of accumulated ozone level above the threshold of 40 ppb (Felzer *et al.,* 2005). Global atmospheric nitrogen deposition data were obtained via https://daac.ornl.gov/CLIMATE/guides/global_N_deposition_maps.html and further interpolated to annual time-step (Wei *et al.*, 2014). The basic soil properties were derived from Harmonized World Soil Database (HWSD) (Wieder *et al.*, 2014). Land use and land cover change data were derived from Synergetic Land Cover Product (SYNMAP) (Jung *et al.,* 2006) and History Database of the Global Environment (HYDE v3.1) (Hurtt *et al.*, 2011). The wetland data were obtained from Global Inundation Extent from Multi-Satellites (GIEMS), which covered the time period from 1993 to 2007 (Prigent *et al.*, 2012). Prior to 1993, we used the mean inundation extent derived from the seasonal variation of inundation dynamic for the 15 years (1993-2007) and assumed the wetland extent remained unchanged after 2007. **Fig. 2.2** shows the contemporary distribution of land use and land cover types in the global terrestrial ecosystem being used in the DLEM. The reconstructed burned area during 1900 to 1995 was obtained from DLEM-fire (Yang *et al.*, 2014) and the burned area during 1996-2014 was derived from GFED4 (Giglio *et al.*, 2013). Further details of the input data were described in the previous publications (Lu & Tian, 2013, Ren *et al.*, 2011, Tian *et al.*, 2015, Tian *et al.*, 2010b).

2.3.4 Model Calibration and Validation

The DLEM estimated CH_4 fluxes have been extensively evaluated against field observations, inventory data, and other process-based and inverse models estimates at multiple scales spanning from sites to global (Lu & Tian, 2013, Melton *et al.*, 2013, Ren *et al.*, 2011, Tian *et al.*, 2015, Tian *et al.*, 2010b, Xu *et al.*, 2010). Previous studies indicated that the DLEM could capture the magnitude and daily/seasonal/annual variations of observed CH_4 fluxes. In this study, we further examined the DLEM performance via 28 observation sites with 552 data pairs for different plant functional types (**Table 2.1; Fig. 2.3**). The daily and seasonal patterns of the DLEM simulated CH_4 fluxes were compared to the data collected at multiple sites (**Fig. 2.3**). In general, the DLEM estimations showed a good agreement with the field observations (slope = 1.1428; $R^2 = 0.9503$; $p < 0.0001$) (**Fig. 2.3**).

2.3.5 Model Implementation

At first, we conducted the initial run, also called the equilibrium run, to make the model reach the equilibrium state and get the initial condition for the spin-up and transient run. All the input data in 1900 were used to drive the model except climate data. For climate data, we used 30-year (1901-1930) long-term mean climate data. Spin-up was used to provide a smooth transition between the equilibrium run and the transient run, which run for another 900 years with de-trended climate data from 1901 to 1930. The transient run was to get the estimation of CH_4 fluxes by considering all the natural and anthropogenic changes during the years 1901-2014.

2.3.6 Calculation of Ruminant Emission

To develop the gridded annual CH_4 emission rate through ruminants during 1993-2014, we used the dataset from the Global Livestock Impact Mapping System (GLIMS) with a spatial resolution of 0.00833 degrees (- a nominal pixel resolution of approximately 1km*1km at the equator) for cattle, pigs, goats, and sheep (Robinson *et al.*, 2014). GLIMS provided the

information on the spatial distribution of different livestock. The annual variation of global livestock number from 1993 to 2014 was controlled by FAOSTAT, which provides country-specific information on the annual stock of livestock (FAOSTAT, 2014) (http://faostat.fao.org/site/291/default.aspx). For those years without the information of livestock populations from FAOSTAT, we applied the annual trend extracted from the HYDE (History Database of the Global Environment) (http://themasites.pbl.nl/tridion/en/themasites/hyde/landusedata/livestock/index-2.html) – livestock numbers based on the continental analysis to calculate the corresponding livestock number. Default emission factors for CH_4 derived from enteric fermentation were obtained from FAO (FAOSTAT, 2014) (http://faostat3.fao.org/download/G1/GE/E).

The development of the time-series CH_4 emission rate from livestock was provided below in more detail. First, we calculated the country-specific ratio of the total head from GLIMS to the total head from FAO.

$$Ratio_{i,j} = \frac{NTH(GLIMS)_{i,j}}{NTH(FAO)_{i,j}}$$

where: *NTH* indicates the national head in total of animal *j* from a specific country *i* (unit: head). Then we calculated the animal density for each country from FAO.

$$Ratio_{i,j} = \frac{D(GLIMS)_{i,j} * A_i}{D(FAO)_{i,j} * A_i} = \frac{D(GLIMS)_{i,j}}{D(FAO)_{i,j}}$$

where: *D* indicates the density of animal *j* from a specific country *i* (unit: head km^{-2}); *A* indicates the area for a specific country *i* (unit: km^2).

Therefore,

$$D(FAO)_{i,j} = \frac{D(GLIMS)_{i,j}}{Ratio_{i,j}}$$

Then we calculated the gridded average CH_4 emission rate by applying the IPCC 2006 guidelines (Tier1).

$$Emission_{(j)} = EF_{(i,j)} \times D(FAO)_{i,j}$$

where $Emissions$ indicates CH_4 emission from Enteric Fermentation for the livestock category *j* (Unit: kg km^{-2} yr^{-1}); $EF_{(i,j)}$ indicates emission factor for the livestock category *j* from a specific country *i* (Unit: kg $head^{-1}$). Here, the ratio of the population for dairy cattle to non- dairy cattle in the conterminous United States was obtained from Yang *et al.* (2016)'s datasets. For other countries in the world, we assumed that each category occupied 50% of the total cattle population.

2.3.7 Description of One-Box Model

One-box model was used to analyze the changes in global CH_4 fluxes via the atmospheric CH_4 concentration and atmospheric growth rate (Dlugokencky *et al.*, 1998). The change in the global burden of CH_4 is given by:

$$\frac{d[CH_4]}{dt} = Q - [CH_4]/\tau$$

where $[CH_4]$ is the global CH_4 burden, Q is the sum of all emissions, and τ is the total atmospheric CH_4 lifetime. The above equation could be rearranged to calculate the annual CH_4 source strength

$$Q = \frac{d[CH_4]}{dt} + [CH_4]/\tau$$

In this equation, the annual increase $\frac{d[CH_4]}{dt}$ is given by yearly-averaged growth rates, and the burden $[CH_4]$ is given by the mole fractions of atmospheric CH_4 concentration. τ is around 9 years. The conversion factor (1nmol mol^{-1} = 2.767 Tg) was used to convert from mol fraction to Tg in mass. The annual CH_4 growth rate was obtained from

http://www.esrl.noaa.gov/gmd/ccgg/trends_ch4/. The atmospheric CH_4 concentration was obtained from ftp://aftp.cmdl.noaa.gov/products/trends/ch4/ch4_annmean_gl.txt.

2.4 Results

2.4.1 Spatial Patterns of Estimated Total CH_4 Fluxes

In this study, we quantified the total CH_4 fluxes from wetlands, rice fields, upland soil, biomass burning, and ruminants during 1993-2014. The estimated total CH_4 flux was 163.9±6.4 Tg C/yr. Among all the CH_4 sources, wetlands contributed almost half (~49.2%) of the global total CH_4 emission, followed by ruminants (~36.8%), rice field (~7.5%) and biomass burning (~6.5%). The upland soil consumed 25.0±0.5 Tg C/yr CH_4 through oxidation, offsetting ~13.2% of the total emitted CH_4 from those four sources.

The tropical regions (30°N-30°S) were the dominant contributor to the estimated net CH_4 flux (~103.6±5.8 Tg C/yr), followed by the northern middle latitude region (NM, 30°N-60°N) (~ 41.7±2.2 Tg C/yr), southern middle latitude region (SM, 30°S-60°S) (~10.0±0.5 Tg C/yr), and northern high latitude region (NH, 60°N -90°N) (~8.6±0.5 Tg C/yr) **(Fig. 2.4)**. The tropical region acted as the largest CH_4 source from wetlands, ruminants, rice fields and biomass burning. Among all the sources, wetlands were found to be the dominant contributor of the net CH_4 fluxes in the tropical region and NH, while ruminant shared the largest portion in the NM and SM.

We further examined the estimated net CH_4 fluxes from six continents **(Fig. 2.5)**, which include Asia, North America, Europe, Africa, South America and Oceania. Asia, the largest rice-growing continent and ruminant-dense region, accounted for over one-third (~38.4%) of the global net CH_4 fluxes. South America shared another 28.2% of the global net CH_4 fluxes, mainly owing to higher tropical wetland emission. Africa and North America together took another one-

third of global CH_4 flux. Despite ~37.7% of CH_4 emissions from biomass burning originated from Africa, CH_4 consumption strength via upland soil was two times larger than biomass burning, which made Africa a small CH_4 source. Europe and Oceania shared the least portion of the global net CH_4 fluxes.

2.4.2 Temporal Patterns of Estimated Total CH_4 Fluxes

The estimated global CH_4 fluxes exhibited substantial inter-annual variation, with the largest CH_4 fluxes occurring in 1997 (~175.5 Tg C/yr) partly owing to the huge release of CH_4 emission from peat fire in Indonesia, and the least in 2000 (148.4 Tg C/yr). The estimated CH_4 emission from wetlands was 92.9±4.2 Tg C/yr and fluctuated greatly during 1993-2014. The Mann–Kendall Trend Test was used to examine the temporal trends in the estimated CH_4 fluxes. The estimated CH_4 emission from wetlands showed a significant decreasing trend at a rate of -1.8 Tg C/yr during 1993-2000 ($p < 0.05$), followed by a significant increasing trend at a rate of 0.8 Tg C/yr during 2004-2014 ($p < 0.05$). The estimated CH_4 emission from ruminants demonstrated a significant upward trend ($p < 0.001$), ranging from 66.5 Tg C/yr in 1999 to 73.1 Tg C/yr in 2014. In contrast, the estimated CH_4 emission from rice field showed a significant downward trend at a rate of 0.2 Tg C/yr ($p < 0.001$). The estimated CH_4 emission from biomass burning was around 12.3±4.0 Tg C/yr during 1993-2014, with peak emission occurred in 1997 (~25.5 Tg C/yr), 2006 (~18.4 Tg C/yr), and 1998 (~17.1 Tg C/yr) due to the large incomplete combustion from peat fire. The consumption of CH_4 fluxes by upland soil was estimated to increase significantly at a rate of -0.05 Tg C/yr ($p < 0.001$).

2.4.3 Attribution of Biogenic and Pyrogenic Sources to Atmospheric CH_4 Variability

To identify the relative contribution of biogenic and pyrogenic sources to atmospheric CH_4 variability, the estimated anomalous fluxes were determined by subtracting the mean annual

CH_4 fluxes during the study period (1993-2014). The Pearson's correlation coefficient was used to evaluate the correlation between the anomalous CH_4 fluxes from each sector (wetlands, ruminants, rice fields, biomass burning and upland soil) and the atmospheric CH_4 growth rate, which was 0.71, 0.62, -0.18, 0.22 and -0.11, respectively (**Fig. 2.6**). Our results revealed that CH_4 emission from wetlands dominated the inter-annual variation of the total CH_4 fluxes from wetlands, ruminants, rice fields, biomass burning and upland soil, and agreed well with the atmospheric CH_4 variation. The accelerated increase in estimated CH_4 emission from ruminants after the early 2000s made its contribution increasingly important to the atmospheric CH_4 variation especially after 2006. Methane emission from biomass burning played a critical role in regulating the inter-annual variation in some specific years (e.g., in 1997, 1998 and 2006), most of which related to the peat fire emission.

2.5 Discussion

2.5.1 Comparison with Other Studies

Various approaches have been used to estimate the CH_4 fluxes from different sources and sinks due to the increasing awareness of the immediate feedback between CH_4 fluxes and climate change. Here, we compared the DLEM-estimated CH_4 fluxes with other studies, which included the estimates from both BU and TD approaches summarized by Kirschke *et al.* (2013) at the continental/country level **(Fig. 2.7)**. The DLEM estimated CH_4 emission from wetlands was within the range of atmospheric inversion model estimation and other bottom-up estimates; and the DLEM-estimated CH_4 uptake from soil was consistent with inversion-estimation. Compared with other BU estimates, ORCHIDEE showed the highest estimation in most parts of the globe. The DLEM estimation was more consistent with the estimation from LPJ-WhyMe. The great differences among BU models estimates were mostly associated with the differences in wetland

extent used by each model (Kirschke *et al.*, 2013, Melton *et al.*, 2013). More specifically, the DLEM-estimated CH_4 flux was at the lower end of estimation from other BU estimates in Africa and South America, and consistent with the estimation from inversion estimation of TM5-4DAVR and LMDZt-SAC. Tropical wetlands were thought to contribute 50%-70% of global wetland emission (Montzka *et al.*, 2011). However, sparse observations for atmospheric concentration and limited field information constrained the ability to assess the spatial and temporal magnitude of CH_4 fluxes in this region for both TD and BU approaches, which further increased the uncertainties of global estimation. The DLEM-estimated CH_4 emission from biomass burning (~12.9 ± 4.2 Tg C/yr) was similar as the estimation from GFED4 (~11.9 ± 4.2 Tg C/yr) during 1997-2014. The DLEM estimated peat fire emission in 1997 (~25.5 Tg C/yr) agreed well with GFED4 estimation (~26.8 Tg C/yr) and was larger in 1998.

2.5.2 Attribution of Biogenic and Pyrogenic Sources to Atmospheric CH_4 Variability

After subtracting the mean wetland CH_4 emission over 1993-2003, the DLEM-estimated CH_4 anomalies from wetlands were -1.2 and 2.2 Tg C/yr in the northern region (> 30°N) in 1997 and 1998, respectively, which agreed well with the previous inversion estimation, indicating a dip in wetland CH_4 emissions anomalies in 1997 and followed by an increase in 1998 (Bousquet *et al.*, 2006). Isotopic measurement together with inter-hemispheric difference of CH_4 mixing ratio analysis showed that large reduction in CH_4 emissions from 312.8±7.5 Tg C /yr to 289.5±3.8Tg C/yr during 1985-2005 in the northern hemisphere, at the rate of 1.1 Tg C /yr (Kai *et al.*, 2011). In this study, the estimated CH_4 emissions from wetland showed a significant decreasing trend at a rate of 0.6 Tg C /yr from 1993 to 2005, which accounted for over 50% of the aforementioned estimation. By using the mean flux over 1999-2007, Bousquet *et al.* (2011) indicated that there was a negative CH_4 anomaly during 2006, however, our study showed a

slightly positive anomaly. For 2007, their results showed global CH_4 anomaly was around 15.8 ± 3Tg C, while estimated anomalous CH_4 emissions from wetland and ruminants by employing the DLEM were around 4.6 Tg C and 3.6 Tg C, respectively, which together accounted for over half of the total anomalies. As suggested by satellite observation and isotopic measurements, post-2006 emission originated from tropical region with ^{13}C-depleted signature (Schaefer *et al.*, 2016). The DLEM-estimated biogenic CH_4 emissions from wetlands, rice fields and ruminants showed a significant increasing trend in the tropical region, at a rate of 0.5 Tg C/yr (p<0.001). Both ruminants and wetlands showed similar contribution to an increase in post-2006 emission.

Asia contributed over 96% of the total emission from the rice field, corresponding to the vast rice area occupancy in this region (Yan *et al.*, 2009). The estimated CH_4 emissions from rice field exhibited small inter-annual variations and the CH_4 consumption from upland soil showed great inter-annual variation, with an overall increasing trend during 1993-2014. South America, Africa savanna and South Asia were found to be the hotspots of CH_4 emission induced by fire in the DLEM estimation, which was due to the sufficient fuel and long dry seasons in these regions (van der Werf *et al.*, 2004, van der Werf *et al.*, 2010, Yang *et al.*, 2014) **(Fig. 2.4**). The inter-annual variability of CH_4 emissions from fire events was determined by the occurrence of fire events, fire types as well as the vegetation types. The long dry season during the largest El Niño in 1997-1998 resulted in large uncontrolled fires (Page *et al.*, 2002). The occurrence of widespread fire in Indonesia and boreal forest in Russia released huge amount of carbon into the atmosphere during 1997-1998, which was consistent with our findings.

2.5.3 Uncertainties

Our results need to be interpreted with caution owing to the uncertainties arising from input data, model representation of different processes and related parameters, and further

investigated. Large differences in the magnitude and spatial distribution of wetlands existed among current datasets. In general, the current global wetland datasets could be classified into two groups: one-phase static wetland datasets (Kaplan, 2007, Lehner & Döll, 2004, Matthews & Fung, 1987) and dynamic wetland datasets (Prigent *et al.*, 2012). GIEMS used in this study for the first time, provided the global coverage and monthly change of inundation extent covering a limited historical temporal record during 1993-2007, which could introduce the uncertainties of the estimated CH_4 emission after 2007. In addition, the inundation datasets derived from multi-satellite observations failed to capture the wetland without standing water, for example in some peatlands, the water table is beneath the soil surface but part of the soil is well saturated which could produce considerable amounts of CH_4 (Melton *et al.*, 2013). Besides, the estimated CH_4 emission from ruminants was based on country-level animal population data together with default emission factor from FAO. However, the uniform emission rate without considering the feed availability and quality across different seasons and various regions for specific livestock type at regional scale could introduce some uncertainties (Ouyang *et al.*, 2013, Rufino *et al.*, 2014). In addition, we used GLIMS to get the spatial distribution of different livestock, which may not be able to provide the accurate information of change in spatial distribution of livestock at sub-national level over time. For instant, the animal population may migrate due to food availability. Therefore, the spatial distribution of different livestock at sub-national scale, such as cattle, sheep, and goat, might be different from the current situation. Besides, GFED4 offered a limited historical temporal record of peat burned fraction, which may underestimate the CH_4 emission from biomass burning due to absent of peat fire before 1996.

2.6 Conclusion

This study examined the global spatial and temporal patterns of CH_4 fluxes from biogenic and pyrogenic sources and upland soil sink during 1993-2014 and also quantified the contribution of each sector on the global atmospheric CH_4 anomalies. Our results suggested that the net CH_4 fluxes from wetlands, rice fields, biomass burning, ruminants and upland soil in total varied from 148.4 to 175.5 Tg C/yr during 1993-2014. Methane emissions from wetland and ruminants together contributed ~86% of the global total CH_4 emission, in which ~13.2% were offset by upland soil. The tropical region shared the largest portion of the estimated net CH_4 fluxes and acted as the largest CH_4 source/sink from each sector. Among six continents, Asia accounted for over one-third (~38.4%) of the global net CH_4 fluxes owing to large rice-growing and ruminant-raising region, followed by South America, Africa, and North America. Europe and Oceania shared the least portion of the global net CH_4 fluxes. Methane emission from wetlands dominated the atmospheric CH_4 variation during 1993-2014. The contribution of CH_4 emission from ruminants became increasingly important, especially after 2006, largely associated with an increase in livestock population. Methane emissions from biomass burning dominated the atmospheric CH_4 variation in some specific years when huge peat fire occurred, which contributed to a release of large amounts of CH_4. This study suggested that biogenic sources, mainly wetlands and ruminants in the tropical region, dominated the atmospheric CH_4 variation. Agricultural emission will likely remain important in regulating the atmospheric CH_4 variation due to the continuous increase in food demand.

2.7 References

Bândă N, Krol M, Weele MV, Noije TV, Röckmann T (2013) Analysis of global methane changes after the 1991 Pinatubo volcanic eruption. Atmospheric Chemistry and Physics, **13**, 2267-2281.

Bousquet P, Ciais P, Miller JB *et al.* (2006) Contribution of anthropogenic and natural sources to atmospheric methane variability. Nature, **443**, 439-443.

Bousquet P, Ringeval B, Pison I *et al.* (2011) Source attribution of the changes in atmospheric methane for 2006–2008. Atmospheric Chemistry and Physics, **11**, 3689-3700.

Ciais P, Sabine C, Bala G *et al.* (2014) Carbon and other biogeochemical cycles. In: *Climate Change 2013: The Physical Science Basis. Contribution of Working Group I to the Fifth Assessment Report of the Intergovernmental Panel on Climate Change*., Cambridge University Press.

Dlugokencky E, Masarie K, Lang P, Tans P (1998) Continuing decline in the growth rate of the atmospheric methane burden. Nature, **393**, 447-450.

Dlugokencky EJ, Bruhwiler L, White JWC *et al.* (2009) Observational constraints on recent increases in the atmospheric CH4 burden. Geophysical Research Letters, **36**.

Dlugokencky EJ, Nisbet EG, Fisher R, Lowry D (2011) Global atmospheric methane: budget, changes and dangers. Philosophical Transactions of the Royal Society a-Mathematical Physical and Engineering Sciences, **369**, 2058-2072.

Faostat (2014) FOOD AND AGRICULTURE ORGANIZATION OF THE UNITED NATIONS STATISTICS DIVISION.

Felzer B, Reilly J, Melillo J *et al.* (2005) Future effects of ozone on carbon sequestration and climate change policy using a global biogeochemical model. Climatic Change, **73**, 345-373.

Giglio L, Randerson J, Van Der Werf G, Kasibhatla P, Collatz G, Morton D, Defries R (2010) Assessing variability and long-term trends in burned area by merging multiple satellite fire products. Biogeosciences, **7**.

Giglio L, Randerson JT, Werf GR (2013) Analysis of daily, monthly, and annual burned area using the fourth-generation global fire emissions database (GFED4). Journal of Geophysical Research: Biogeosciences, **118**, 317-328.

Houweling S (2000) *Global modeling of atmospheric methane sources and sinks*, Utrecht University Utrecht.

Hurtt GC, Chini LP, Frolking S *et al.* (2011) Harmonization of land-use scenarios for the period 1500-2100: 600 years of global gridded annual land-use transitions, wood harvest, and resulting secondary lands. Climatic Change, **109**, 117-161.

Jung M, Henkel K, Herold M, Churkina G (2006) Exploiting synergies of global land cover products for carbon cycle modeling. Remote Sensing of Environment, **101**, 534-553.

Kai FM, Tyler SC, Randerson JT, Blake DR (2011) Reduced methane growth rate explained by decreased Northern Hemisphere microbial sources. Nature, **476**, 194-197.

Kaplan JO (2007) A composite map of global wetland distribution at 0.5 degree resolution. Digital dataset available at http://arve.epfl.ch/pub/wetlands/index.html.

Kirschke S, Bousquet P, Ciais P *et al.* (2013) Three decades of global methane sources and sinks. Nature Geoscience, **6**, 813-823.

Lehner B, Döll P (2004) Development and validation of a global database of lakes, reservoirs and wetlands. Journal of Hydrology, **296**, 1-22.

Lu CQ, Tian HQ (2013) Net greenhouse gas balance in response to nitrogen enrichment: perspectives from a coupled biogeochemical model. Global Change Biology, **19**, 571-588.

Matthews E, Fung I (1987) Methane emission from natural wetlands: Global distribution, area, and environmental characteristics of sources. Global Biogeochemical Cycles, **1**, 61-86.

Melton JR, Wania R, Hodson EL *et al.* (2013) Present state of global wetland extent and wetland methane modelling: conclusions from a model inter-comparison project (WETCHIMP). Biogeosciences, **10**, 753-788.

Montzka SA, Dlugokencky EJ, Butler JH (2011) Non-CO2 greenhouse gases and climate change. Nature, **476(7358)**, 43-50.

Nisbet EG, Dlugokencky EJ, Bousquet P (2014) Methane on the Rise-Again. Science, **343**, 493-495.

Ouyang W, Hao F, Wei X, Huang H (2013) Spatial and temporal trend of Chinese manure nutrient pollution and assimilation capacity of cropland and grassland. Environmental Science and Pollution Research, **20**, 5036-5046.

Page SE, Siegert F, Rieley JO, Boehm H-DV, Jaya A, Limin S (2002) The amount of carbon released from peat and forest fires in Indonesia during 1997. Nature, **420**, 61-65.

Pan S, Tian H, Dangal SR *et al.* (2014) Modeling and monitoring terrestrial primary production in a changing global environment: toward a multiscale synthesis of observation and simulation. Advances in Meteorology, **2014**.

Pison I, Ringeval B, Bousquet P, Prigent C, Papa F (2013) Stable atmospheric methane in the 2000s: key-role of emissions from natural wetlands. Atmospheric Chemistry and Physics, **13**, 11609-11623.

Prigent C, Papa F, Aires F, Jimenez C, Rossow WB, Matthews E (2012) Changes in land surface water dynamics since the 1990s and relation to population pressure. Geophysical Research Letters, **39**.

Prigent C, Papa F, Aires F, Rossow W, Matthews E (2007) Global inundation dynamics inferred from multiple satellite observations, 1993–2000. Journal of Geophysical Research: Atmospheres, **112**.

Ren W, Tian HQ, Tao B, Huang Y, Pan SF (2012) China's crop productivity and soil carbon storage as influenced by multifactor global change. Global Change Biology, **18**, 2945-2957.

Ren W, Tian HQ, Xu XF *et al.* (2011) Spatial and temporal patterns of CO2 and CH4 fluxes in China's croplands in response to multifactor environmental changes. Tellus Series B-Chemical and Physical Meteorology, **63**, 222-240.

Robinson TP, Wint GRW, Conchedda G *et al.* (2014) Mapping the Global Distribution of Livestock. Plos One, **9**.

Rufino M, Brandt P, Herrero M, Butterbach-Bahl K (2014) Reducing uncertainty in nitrogen budgets for African livestock systems. Environmental Research Letters, **9**, 105008.

Schaefer H, Fletcher SEM, Veidt C *et al.* (2016) A 21st-century shift from fossil-fuel to biogenic methane emissions indicated by 13CH4. Science, **352**, 80-84.

Tian H, Lu C, Ciais P *et al.* (2016) The terrestrial biosphere as a net source of greenhouse gases to the atmosphere. Nature, **531**, 225-228.

Tian HQ, Chen GS, Liu ML *et al.* (2010a) Model estimates of net primary productivity, evapotranspiration, and water use efficiency in the terrestrial ecosystems of the southern United States during 1895-2007. Forest Ecology and Management, **259**, 1311-1327.

Tian HQ, Chen GS, Lu CQ *et al.* (2015) Global methane and nitrous oxide emissions from terrestrial ecosystems due to multiple environmental changes. Ecosystem Health and Sustainability, **1**, art4.

Tian HQ, Xu XF, Liu ML, Ren W, Zhang C, Chen GS, Lu CQ (2010b) Spatial and temporal patterns of CH4 and N2O fluxes in terrestrial ecosystems of North America during 1979-2008: application of a global biogeochemistry model. Biogeosciences, **7**, 2673-2694.

Van Der Werf GR, Randerson JT, Collatz GJ *et al.* (2004) Continental-scale partitioning of fire emissions during the 1997 to 2001 El Nino/La Nina period. Science, **303**, 73-76.

Van Der Werf GR, Randerson JT, Giglio L *et al.* (2010) Global fire emissions and the contribution of deforestation, savanna, forest, agricultural, and peat fires (1997–2009). Atmospheric Chemistry and Physics, **10**, 11707-11735.

Walter BP, Heimann M, Matthews E (2001) Modeling modern methane emissions from natural wetlands 1. Model description and results. Journal of Geophysical Research-Atmospheres, **106**, 34189-34206.

Wei Y, Liu S, Huntzinger DN *et al.* (2014) The North American Carbon Program Multi-scale Synthesis and Terrestrial Model Intercomparison Project - Part 2: Environmental driver data. Geoscientific Model Development, **7**, 2875-2893.

Wieder WR, Boehnert J, Bonan GB, Langseth M (2014) Regridded Harmonized World Soil Database v1.2. Data set. Available on-line [http://daac.ornl.gov] from Oak Ridge National Laboratory Distributed Active Archive Center, Oak Ridge, Tennessee, USA.

Wmo (2015) World Meteorlogical Organization Greenhouse Gas Bulletin. pp Page, Citeseer.

Xu XF, Tian HQ, Zhang C *et al.* (2010) Attribution of spatial and temporal variations in terrestrial methane flux over North America. Biogeosciences, **7**, 3637-3655.

Yan XY, Akiyama H, Yagi K, Akimoto H (2009) Global estimations of the inventory and mitigation potential of methane emissions from rice cultivation conducted using the 2006 Intergovernmental Panel on Climate Change Guidelines. Global Biogeochemical Cycles, **23**.

Yang J, Tian H, Tao B, Ren W, Kush J, Liu Y, Wang Y (2014) Spatial and temporal patterns of global burned area in response to anthropogenic and environmental factors: Reconstructing global fire history for the 20th and early 21st centuries. Journal of Geophysical Research: Biogeosciences, **119**, 249-263.

Yang J, Tian H, Tao B *et al.* (2015) Century-scale patterns and trends of global pyrogenic carbon emissions and fire influences on terrestrial carbon balance. Global Biogeochemical Cycles, **29**, 1549-1566.

Yang Q, Tian H, Li X, Ren W, Zhang B, Zhang X, Wolf J (2016) Spatiotemporal patterns of livestock manure nutrient production in the conterminous United States from 1930 to 2012. Science of The Total Environment, **541**, 1592-1602.

Table 2.1 Site information for observed data

Site	Longitude	Latitude	PFTs	Reference
Eeath University	-83.57°W	10.22°N	Herbaceous wetland	Nahlik et al., 2011
Florida Typha	-84.25°W	30.5°N	wetland	Whiting et al., 2001
Can. Boreal Fen	-113°W	54°N	Fen	Whiting et al., 2001
Smith Lake	147.85W	64.87N	Tundra	Whalen et al., 1988
Albert Canada	113°W	55°N	Sedge Meadow	Vitt et al., 1990
Quebec Canada	66°W	54°N	Fen	Moore et al., 1990
Central Canada	78°W	45°N	Wetland	Roulet et al., 1992
Ellergower Moss	4°W	55°N	Bog	Clymo et al., 1971
Tapjos National Forest	54.95°W	2.90°S	Forest	Davidson et al., 2008
Canada Boreal Forest	105°W	53°N	Boreal forest	Matson et al., 2009
Louisiana, USA	90.11°W	29.8°'N	Forested wetland	Yu et al., 2008
Nanjing, China	118°E	32°'N	Rice paddies	Xiong et al., 2007
Jean Lafitte National Historic Park	-90.11°W	29.81°N	Bottomland Hardwood Frest	Yu et al., 2008
National Botanical Research Institute, Lucknow	80.85°E	26.75°N	Deepwater wetland	Singh et al., 2000
Manaus, Brazil	-60.03°W	-3.10°S	Flooded Forest	Devol et al., 1988
Schefferville, Quebec, Canada	-66.70°W	54.72°N	Temperate and Subartic Forest	Adamsen et al., 1993
Yukon Delta, Alaska, US	-161.75°W	60.75°N	Dry Tundra	Bartlett et al., 1992
Moosonee, Ontario, Canada	-81.83°W	51.33°N	bog	Klinger et al., 1994
Jasper Ridge Biological Preserve	122.23°W	37.4°N	Grassland	Blankinship et al., 2010
Wild rice bed	95.17°W	47.25°N	Rice	Harriss et al., 1985
Canton of Graubunden	9.87°E	46.78°N	Grassland	Merbold et al., 2013
Bonanza Creek LTER	-148.33°W	64.64°N	Bog	Myers Smith 2005
Kellogg Biological Station in southwest Michigan	-85.40°W--85.37°W	42.42°N-42.39°N	Crop	Robertson 2013
Buck Hollow Bog	84°01'W	42°27'N	Bog	Tang et al., 2010
Buck Hollow Peatland	84°01'W	42°27'N	Peatland	Shannon et al., 1994
Wisconsin mixed temperate/boreal lowland and wetland forest site	90°16'W	45°56'N	Wetland	Werner et al., 2003

Minnesota Peatland	93°28’W	47°32’N	Peatland	Dise et al., 1993
King bog lake	121.78°W	47.60°N	Bog	Lansdown et al., 1992

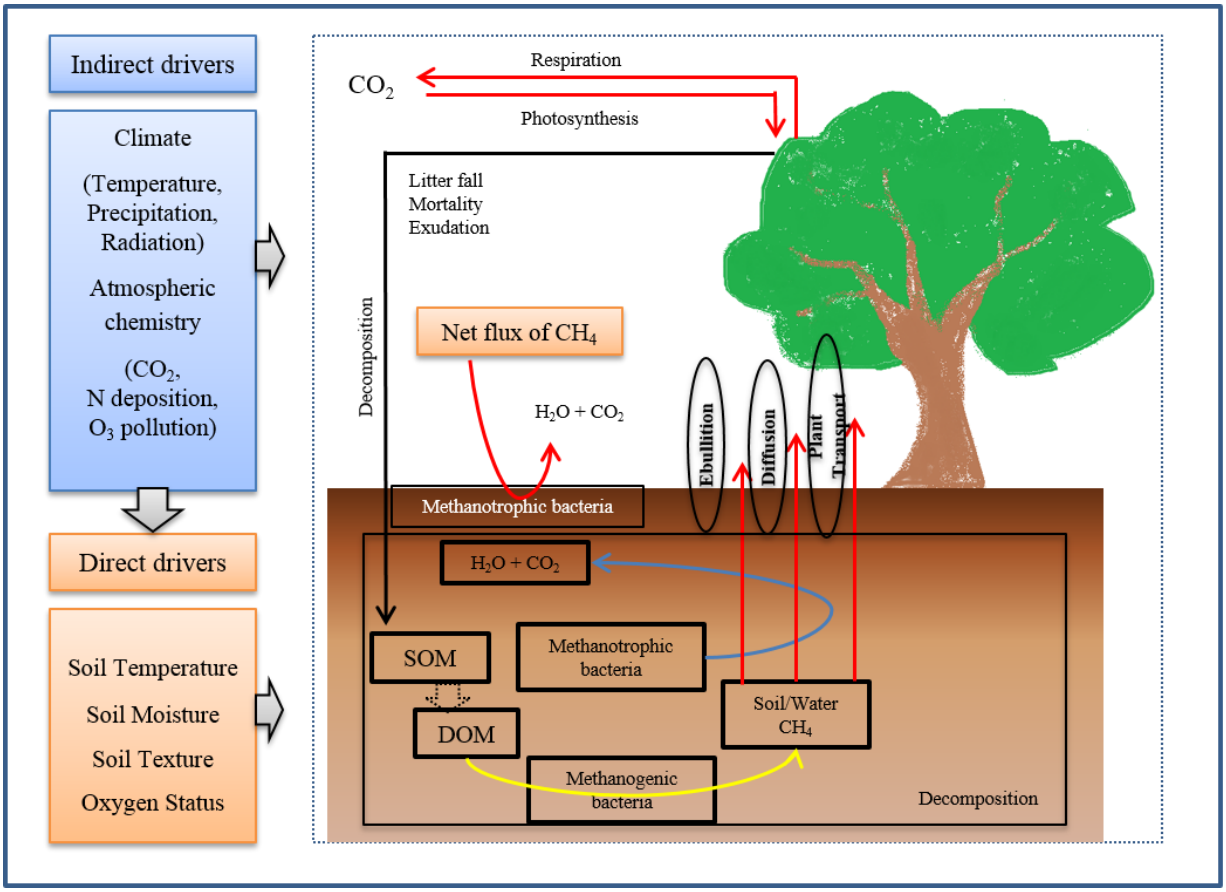

Figure 2.1 Framework of key biological processes controlling biogenic CH_4 fluxes in the DLEM, including direct and indirect drivers

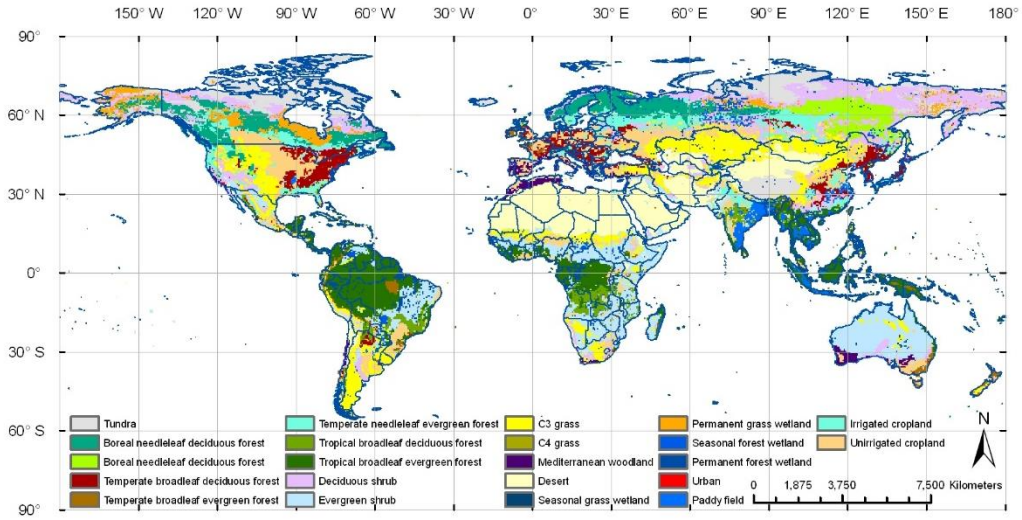

Figure 2.2 Contemporary distribution of land use and land cover types in the global terrestrial ecosystem being used in the DLEM

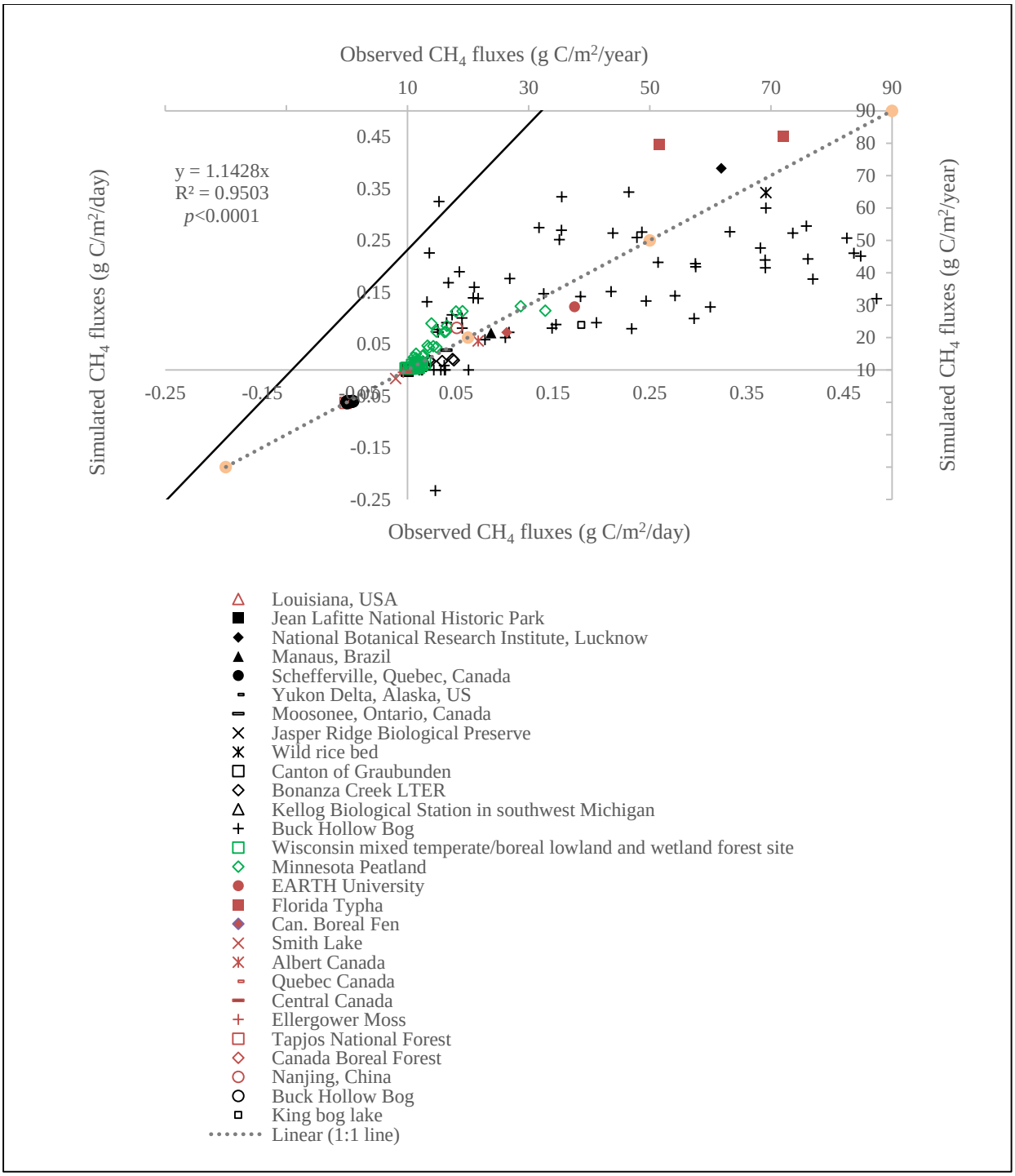

Figure 2.3 Evaluation of DLEM-estimated daily/monthly/yearly CH_4 fluxes against observed data at multiple sites.

Note: The black maker and the green maker used the primary axis, and indicates the units of CH_4 flux are g C/m^2/day. The orange maker used the secondary axis and indicates the units of CH_4 flux are g C/m^2/year.

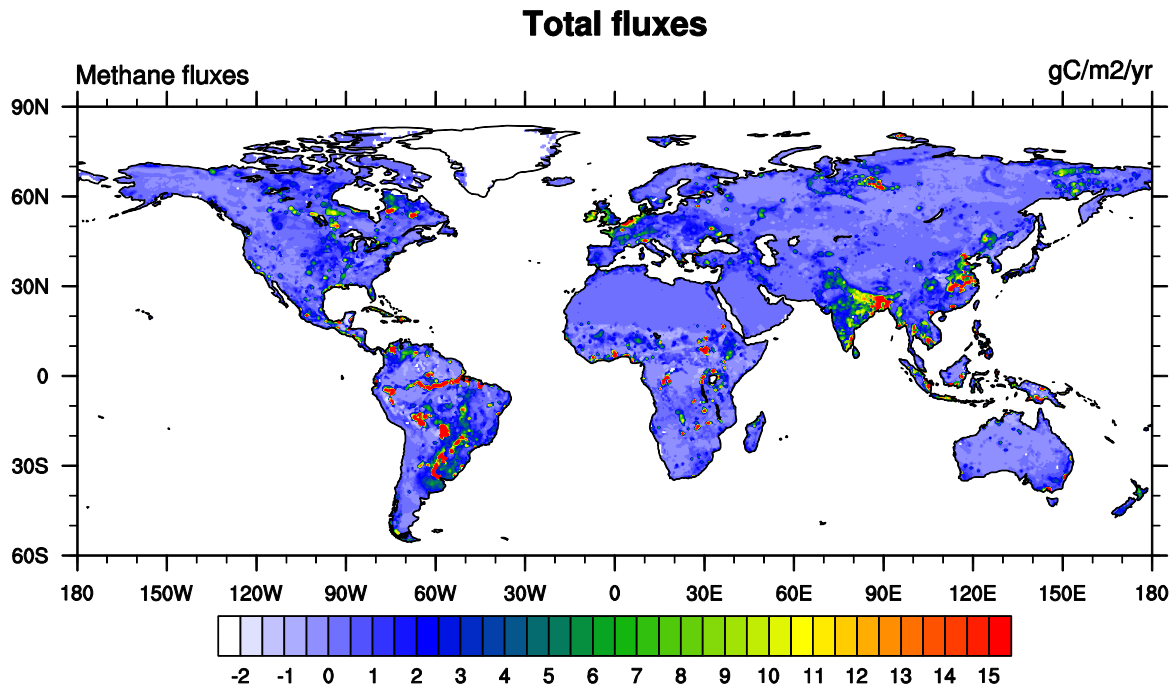

Figure 2.4 The estimated total CH_4 fluxes from wetlands, rice fields, biomass burning, ruminants and upland soil during 1993-2014

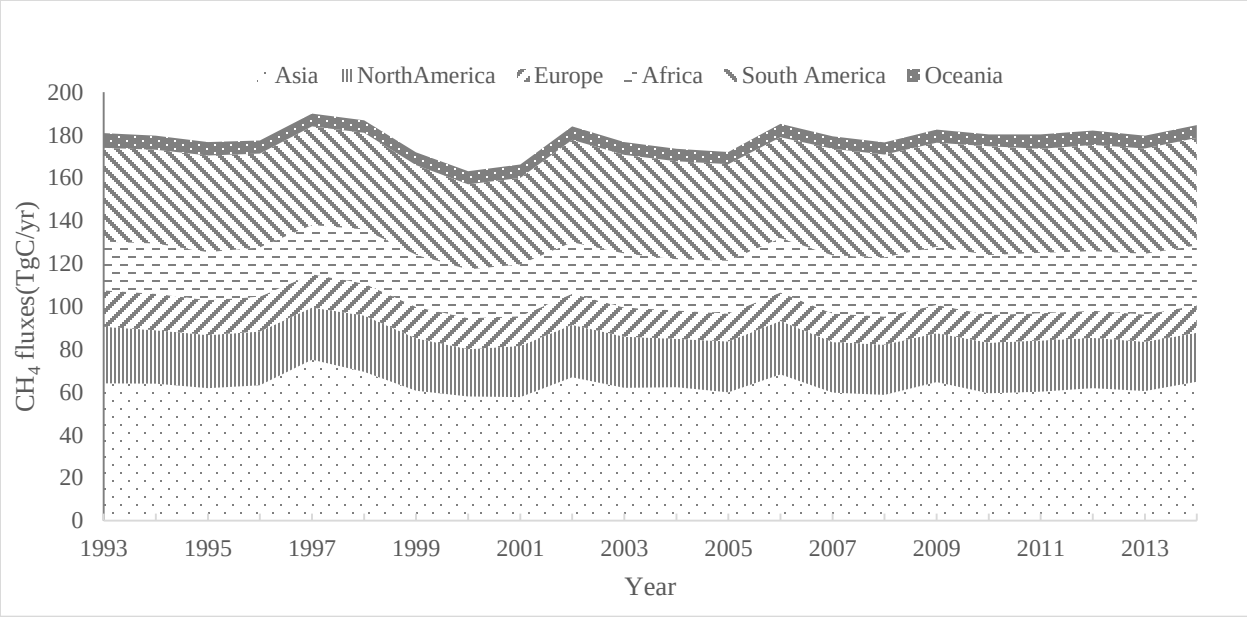

Figure 2.5 Temporal variation of total CH_4 fluxes from wetlands, rice fields, biomass burning, ruminants and upland soil at continental scale during 1993-2014

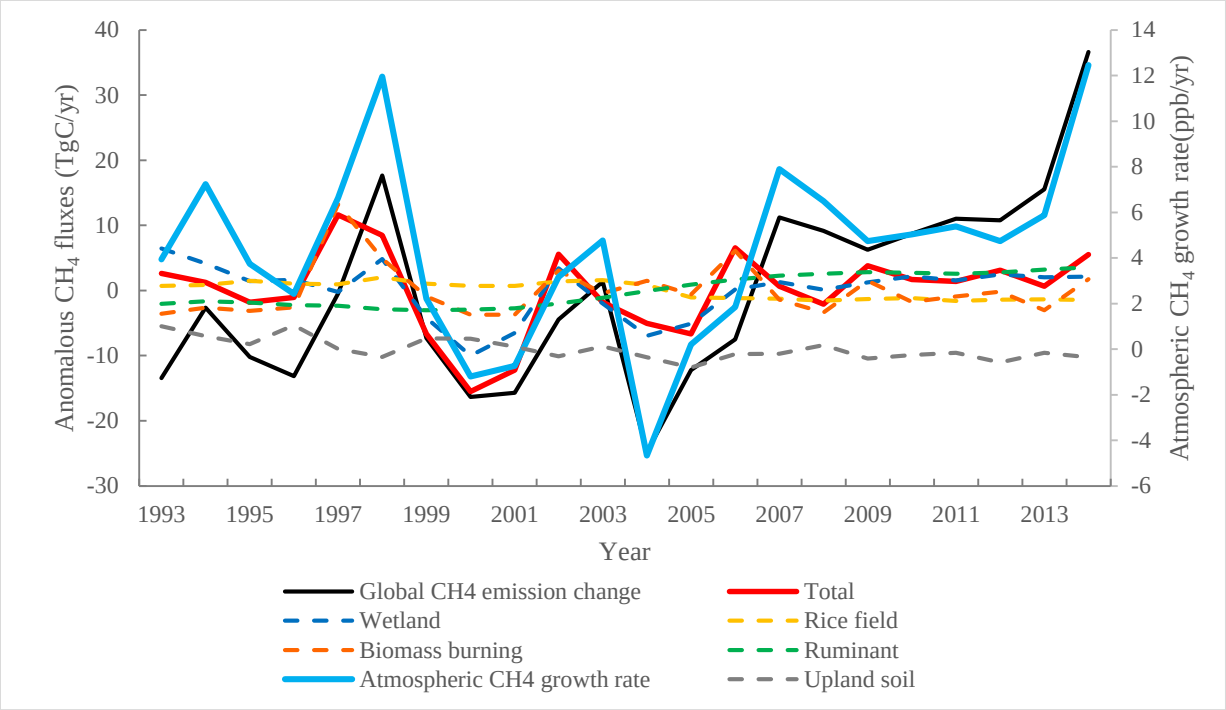

Figure 2.6 The comparison between atmospheric CH_4 growth rate (NOAA), Global CH_4 emission changes derived from one-box model, and estimated CH_4 anomalies from wetlands, rice fields, biomass burning, ruminants and upland soil

Note: the anomalous fluxes are determined by subtracting mean annual total fluxes from 1993-2014

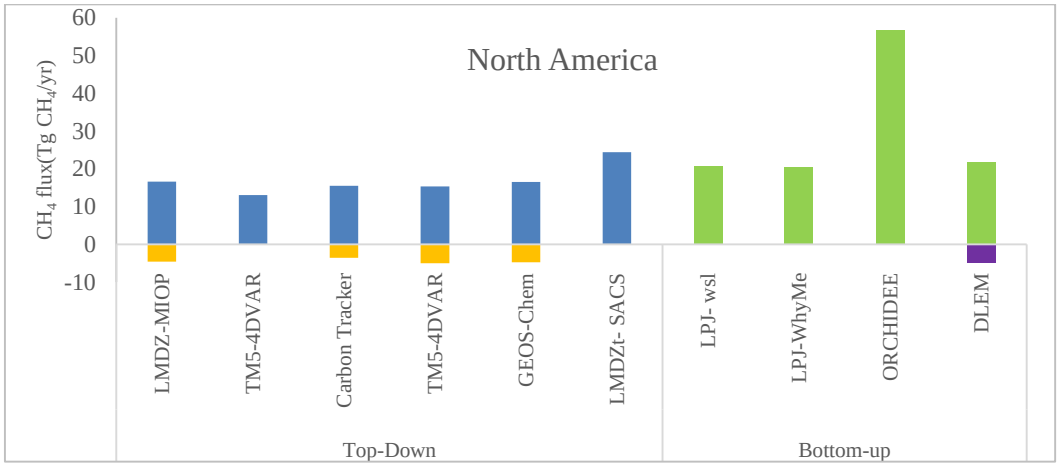
North America
CH4 flux(Tg CH4/yr)
60
50
40
30
20
10
0
-10
LMDZ-MIOP
TM5-4DVAR
Carbon Tracker
TM5-4DVAR
GEOS-Chem
LMDZt- SACS
LPJ- wsl
LPJ-WhyMe
ORCHIDEE
DLEM
Top-Down
Bottom-up

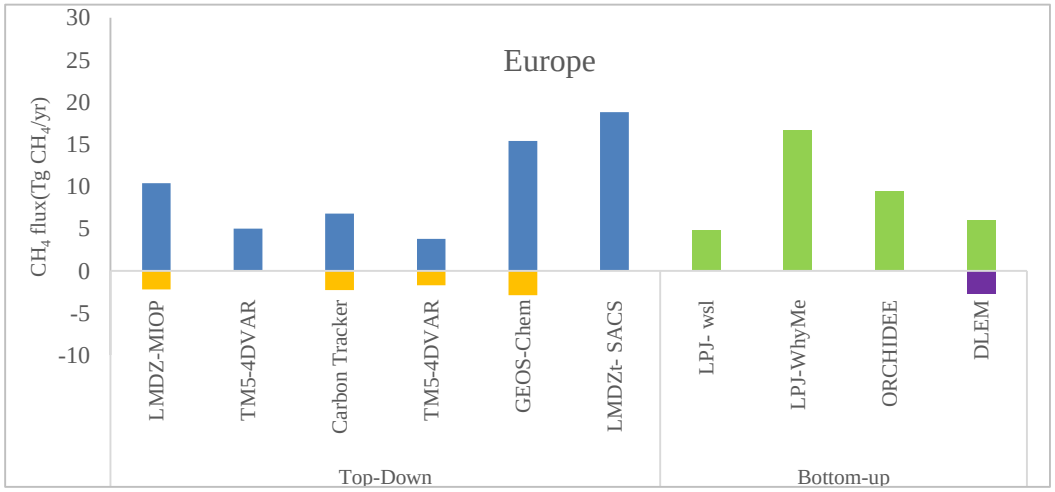
Europe
CH4 flux(Tg CH4/yr)
30
25
20
15
10
5
0
-5
-10
LMDZ-MIOP
TM5-4DVAR
Carbon Tracker
TM5-4DVAR
GEOS-Chem
LMDZt- SACS
LPJ- wsl
LPJ-WhyMe
ORCHIDEE
DLEM
Top-Down
Bottom-up

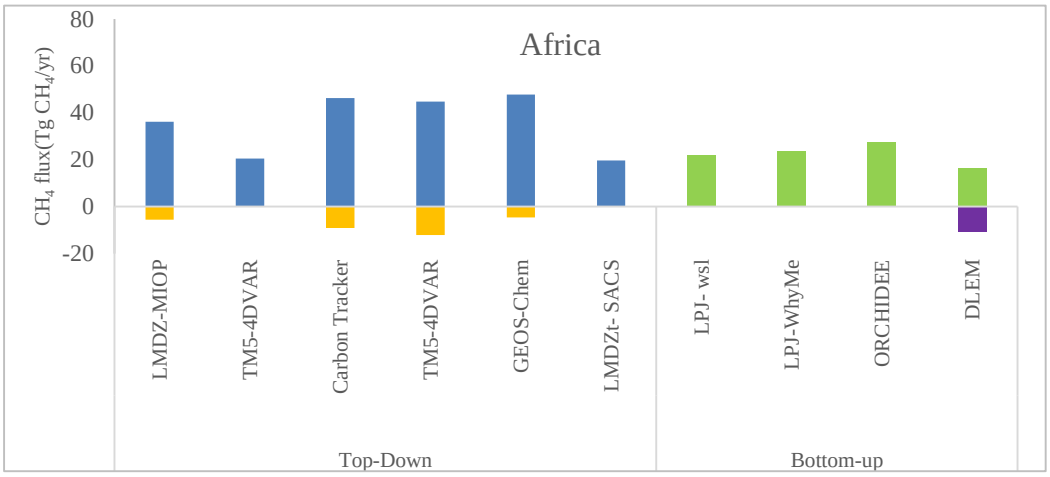
Africa
CH4 flux(Tg CH4/yr)
80
60
40
20
0
-20
LMDZ-MIOP
TM5-4DVAR
Carbon Tracker
TM5-4DVAR
GEOS-Chem
LMDZt- SACS
LPJ- wsl
LPJ-WhyMe
ORCHIDEE
DLEM
Top-Down
Bottom-up

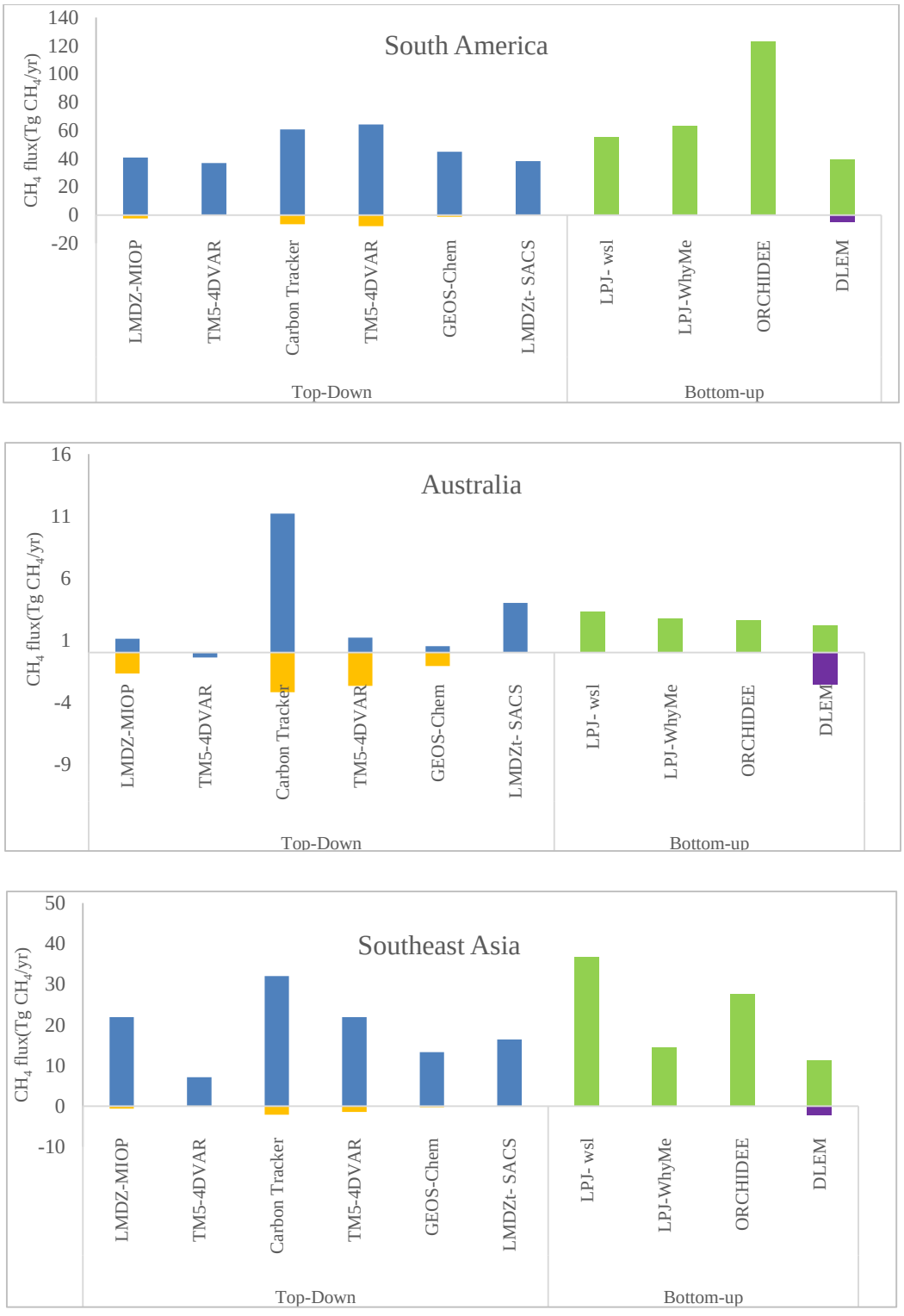

Figure 2.7 Comparison of the DLEM-estimated CH_4 fluxes with other studies

Notes: Blue and green column indicated the estimated CH_4 fluxes from wetland by using both top-down approach and bottom-up approach, respectively. Orange and purple column indicated the estimated CH_4 fluxes from soil by using both top-down approach and bottom-up approach, respectively.

Chapter 3

Methane Emissions from Global Rice Fields: Magnitude, Spatio-Temporal Patterns and Environmental Controls

3.1 Abstract

Given the importance of the potential positive feedback between methane (CH_4) emissions and climate change, it is critical to accurately estimate the magnitude and spatio-temporal patterns of CH_4 emissions from global rice fields and better understand the underlying determinants governing the emissions. Here, we used a coupled biogeochemical model in combination with satellite-derived contemporary inundation area to quantify the magnitude and spatio-temporal variation of CH_4 emissions from global rice fields and attribute the environmental controls of CH_4 emissions during 1901-2010. Our study estimated that CH_4 emissions from global rice fields varied from 18.3±0.1 Tg CH_4/yr (Avg. ± 1 std. dev.) under intermittent irrigation to 38.8±1.0 Tg CH_4/yr under continuous flooding in the 2000s, indicating that the magnitude of CH_4 emissions from global rice fields was largely dependent on different water schemes. Over the past 110 years, our simulated results showed that global CH_4 emissions from rice cultivation increased 85%. The expansion of rice fields was the dominant factor for the increasing trends of CH_4 emissions, followed by elevated CO_2 concentration, and nitrogen fertilizer use. On the contrary, climate had the negative effect on the cumulative CH_4 emissions for most of the years over the study period. Our results imply that CH_4 emissions from global rice fields could be reduced through implementation of optimized irrigation practices. Therefore,

the future magnitude of CH_4 emissions from rice fields will be determined by the human demand for rice production as well as the implementation of optimized water management practices.

3.2 Introduction

Methane (CH_4) emissions from rice cultivation have long been recognized as one of the dominant contributors to anthropogenic greenhouse gas emissions (Ciais *et al.*, 2014, Tian *et al.*, 2016a). Rice field, a unique human-dominated ecosystem, shares the fundamental set of controls as natural wetlands and meanwhile incorporates different agronomic practices, such as irrigation and fertilizer use (Bridgham *et al.*, 2013). The net CH_4 flux is determined by both the production from methanogens and the consumption from methanotrophs (Lee *et al.*, 2014, Tian *et al.*, 2010). Previous studies have shown that the CH_4 emissions from rice fields were influenced by farming types (irrigated, rainfed and/or deepwater) (Yan *et al.*, 2009), nitrogen fertilizer use (Banger *et al.*, 2012), organic input (Chen *et al.*, 2013, Yan *et al.*, 2009), and rice varieties (Zhang *et al.*, 2014). In the last 50 years, global rice harvest area increased by 40% due to rice expansion and intensification (Burney *et al.*, 2010, FAOSTAT, 2014), which has greatly increased CH_4 emissions. The rapid increase in CH_4 emissions is expected to continue in the near future to meet the increasing food demand (US-EPA, 2012). Therefore, it is vital to better understand the current magnitude and spatio-temporal patterns of global CH_4 emissions from rice fields.

Over the last three decades, substantial progress has been made in estimating the CH_4 emissions from rice fields globally; however, large discrepancies exist among various studies in both magnitude, ranging from 25.6 Tg CH_4/yr to 115 Tg CH_4/yr (Aselmann & Crutzen, 1989, Chen & Prinn, 2006, Frankenberg *et al.*, 2005, Yan *et al.*, 2009), and spatial distribution (Monfreda *et al.*, 2008, Xiao *et al.*, 2005) due to multiple environmental factors and complicated agricultural activities involved (Zhang *et al.*, 2011a, Zhang *et al.*, 2011b). Clearly, it is essential to quantify effects of those influencing factors on CH_4 emissions from rice fields and explore the underlying mechanisms.

Previous studies have illustrated the complicated environmental controls on CH_4 emissions. For example, global warming could increase the rate of root decay, which provides quantitatively important substrates for CH_4 production (Tokida *et al.*, 2011). On the other hand, rice is very vulnerable to high temperature and overheating and a few hours of exposure could cause complete sterility and poor milling quality (Laborte *et al.*, 2012), which may reduce carbon substrates for CH_4 emissions. Precipitation could influence the water availability of the rice fields, especially for the rainfed rice. The shortage of water could greatly reduce the CH_4 emissions. Elevated atmospheric CO_2 concentration may stimulate the CH_4 emissions by providing more methanogen-favored carbon substrate (Dijkstra *et al.*, 2012, van Groenigen *et al.*, 2011). The effects of nitrogen fertilizer use are complex and can either stimulate or inhibit the CH_4 emissions by influencing microbial activities (Banger *et al.*, 2012). Irrigation could change the water status of the soil, which further determines the oxygen availability of the soil and greatly affects the CH_4 producing, and oxidizing capability. Elevated ozone concentration could reduce the rice productivity, inhibit the microbial activities and suppress the belowground carbon processes, which together decrease the CH_4 emissions (Ren *et al.*, 2007, Zheng *et al.*, 2011). These environmental factors could individually and interactively affect the CH_4 processes. However, the response of CH_4 to changes in multiple environmental factors from rice fields has not yet been well investigated at the global scale.

Various approaches have been applied to estimate CH_4 emissions from rice fields. Inventory method provides regional-scale estimations of CH_4 emissions from rice fields based on country-specific (or county-specific if applied) statistical data of harvest area, emission factor and scaling factor (Chen *et al.*, 2013, Chen & Prinn, 2006, Yan *et al.*, 2009, Zhang *et al.*, 2014). In the top-down approach, atmospheric CH_4 measurements with prior information and transport

model are used to estimate the CH_4 emissions. However, both approaches have large limitations when estimating the CH_4 emissions from rice fields. For example, universal emission factors used in inventory methods over large areas without considering the environment heterogeneities, limit our ability to predict the feedback between climate change and rice CH_4 emissions. On the other hand, top-down approach is hard to differentiate multiple sources. It has been suggested that transport model itself could lead to 5% to 48% errors (Locatelli *et al.*, 2013). Meanwhile, reliable estimation of top-down approach may also be constrained by the prior information used, which is usually derived from either inventory estimation or bottom-up estimation (Bergamaschi *et al.*, 2007, Bloom *et al.*, 2010, Frankenberg *et al.*, 2005). Bottom-up approach, i.e., process-based models which consider multiple environmental factors, land surface heterogeneities, and major pathways of CH_4 processes (e.g., CH_4 production, CH_4 oxidation, and CH_4 transportation), provides spatially-explicit estimates of annual CH_4 emissions (Tian *et al.*, 2010). Meanwhile, it has the capability to quantify the relative contribution of driving factors, such as, atmospheric CO_2 concentration, climatic variability, nitrogen enrichment, and cropland management practices, which is vital for policy decisions on climate change mitigation (Bridgham *et al.*, 2013).

Globally, Southeast Asia dominates the CH_4 emissions from rice fields, due to the large rice area occupancy in this region (Yan *et al.*, 2009). China and India, as the most populous countries in the world, account for 20.0% and 28.5% of the global rice area, respectively (FAOSTAT, 2014). Approximately 90% of the rice fields are sufficiently irrigated in China, with high spatial-temporal variations in water regimes due to various irrigation strategies in recent decades (Chen *et al.*, 2013). Over 46% of rice cultivation area is irrigated in India (Banger *et al.*, 2015b, Jain *et al.*, 2000). Thus, up-to-date rice area information with accurate water management

information in those two countries could greatly improve our understanding of global estimation of rice emission.

In this study, we used the Dynamic Land Ecosystem Model version 2.0 (DLEM v2.0) (Tian *et al.*, 2015b) to quantify the effects of multiple environmental factors on the magnitude and spatio-temporal variation of CH_4 emissions from global rice fields during 1901-2010. The specific objectives of this study are (1) to estimate the magnitude of CH_4 emissions from global rice fields by applying different water schemes; (2) to investigate the spatial and temporal variation of CH_4 emissions from rice fields; (3) to quantify the relative contributions of multiple environmental factors to CH_4 emissions from rice fields; and (4) to discuss potential CH_4 mitigation strategies through water regime practices in the rice fields.

3.3 Materials and Methods

3.3.1 The Dynamic Land Ecosystem Model (DLEM)

In this study, we used the DLEM v2.0, which has the capability to simulate the carbon, water, and nitrogen fluxes and storages within the terrestrial ecosystem, and also the exchanges of greenhouse gases (CO_2, CH_4, and N_2O) between terrestrial ecosystems and the atmosphere. Five key components (biophysics, plant physiology, soil biogeochemistry, land use, disturbance and land management, and vegetation dynamics) are interconnected in the model. In brief, the biophysics component simulates the water and energy fluxes within the terrestrial ecosystems and their interactions with the environments. The plant physiology component simulates the key physiological processes, such as photosynthesis, respiration, allocation, and evapotranspiration. The soil biogeochemistry component simulates the processes of decomposition, nitrogen mineralization/immobilization, nitrification/denitrification, fermentation and some other major biogeochemical processes in the soil including CH_4 production/oxidation and related processes.

The land use, disturbance, and land management component simulates the impact of natural and human disturbance on the water and nutrient fluxes and storages in the land ecosystems. The DLEM is able to simulate the exchange of water, carbon and nitrogen fluxes for both natural and human-dominated ecosystems (such as major crop types, i.e., rice, wheat, soybean) at daily time step. In this study, we only focus on rice.

The DLEM simulation results have been extensively validated against a large number of field observations and measurements at the site level (Lu & Tian, 2013, Ren *et al.*, 2011, Tao *et al.*, 2013, Tian *et al.*, 2010, Tian *et al.*, 2011). The DLEM-estimated fluxes and storages of water, carbon and nutrients are also compared with the estimates from other approaches, such as statistical-based empirical modeling, top-down inversion or other process-based modeling approaches, at regional, continental and global scale (Pan *et al.*, 2014a, Pan *et al.*, 2014b, Tian *et al.*, 2015a, Tian *et al.*, 2015b, Yang *et al.*, 2014). The previous results indicated that the DLEM is able to realistically simulate the exchange of trace gases, such as CH_4, at different temporal and spatial scales.

3.3.2 Description of the Agricultural Module in the DLEM

The agricultural module of the DLEM model (DLEM-Ag) incorporates the influences of agronomic practices on crop growth and phenology and other biogeochemical processes (Ren *et al.*, 2012, Ren *et al.*, 2011, Tian *et al.*, 2012). The DLEM-Ag has the capability to estimate the crop productivity (net primary production-NPP) and crop yield. The DLEM-Ag estimated crop yield has been compared with census data at the provincial level and site-level observations in China (Ren *et al.*, 2012, Tian *et al.*, 2016b), India (Banger *et al.*, 2015a), Africa (Pan *et al.*, 2015) and other regions of the world (Pan *et al.*, 2014b). Previous studies suggested that the

DLEM could capture both the trend and magnitude of regional responses of crop production to global environmental changes (Tian *et al.*, 2016b).

The main crop categories in each grid were first identified according to the global crop geographic distribution map (Leff *et al.*, 2004), and were then refined based on FAOSTAT census data. The prescribed crop phenology was derived from large numbers of field observations and remote sensing data (i.e., Moderate Resolution Imaging Spectroradiometer leaf area index, MODIS LAI and Advanced Very High Resolution Radiometer, AVHRR), which encompassed the onset and development of foliage and also the dynamic of leaf loss (Ren *et al.*, 2012). Since Global 1 km MODIS LAI is only available after 2000, we assumed the phenology unchanged before 2000. To improve the accuracy of rice distribution in China and India, we further refined the data of land use/land cover and cropping systems by incorporating the data extracted from the Chinese Academy of Agricultural Sciences (http://www.caas.net.cn) and multi-temporal remote sensing images in China (Liu & Tian, 2010), and high-resolution remote sensing datasets from Resourcesat-1 with historical archives at district and state levels in India (Tian *et al.*, 2014).

In this study, the major agronomic management practices, including rotation, nitrogen fertilizer use, and irrigation were identified. We considered three major cropping systems, i.e., the single cropping system, double cropping system, and triple cropping system. The rotation types were identified by incorporating the phenological characteristics from multi-temporal remote sensing images (Yan *et al.*, 2005). Multi-temporal data refers to a series of temporal data derived from AVHRR. We used the 10-day composited NDVI (Normalized Difference Vegetation Index) from AVHRR. Based on 36 time-phase data within a year, we could extract the information for crop growth. We assumed that the cropping systems remain unchanged over

the study period. Nitrogen fertilizer use rates for China, India, and the United States were derived from county-level census data (Tian *et al.*, 2012; Tian *et al*., 2015; Banger *et al.*, 2015), while information in other regions were based on Food and Agriculture Organization (FAO) country-level statistical data (http://faostat3.fao.org/download/E/EF/E).

Different from previous studies, we designed three scenarios to depict the potential water management practices based on available data sets and a few assumptions, and to determine the impact of water management practices on the rice CH_4 emission. In the Scheme 1 (SC1), we used the dynamic inundation data derived from Global Inundation Extent from Multi-Satellite (GIEMS) observations to determine the water status in the rice fields (Prigent *et al.*, 2012). GIEMS provides the surface water extent and dynamics at monthly time-step during 1993-2007 with a spatial resolution of 0.5° × 0.5° longitude/latitude. Prior to 1993, we used the mean inundation extent derived from the seasonal variation of inundation dynamic for the 15 years (1993-2007). During the model simulation, once the grid cell was identified as rice fields, the inundation status would be checked against Prigent's data. If it was inundated, that grid cell would be irrigated until the soils reach inundation; or the CH_4 fluxes would be estimated based on the DLEM-simulated soil moisture status in that grid cell. More details about the representation of soil moisture in the DLEM could be found in the supplementary material. We considered SC1 as our best estimate because the dynamic inundation data was derived from multi-satellite observation and reflected the irrigation status in the real world to a large extent. In the Scheme 2 (SC2), we used the global data set of monthly irrigated and rainfed rice areas around the year 2000 (MIRCA2000) to determine the irrigation status in the rice fields for the whole study period (Portmann *et al.*, 2010). In the SC2, the grid cell with rice field would be checked whether it was irrigated or rainfed rice field against Portmann's data. If it was irrigated,

or rainfed and at the same time identified as inundation according to Prigent's data, we assumed its soil water content would reach saturation. Otherwise, the soil moisture status will be calculated based on local climate and soil properties in that grid cell. The application of both Prigent and Portmann's data was to improve the estimation accuracy of irrigation and inundation status from multiple data sources. In the Scheme 3 (SC3), the rice fields were assumed to continuously flood. Although the long-term (1901-2010) irrigation dataset is not available, the irrigation area could change along with the change in rice growing area. For instance, the mean inundation extent derived from dynamic inundation data does not change over time, but the rice growing area could vary year to year according to HYDE data (http://themasites.pbl.nl/tridion/en/themasites/hyde/landusedata/index-2.html). Thus the corresponding irrigation area, which needs to be identified as rice and meanwhile be inundated, could change over the time.

3.3.3 Description of the CH_4 Module in the DLEM

In the DLEM, the CH_4-related processes are assumed to occur only in the top 50 cm of soil (Tian *et al*., 2010). The DLEM only consider CH_4 produced from dissolved organic carbon (DOC), which is the byproduct of the decomposition of litterfall and soil organic matter, and allocation of gross primary production (GPP). Methane production, oxidation, and transportation from soil pore water to the atmosphere are involved in the calculation of CH_4 exchanges between the rice fields and the atmosphere. The net CH_4 flux between the atmosphere and soil is determined by the following equation:

$$F_{CH_4} = F_P - F_O + \Delta[CH_4]$$

where F_{CH_4} is the flux of CH_4 between soil and the atmosphere (g C m^{-2} d^{-1}); F_P is the CH_4 production (g C m^{-2} d^{-1}); F_O is the CH_4 oxidation (g C m^{-2} d^{-1}); $\Delta[CH_4]$ is the net CH_4 fluxes changed within the soil column.

The DLEM considers CH_4 production from DOC, which is a function of environmental factors including soil pH, temperature and soil moisture content (Fig. 1).

$$CH_{4_{prod}} = V_{prod,max} * \frac{[DOC]}{[DOC] + Km_{prod}} * f(T_{soil}) * f(pH) * f_{prod}(vwc)$$

where $V_{prod,max}$ is the maximum rate of CH_4 production (g C m^{-3} d^{-1}); [DOC] is the concentration of DOC (g C m^{-3}); Km_{prod} is the half-saturation coefficient of CH_4 production (g C m^{-3}); $f(T_{soil})$ is a multiplier that describes the effect of soil temperature on CH_4 production and oxidation; $f(pH)$ is a multiplier that describes the effect of soil pH on CH_4 production and oxidation; $f_{prod}(vwc)$ is a multiplier that describes the effect of soil moisture on CH_4 production and oxidation.

Three pathways are considered in the DLEM for CH_4 oxidation: (1) Atmospheric CH_4 oxidation; (2) CH_4 oxidation in the soil pore water; and (3) CH_4 oxidation during plant-mediated transport. In this model, ebullition, diffusion, and plant-mediated transport are considered as three pathways by which CH_4 can be transported from soil pore water to the atmosphere. More detailed information about the features of the CH_4 module in the DLEM could be found in Tian *et al.* (2010). CH_4 module in the DLEM has already been validated at regional scales, such as West Siberian Lowland and Sanjiang Plain (Bohn *et al.*, 2015, Song *et al.*, 2013), at country level, such as China (Ren *et al.*, 2011), and Canada (Miller *et al.*, 2014), at continental level, such as North America (Tian *et al.*, 2010), and at global level (Melton *et al.*, 2013, Tian *et al.*, 2015a, Wania *et al.*, 2013)**.**

3.3.4 Other Input Data

Several sets of geo-referenced and time series input data are compiled to drive the DLEM model, including (1) daily climate data (maximum, minimum, and mean air temperature, precipitation, relative humidity, and downward shortwave radiation); (2) atmospheric chemical components (atmospheric CO_2 concentration, AOT40 O_3 index and nitrogen deposition); (3) soil properties (soil texture, soil pH, and soil bulk density); (4) land use and land cover data; (5) agricultural management practices (irrigation, nitrogen fertilizer use, and rotation etc.) and other ancillary data, such as river network and topographic data. More specifically, daily climate variables during 1901-2010 were derived from CRUNCEP 6-hourly climate datasets (http://dods.extra.cea.fr/store/p529viov/cruncep/V4_1901_2012/readme.htm). Atmospheric CO_2 concentration data was obtained from a spline fit of the Law Dome before 1959 (http://cdiac.ornl.gov/ftp/trends/co2/lawdome.smoothed.yr20), and from NOAA (http://www.esrl.noaa.gov/gmd/ccgg/trends/global.html) during 1959-2010. Monthly atmospheric ozone concentration was represented by AOT 40 (Felzer *et al.*, 2005) and further interpolated to daily data (Ren *et al.*, 2007). Atmospheric nitrogen deposition data was obtained from North American Carbon Program Multi-scale Synthesis and Terrestrial Model Intercomparison Project (Wei *et al.*, 2014). The basic soil physical and chemical properties, such as soil texture, bulk density, soil pH etc., were obtained from Harmonized World Soil Database (HWSD) (Wieder *et al.*, 2014). Cropland distribution was derived from the 5-arc minute resolution HYDE v3.1 data and aggregated to half-degree (Goldewijk *et al.*, 2011). Inundation data from multi-satellite observations were obtained from global wetland extent and wetland CH_4 inter-comparison of models project (WETCHIMP) (Prigent *et al.*, 2012). Further details of other

input data could be found in the previous publications (Ren *et al.*, 2011, Tian *et al.*, 2015a, Xu *et al.*, 2010, Yang *et al.*, 2014).

3.3.5 Simulation Experiments Design

To determine the spatial and temporal patterns of CH_4 emissions and quantify the relative contribution of multiple environmental factors, we conducted ten simulations in total (Table 3.1). The model was first run to reach the equilibrium state and get the initial condition for the spin-up and transient simulations. In the equilibrium run, all the input data in 1900 was used to drive the model except climate data and inundation data. For climate data, we used long-term mean climate data during 1901-1930. For inundation data, we derived the seasonal variation patterns from 15-year (1993-2007) mean inundation extent. After the equilibrium run, the model was run another 900 years for the spin-up with de-trend climate data from 1901 to 2010. The spin-up was to smooth the transition from the equilibrium state to the transient run. The transient runs for all-combined simulation were to get the estimation of CH_4 fluxes by considering all the natural and anthropogenic changes during 1901-2010 ($S_{all\text{-}combined}$). We conducted six simulations to quantify the effects of individual environmental factors (S_{single}), such as climate, atmospheric chemistry, land cover change, and land management practices on the CH_4 fluxes. For example, for the experiment without climate considered, we let all other input data change with time except climatic data, which was kept at the level of 1901. Then the effect of climate on the CH_4 fluxes was determined by $S_{all\text{-}combined}$ versus $S_{single(climate)}$.

3.3.6 Model Evaluation against Field Observations at Site Level

The key parameters for the CH_4-related processes are derived from field observations (**Table 3.2**). In this study, we further evaluated the DLEM performance of the CH_4 emissions from rice fields at 31 observation sites (**Fig. 3.2-3.4; Table S3.1**). The comparisons of the

DLEM estimated CH_4 with site-level observations indicates that the DLEM can capture the daily or seasonal patterns of CH_4 emissions (**Fig. 3.2-3.4**). In general, the DLEM estimations showed a good agreement with the field observations (n=31; slope = 0.9021; R^2 = 0.9545; p <0.0001). The big differences of CH_4 emissions between the observations and the DLEM-estimations at PhilRice Central Experimental Station in Mayligaya during 1996 were probably caused by the commence use of organic amendments in that year at the experimental site. The addition of organic amendments could provide the rich substrate for the methanogens which greatly stimulate the CH_4 emissions in that year. Thus, the observed CH_4 emissions during the dry and wet season in 1996 were obviously higher than the other years. Compared with the dry season, the amount of CH_4 emissions during the wet season were much greater at PhilRice Central Experimental Station and the DLEM was able to capture the seasonal variation of CH_4 emissions. For the double rice cropping system, the DLEM estimated CH_4 emissions were comparable with the observations during the 5-year experiment in southeast China (Lu *et al.*, 2000).

3.4 Results

3.4.1 Multiple Environmental Changes in the Global Rice Field during 1901-2010

During 1901-2010, global rice fields increased at a rate of 0.43 Mha/yr and meanwhile experienced substantial environmental changes **(Fig. 3.5**). Atmospheric CO_2 concentration steadily increased from 296.4 ppm to 391.9 ppm. At the same time, both precipitation and temperature showed large inter-annual variations in overall significant increasing trends of 6.2 mm/decade and 0.075 °C/decade (p < 0.01). AOT40 increased rapidly since the 1950s, with the largest increase occurred in Asia. Rice fields received more amount of nitrogen through fertilizer use than deposition. The amount of nitrogen through atmospheric deposition was around 1/5 of

the amount of fertilizer use in the 2000s. Both nitrogen fertilizer use and deposition increased slowly before the 1960s and then enhanced dramatically afterward, at an overall increasing trend of 1 and 0.12 kg N/ha/year, respectively.

3.4.2 Temporal Changes in Global CH_4 Emissions

In this study, we quantified the CH_4 emissions from global rice fields during 1901-2010. For the SC1, we determined the inundation status in the rice fields based on multi-satellite observations, the estimated CH_4 emissions increased from 10.4±0.2 (Avg. ± 1 std. dev., same hereafter) Tg CH_4/yr in the 1900s to 19.2±1.9 Tg CH_4/yr in the 2000s with a significant increasing trend (0.1 Tg CH_4/yr, $p < 0.01$) **(Fig. 3.6**). The dynamic inundation data only covers 1993 to 2007, hence, the estimate of CH_4 emissions during this period was 20.5±1.4 Tg CH_4/yr. For the SC2, the DLEM estimated CH_4 emissions were 18.3±0.1 Tg CH_4/yr when soil moisture is determined by one-phase monthly irrigation/rainfed maps. For the SC3, we assumed that the rice fields were continuously flooded, and the DLEM estimated CH_4 emissions were 38.8±1.0 Tg CH_4/yr during the 2000s. Compared with the SC1 and the SC2, continuously flooding could double the CH_4 emissions from the global rice fields.

For the intra-annual variation, the DLEM estimation showed CH_4 emissions increased from early February and reached a peak emission during July to August, which is partly due to the larger area of rice planted and the high rates of CH_4 emissions during this time period, and then leveled off from September (**Fig. 3.7**). The seasonal contribution of the CH_4 emissions varied at different continents. In Asia, the estimated CH_4 emissions in spring, summer, autumn and winter contributed 22%, 38%, 25% and 15% of the annual emission, respectively. In North America, the CH_4 emissions in spring, summer, autumn and winter contributed 28%, 32%, 21% and 19% of the annual emission, respectively. The DLEM estimated CH_4 emissions during the

growing and non-growing season accounted for 76% and 24% of the annual emission, respectively.

3.4.3 Spatial Patterns of Global CH_4 Emissions

When investigating CH_4 emissions in the SC1 along the latitudinal gradient, our results showed that the estimated CH_4 emission from rice fields peaked (1 Tg CH_4/0.5 latitude) around 21°N-22°N and 23°N-24°N, mainly due to the distribution of large rice fields in subtropical and tropical Asia **(Fig. 3.8**). Further analysis suggested that tropical region (30°N-30°S) contributed 85% of the estimated global rice emission, followed by northern mid-latitude (30°N-60°N) and southern mid-latitude (30°S-60°S). From the continental perspective, Asia was the primary emitter, which contributed around 94% of the total rice emissions. Country-level analysis showed that India and China were two biggest contributors to the global rice emissions. DLEM estimated rice CH_4 emissions were around 4.99±0.36 Tg CH_4/yr in India, and 3.61±0.16 Tg CH_4/yr in China, which accounted for 24% and 18% of the estimated CH_4 emissions from global rice fields, respectively.

3.4.4 Relative Contributions of Multiple Environmental Factors

Through factorial simulation experiments, we further quantified the relative contribution of environmental factors to the cumulative rice emission. Our simulations indicated that land conversion from natural vegetation to rice fields played the dominant role in the increase of the rice emissions, which was around 49.44% (4.36 Tg CH_4/yr) of the total increase in global CH_4 emissions from rice fields (**Fig. 3.6**).

Elevated atmospheric CO_2 concentration induced an increase of 2.25 Tg CH_4/yr in estimated CH_4 emissions from the 1900s to the 2010s, which roughly accounts for 25.52% of the total increase in global CH_4 emissions from rice fields. Both nitrogen fertilizer use and nitrogen

deposition had a positive influence on the CH_4 emissions (**Fig. 3.5c, 3.5d**). In the 2000s, nitrogen fertilizer use and deposition increased the CH_4 emissions by 0.61 and 0.08 Tg CH_4/yr, respectively (**Fig. 3.6**). Elevated O_3 concentration had a minor influence on the global rice emissions over time compared with other factors. On the contrary, climate decreased the CH_4 emissions for most of the years over the study period. Particularly in the 2000s, the warmest decade compared with all the previous decades in the instrumental record (Stocker *et al.*, 2013), which induced a reduction of 0.27 Tg CH_4/yr in the CH_4 emission (**Fig. 3.6**).

3.5 Discussion

3.5.1 Comparison with Other Studies

Over the last two decades, due to the increasing number of field measurements, availability of remote sensing observations, improved understanding of mechanisms responsible for the CH_4 emissions in rice fields, the accuracy of CH_4 emissions from rice fields has been improved and the magnitude of the estimated rice emissions turned out a downward trend in previous studies (Chen & Prinn, 2006). In this study, the DLEM-estimated CH_4 emissions from rice fields were 18.3±0.1 ~ 38.8±1.0 Tg CH_4/yr during the 2000s based on different water schemes. The assumption of continuous flooding for the rice fields resulted in an overestimation of CH_4 emissions. Here we compared our results with the studies from recent ten years at both global and country levels. In general, the estimations from top-down approaches (44-115 Tg CH_4/yr) were much higher than those from both inventory (25.6-41.7 Tg CH_4/yr) and bottom-up (24.8-44.9 Tg CH_4/yr) approaches, which is likely associated with uncertainties in prior information of either rice fields distribution or the estimated CH_4 emissions being used in top-down studies (Bergamaschi *et al.*, 2007, Bloom *et al.*, 2010, Chen & Prinn, 2006) (**Table. S3.2**). To the best of our understanding, our study incorporated the "state-of-the-art" information from

multi-satellite observations-derived inundation data and inventory-based, monthly-irrigated rice area to determine the water status in the rice fields and narrow down the current estimation of CH_4 emissions from rice field. Most of the previous ecosystem models treated rice as one type of wetland and applied the same schemes to calculate the CH_4 fluxes. Due to the consideration of the non-inundation status in the rice fields, the estimated annual CH_4 emissions were largely reduced.

For the contemporary period (1990~2010), FAO (http://faostat3.fao.org/home/E), EDGAR (http://edgar.jrc.ec.europa.eu/part_CH4.php) and EPA (http://epa.gov/climatechange/ghgemissions/gases/ch4.html) provided time series estimation of CH_4 emissions from rice fields. The magnitudes of DLEM-simulated CH_4 emissions were comparable with other estimations; however, the inter-annual variation in CH_4 emissions showed divergence when compared with each other. For example, CH_4 emissions estimates based on FAO showed no significant inter-annual variation, while CH_4 emissions estimates from EDGAR decreased during 2000-2004, but then started to increase afterward until 2010 (37.6 Tg CH_4/yr) (**Fig. 3.9**). Variability in CH_4 emissions based on FAO which may be attributed to the similar trend in harvest area during the 2000s (FAOSTAT, 2014). It is worth noting that the increase of CH_4 emission after 2007 may also contribute to the resumption of atmospheric CH_4 concentration increase. For the DLEM-estimated CH_4 fluxes, the annual variation is determined by both the spatial and temporal variation of inundation status and environmental heterogeneity in the rice fields. In the SC1, DLEM-estimated CH_4 emissions showed large reduction after 2004, which is likely caused by climatic change **(Fig. 3.9**). Further analysis indicated that South and Southeast Asia contributed over 85% of the reduced CH_4 fluxes. At the country level, India and Indonesia played a major contribution to CH_4 emissions. Previous studies suggested that severe drought

happened in Northeast India during the summer monsoon in 2006 (Bergamaschi *et al.*, 2007), which may reduce the CH_4 emissions. In Indonesia, the monthly mean temperature in February and March during 2005-2007 was 0.73°C and 0.43°C lower than that during 1993-2004, and the mean temperature from October to March was 0.22°C lower during 2005-2007 compared with that during 1993-2004. In most areas of Indonesia, the rice planting season starts from October to March, with the highest rainfall from December to March. The lower temperature could reduce microbial activities, which might have contributed to the reduction of CH_4 emissions during 2005-2007.

The DLEM-simulated intra-annual variations in CH_4 fluxes showed consistent patterns with the column-averaged CH_4 mixing ratio from atmospheric inversion estimation (Bergamaschi *et al.*, 2007). The estimated CH_4 emissions during winter also contributed a small portion of the total amount emitted annually. At the global scale, the estimated CH_4 emissions during the non-growing season accounts for almost one-fifth of the annual emission, which is within the range estimated by Weller et al., (2016). In the United States and China, some of the rice fields during the non-growing season are still being flooded in order to provide habitat for waterfowl and migratory birds (Wood et al., 2010), which may lead to CH_4 emissions.

Most country-level analyses of CH_4 emissions from rice cultivation were inventory-based (**Table S3.2**). Previous estimation of rice emission in China ranged from 5.2 to 11.4 Tg CH_4/yr as estimated by inventory studies (Chen *et al.*, 2013, SNCCCC, 2012, Yan *et al.*, 2009, Zhang & Chen, 2014, Zhang *et al.*, 2014) and ranged from 4.1 to 7.5 Tg CH_4/yr as estimated by bottom-up approach (Kai *et al.*, 2010, Wang *et al.*, 2008, Zhang *et al.*, 2011a). The DLEM-estimated rice emissions were around 3.2~5.6 Tg CH_4/yr. The differences among studies were probably caused by various water regimes being used. During the last two decades, China has already improved

water management and fertilizer use in rice fields. Intermittent drainage together with other water management practices have been applied to a large portion of rice fields over China, and field observations also confirmed that water-saving management could largely reduce or even cease CH_4 emissions (Chen *et al.*, 2013). In India, 55% of rice fields were irrigated and the rest were rainfed (Bhatia *et al.*, 2013). By applying the Intergovernmental Panel on Climate Change (IPCC) 2006 guideline, estimated CH_4 emissions from rice cultivation in India were around 3.4 to 6.1 Tg CH_4/yr (Bhatia *et al.*, 2013, Garg *et al.*, 2011, Yan *et al.*, 2009). The DLEM simulated results showed an emission estimates of 4.99 Tg CH_4/yr, which is within the range (3.4-6.1Tg CH_4/yr), as estimated by IPCC (2006) guidelines for rice fields in India.

3.5.2 Climate Effects on CH_4 Emissions

Our simulated results showed that over the study period, climate variability/change had reduced CH_4 emissions from rice field. Both China and India experienced warming (Jain & Kumar, 2012, Li *et al.*, 2010), which changed the availability of soil moisture content and carbon substrate, and further affected the CH_4 emissions from rice fields (Laborte *et al.*, 2012, Tokida *et al.*, 2011). Precipitation is another key climatic factor which governed the CH_4 emissions, especially in Southeast Asia, such as Indonesia, Myanmar, and Thailand, where 40%, 79% and 35% of the rice area was under rainfed, respectively (Redfern *et al.*, 2012). The reduction in precipitation or shifting in timing and magnitude of rainfall event may cause crop failure, which could further reduce CH_4 emissions from the rice fields.

3.5.3 Effects of Land Use and Water Use on CH_4 Emissions

Land cover and land use change, including land conversion, irrigation, and nitrogen fertilizer use, had significant impacts on the CH_4 emissions. Our input data indicates that the rice cultivation area between the 1900s and the 2000s increased around 38%, which was partially

supported by the global rice harvest area derived from FAO and U. S. Department of Agriculture (USDA) from 1964 to 2010. The expansion of rice cultivation is the primary factor that led to an increase in rice CH_4 emission. Water management regimes, like different irrigation practices, could effectively mitigate CH_4 emissions, which are well documented in Asian countries (Corton *et al.*, 2000). Intermittent irrigation could reduce CH_4 emissions by 22-80% as compared with continuous flooding (Jain *et al.*, 2000, Lu *et al.*, 2000, Wang *et al.*, 2000, Wassmann *et al.*, 2000).

Previous study suggested that the improved water use efficiency and the rapid rise in chemical fertilizer use were the dominant contributor to the reduction in CH_4 emission between 1980 and 2005 (Kai *et al.*, 2011), which is partially inconsistent to our results. In Kai *et al.* (2011), they attributed the change of CH_4 fluxes since 1980 to the reduction of CH_4 emission from the rice field by assuming that there was no significant change in both wetland area in the northern hemisphere and CH_4 emission from global wetlands. However, Prigent's data revealed that the global inundation extent decreased dramatically, at the rate of 67,700 km^2/yr during Jan-1993 to mid-2000 (Prigent *et al.*, 2012). In addition, DLEM estimated CH_4 emission from wetland showed an overall decreasing trend from 1993 to 2007 (unpublished data), which was supported by the inversion model of atmospheric transport and chemistry (Bousquet *et al.*, 2006, Pison *et al.*, 2013). Meanwhile, Kai *et al.* (2011) suggested that the use of inorganic fertilizer could reduce the CH_4 emission in rice fields partly due to the displacement of organic amendments. However, in their empirical-based model, they just simply incorporated the mechanisms that the use of inorganic fertilizer decreased the CH_4 emission in rice fields without considering the organic amendments, ignoring complex effects of nitrogen fertilizer use on both CH_4 production and oxidation processes (Banger *et al.*, 2012). Liu [2009] demonstrated that in

the anaerobic agricultural system, CH_4 emissions increase by 0.008±0.004 kg/ha/yr per l kg N/ha/yr fertilizer use. Banger et al. [2012] analyzed 155 data pairs in rice fields and 64% of them showed CH_4 emissions increase in response to nitrogen fertilizer application. In our study, nitrogen fertilizer use could promote the crop production, which provided higher litter input, root biomass and root exudation for the carbon substrate of methanogens and stimulated the CH_4 production. At the same time, it could accelerate water transpiration in N-limited area, lowered soil water content given a certain amount of rainfall, and thus increased CH_4 oxidation while depressing its production (Lu & Tian, 2013). Our study agreed with Kai *et al.* (2011) that the improved water management could reduce the CH_4 emissions in rice field.

3.5.4 Effects of Other Atmospheric Chemistry Components

In our study, atmospheric CO_2 concentration enrichment has induced an increase of 2.25 Tg CH_4/yr in CH_4 emissions from global rice fields between the 1900s and the 2010s (**Fig. 3.6**). Elevated CO_2 could stimulate belowground carbon production, which may provide more substrate for methanogens activity (Allen *et al.*, 2003, Jackson *et al.*, 2009, Pregitzer *et al.*, 2008, Zak *et al.*, 2000). Field observation has confirmed that under free-air CO_2 enrichment (FACE) experiment, CH_4 production from the rice fields was significantly greater than that under ambient conditions (Inubushi *et al.*, 2003). Chen (2013) found the increasing trend of CH_4 emissions from the rice fields in China as a result of elevated atmospheric CO_2 concentration. Meta-data analysis for the effect of elevated CO_2 on CH_4 emissions revealed that CO_2 enrichment could stimulate CH_4 by 43.4% in the rice fields (van Groenigen *et al.*, 2011). Under the future climate scenarios, atmospheric CO_2 concentrations are expected to continuously increase, which may further stimulate the CH_4 emission in the rice fields (Stocker *et al.*, 2013).

During 1901-2010, global nitrogen deposition enhanced at an increasing rate of 0.12 kg N/ha/year. Nitrogen addition could promote crop growth and provide more carbon substrate for the microbial activity, which could further stimulate CH_4 emission. In the 2000s, nitrogen deposition increased the CH_4 emissions by 0.08 Tg CH_4/yr (**Fig. 3.6**). The level of tropospheric ozone as indicated by AOT40 has significantly increased especially after the 1990s in China and India (Ren *et al.*, 2007), which reduced the CH_4 emissions (Bhatia *et al.*, 2011, Zheng *et al.*, 2011). At a global level, however, this study showed that tropospheric ozone pollution had a minor influence on rice CH_4 emission compared with other factors.

3.5.5 Uncertainties and Future Research Need

Our estimation of CH_4 emissions from rice cultivation must be used with caution because of much uncertainty resulting from input data, model structure and parameters. Uncertainties may be resulted from the inaccurate spatial distribution of rice cultivation, and agronomic practices being applied. In this study, we have incorporated the map of global crop geographic distribution with regional agricultural census data derived from FAOSTAT along with the multiple rotation types to generate the distribution of rice fields, however, there are still discrepancies among various rice distribution maps due to the differences in geo-referenced resolution as well as the lack of information on rice cultivation over some regions of the world. In addition, we applied different irrigation schemes to determine the impact of irrigation on the CH_4 emission from global rice fields. In the SC1, we identified the inundation status of rice cultivation based on multi-satellite observation, which only covers the time period between 1993-2007. This may bring large uncertainties to the estimated CH_4 emission from other years. Besides, the satellite datasets may underestimate some small paddy field (few hectares) (Prigent *et al.*, 2007), which could result in the underestimation of CH_4 emission. The DLEM inexplicitly

addressed CH_4 emission associated with the crop residues through model parameterization. However, DLEM used time-invariant parameter to estimate the amount of crop residue returning to the field, which could introduce some uncertainties. More explicitly representation of such processes is needed to reduce the uncertainties.

Several additional issues have been identified for advancing our research in the future, including (1) improving spatial resolution of input data and sub-grid heterogeneity for driving the model, and (2) improving model representation of additional processes that regulate the CH_4 emission in rice field. Finer resolution data is needed for future model application at multiple spatial scales, which will serve to make more realistic assumptions based on conditions that are truly happening in the real world (Pan *et al.*, 2014a). In this study, all the datasets have a spatial resolution of 0.5° × 0.5° longitude/latitude. However, in reality, the water regimes might be highly variable at the local scale, such as field to field variation or variation within field. The current assumption of homogeneous water regimes applied in each individual grid needs to be improved by considering the sub-grid variability in water regimes.

In addition, the model representations of rice varieties and iron reduction/oxidation are needed to better estimate CH_4 emission in rice field. Rice variety is a key factor to regulate the CH_4 fluxes (Zhang *et al.*, 2014). Different types of rice could provide various amounts of root-derived carbon, and also differ in structures, which regulate the pathway to diffuse the oxygen flux to the soil and transport CH_4 to the atmosphere. At the same time, the improvement in rice varieties over time could contribute to the variation of CH_4 emission. For example, modern rice varieties often shorten vegetation periods and meanwhile may adapt to multiple environmental changes, such as extreme climate, which directly and indirectly regulate the total CH_4 emissions. Other critical factors, such as iron reduction/oxidation processes (Van Bodegom *et al.*, 2002),

were missing in the current version of the DLEM. These factors or local practices are very important in regulating the CH_4 emission, but have a large spatial and temporal variability, which are very difficult to collect at the large scale (Van Bodegom *et al.*, 2002). This limitation of data over a large scale makes it impossible to incorporate such information and processes into the model for a global level estimation at the current stage of study.

3.6 Conclusion

Given the importance of the CH_4 emissions from the global rice fields, it is vital to provide robust estimation before developing climate mitigation strategies. Rice fields serve about half of the world population. The production and management practices for the rice fields affect food security, water scarcity and the feedback to climate change. It can be anticipated that to meet the demand of boost population, rice cultivation area is expected to increase, which could result in more CH_4 emissions. Despite some remaining uncertainties, our process-based modeling study provides the state-of-the-art estimate on the magnitude and spatial-temporal variability of CH_4 emissions from global rice field. Our results suggest that CH_4 emissions from global rice field varied from 18.3±0.1 to 38.8±1.0 Tg CH_4/yr during the 2000s depending on different water management practices. The estimated CH_4 emission from the global rice field under continuous flooding could be reduced by more than 50% if intermittent irrigation would be applied. The optimized irrigation strategies could have potentials to attenuate the water scarcity, and meanwhile, reduce the CH_4 emissions. Thus, more work needs to be done to determine the optimum level of water content to simultaneously reduce CH_4 emissions as well as achieve sustainable rice production.

3.7 References

Allen LH, Albrecht SL, Colon-Guasp W, Covell SA, Baker JT, Pan DY, Boote KJ (2003) Methane emissions of rice increased by elevated carbon dioxide and temperature. Journal of Environmental Quality, **32**, 1978-1991.

Aselmann I, Crutzen PJ (1989) Global Distribution of Natural Fresh-Water Wetlands and Rice Paddies, Their Net Primary Productivity, Seasonality and Possible Methane Emissions. Journal of Atmospheric Chemistry, **8**, 307-358.

Banger K, Tian HQ, Lu CQ (2012) Do nitrogen fertilizers stimulate or inhibit methane emissions from rice fields? Global Change Biology, **18**, 3259-3267.

Banger K, Tian HQ, Tao B, Ren W, Pan SF, Dangal SRS, Yang J (2015a) Terrestrial net primary productivity in India during 1901–2010: contributions from multiple environmental changes. Climatic Change, **132**, 575-588.

Banger K, Tian HQ, Zhang BW, Lu CQ, Ren W, Tao B (2015b) Biosphere-atmosphere exchange of methane in India as influenced by multiple environmental changes during 1901-2010. Atmospheric Environment, 192-200.

Bergamaschi P, Frankenberg C, Meirink JF *et al.* (2007) Satellite chartography of atmospheric methane from SCIAMACHYon board ENVISAT: 2. Evaluation based on inverse model simulations. Journal of Geophysical Research-Atmospheres, **112**.

Bhatia A, Ghosh A, Kumar V, Tomer R, Singh SD, Pathak H (2011) Effect of elevated tropospheric ozone on methane and nitrous oxide emission from rice soil in north India. Agriculture Ecosystems & Environment, **144**, 21-28.

Bhatia A, Jain N, Pathak H (2013) Methane and nitrous oxide emissions from Indian rice paddies, agricultural soils and crop residue burning. Greenhouse Gases-Science and Technology, **3**, 196-211.

Bloom AA, Palmer PI, Fraser A, Reay DS, Frankenberg C (2010) Large-Scale Controls of Methanogenesis Inferred from Methane and Gravity Spaceborne Data. Science, **327**, 322-325.

Bohn TJ, Melton JR, Ito A *et al.* (2015) WETCHIMP-WSL: intercomparison of wetland methane emissions models over West Siberia. Biogeosciences, **12**, 3321-3349.

Bousquet P, Ciais P, Miller JB *et al.* (2006) Contribution of anthropogenic and natural sources to atmospheric methane variability. Nature, **443**, 439-443.

Bridgham SD, Cadillo-Quiroz H, Keller JK, Zhuang QL (2013) Methane emissions from wetlands: biogeochemical, microbial, and modeling perspectives from local to global scales. Global Change Biology, **19**, 1325-1346.

Burney JA, Davis SJ, Lobell DB (2010) Greenhouse gas mitigation by agricultural intensification. Proceedings of the National Academy of Sciences, **107**, 12052-12057.

Chen H, Zhu QA, Peng CH *et al.* (2013) Methane emissions from rice paddies natural wetlands, lakes in China: synthesis new estimate. Global Change Biology, **19**, 19-32.

Chen YH, Prinn RG (2006) Estimation of atmospheric methane emissions between 1996 and 2001 using a three-dimensional global chemical transport model. Journal of Geophysical Research-Atmospheres, **111**.

Ciais P, Sabine C, Bala G *et al.* (2014) Carbon and other biogeochemical cycles. In: *Climate Change 2013: The Physical Science Basis. Contribution of Working Group I to the Fifth*

Assessment Report of the Intergovernmental Panel on Climate Change. pp Page., Cambridge University Press.

Corton TM, Bajita JB, Grospe FS *et al.* (2000) Methane emission from irrigated and intensively managed rice fields in Central Luzon (Philippines). Nutrient Cycling in Agroecosystems, **58**, 37-53.

Dijkstra FA, Prior SA, Runion GB, Torbert HA, Tian H, Lu C, Venterea RT (2012) Effects of elevated carbon dioxide and increased temperature on methane and nitrous oxide fluxes: evidence from field experiments. Frontiers in Ecology and the Environment, **10**, 520-527.

Faostat (2014) FOOD AND AGRICULTURE ORGANIZATION OF THE UNITED NATIONS STATISTICS DIVISION.

Felzer B, Reilly J, Melillo J *et al.* (2005) Future effects of ozone on carbon sequestration and climate change policy using a global biogeochemical model. Climatic Change, **73**, 345-373.

Frankenberg C, Meirink JF, Van Weele M, Platt U, Wagner T (2005) Assessing methane emissions from global space-borne observations. Science, **308**, 1010-1014.

Garg A, Kankal B, Shukla PR (2011) Methane emissions in India: Sub-regional and sectoral trends. Atmospheric Environment, **45**, 4922-4929.

Goldewijk KK, Beusen A, Van Drecht G, De Vos M (2011) The HYDE 3.1 spatially explicit database of human-induced global land-use change over the past 12,000 years. Global Ecology and Biogeography, **20**, 73-86.

Inubushi K, Cheng WG, Aonuma S *et al.* (2003) Effects of free-air CO2 enrichment (FACE) on CH4 emission from a rice paddy field. Global Change Biology, **9**, 1458-1464.

Jackson RB, Cook CW, Pippen JS, Palmer SM (2009) Increased belowground biomass and soil CO2 fluxes after a decade of carbon dioxide enrichment in a warm-temperate forest. Ecology, **90**, 3352-3366.

Jain MC, Kumar S, Wassmann R *et al.* (2000) Methane emissions from irrigated rice fields in northern India (New Delhi). Nutrient Cycling in Agroecosystems, **58**, 75-83.

Jain SK, Kumar V (2012) Trend analysis of rainfall and temperature data for India. Current Science, **102**, 37-49.

Kai FM, Tyler SC, Randerson JT (2010) Modeling methane emissions from rice agriculture in China during 1961-2007. Journal of Integrative Environmental Sciences, **7**, 49-60.

Kai FM, Tyler SC, Randerson JT, Blake DR (2011) Reduced methane growth rate explained by decreased Northern Hemisphere microbial sources. Nature, **476**, 194-197.

Laborte A, Nelson A, Jagadish K, Aunario J, Sparks A, Ye C, Redoña E (2012) Rice feels the heat. International Rice Research Institute.

Lee HJ, Kim SY, Kim PJ, Madsen EL, Jeon CO (2014) Methane emission and dynamics of methanotrophic and methanogenic communities in a flooded rice field ecosystem. Fems Microbiology Ecology, **88**, 195-212.

Leff B, Ramankutty N, Foley JA (2004) Geographic distribution of major crops across the world. Global Biogeochemical Cycles, **18**.

Li QX, Dong WJ, Li W, Gao XR, Jones P, Kennedy J, Parker D (2010) Assessment of the uncertainties in temperature change in China during the last century. Chinese Science Bulletin, **55**, 1974-1982.

Liu ML, Tian HQ (2010) China's land cover and land use change from 1700 to 2005: Estimations from high-resolution satellite data and historical archives. Global Biogeochemical Cycles, **24**.

Locatelli R, Bousquet P, Chevallier F *et al.* (2013) Impact of transport model errors on the global and regional methane emissions estimated by inverse modelling. Atmospheric Chemistry and Physics, **13**, 9917-9937.

Lu CQ, Tian HQ (2013) Net greenhouse gas balance in response to nitrogen enrichment: perspectives from a coupled biogeochemical model. Global Change Biology, **19**, 571-588.

Lu WF, Chen W, Duan BW *et al.* (2000) Methane emissions and mitigation options in irrigated rice fields in southeast China. Nutrient Cycling in Agroecosystems, **58**, 65-73.

Melton JR, Wania R, Hodson EL *et al.* (2013) Present state of global wetland extent and wetland methane modelling: conclusions from a model inter-comparison project (WETCHIMP). Biogeosciences, **10**, 753-788.

Miller SM, Worthy DEJ, Michalak AM *et al.* (2014) Observational constraints on the distribution, seasonality, and environmental predictors of North American boreal methane emissions. Global Biogeochemical Cycles, **28**, 146-160.

Monfreda C, Ramankutty N, Foley JA (2008) Farming the planet: 2. Geographic distribution of crop areas, yields, physiological types, and net primary production in the year 2000. Global Biogeochemical Cycles, **22**.

Pan S, Dangal SR, Tao B, Yang J, Tian H (2015) Recent patterns of terrestrial net primary production in Africa influenced by multiple environmental changes. Ecosystem Health and Sustainability, **1**, 1-15.

Pan S, Tian H, Dangal SR *et al.* (2014a) Modeling and monitoring terrestrial primary production in a changing global environment: toward a multiscale synthesis of observation and simulation. Advances in Meteorology, **2014**.

Pan SF, Tian HQ, Dangal SRS *et al.* (2014b) Complex Spatiotemporal Responses of Global Terrestrial Primary Production to Climate Change and Increasing Atmospheric CO2 in the 21st Century. Plos One, **9**.

Pison I, Ringeval B, Bousquet P, Prigent C, Papa F (2013) Stable atmospheric methane in the 2000s: key-role of emissions from natural wetlands. Atmospheric Chemistry and Physics, **13**, 11609-11623.

Portmann FT, Siebert S, Doll P (2010) MIRCA2000-Global monthly irrigated and rainfed crop areas around the year 2000: A new high-resolution data set for agricultural and hydrological modeling. Global Biogeochemical Cycles, **24**.

Pregitzer KS, Burton AJ, King JS, Zak DR (2008) Soil respiration, root biomass, and root turnover following long-term exposure of northern forests to elevated atmospheric CO2 and tropospheric O3. New Phytologist, **180**, 153-161.

Prigent C, Papa F, Aires F, Jimenez C, Rossow WB, Matthews E (2012) Changes in land surface water dynamics since the 1990s and relation to population pressure. Geophysical Research Letters, **39**.

Prigent C, Papa F, Aires F, Rossow W, Matthews E (2007) Global inundation dynamics inferred from multiple satellite observations, 1993–2000. Journal of Geophysical Research: Atmospheres, **112**.

Redfern SK, Azzu N, Binamira JS (2012) Rice in Southeast Asia: facing risks and vulnerabilities to respond to climate change. Building resilience for adaptation to climate change in the agriculture sector, **23**, 295.

Ren W, Tian HQ, Liu ML *et al.* (2007) Effects of tropospheric ozone pollution on net primary productivity and carbon storage in terrestrial ecosystems of China. Journal of Geophysical Research-Atmospheres, **112**.

Ren W, Tian HQ, Tao B, Huang Y, Pan SF (2012) China's crop productivity and soil carbon storage as influenced by multifactor global change. Global Change Biology, **18**, 2945-2957.

Ren W, Tian HQ, Xu XF *et al.* (2011) Spatial and temporal patterns of CO2 and CH4 fluxes in China's croplands in response to multifactor environmental changes. Tellus Series B-Chemical and Physical Meteorology, **63**, 222-240.

Sncccc (2012) Second National Communication on Climate Change of The People's Republic of China.

Song CC, Wang LL, Tian HQ *et al.* (2013) Effect of continued nitrogen enrichment on greenhouse gas emissions from a wetland ecosystem in the Sanjiang Plain, Northeast China: A 5 year nitrogen addition experiment. Journal of Geophysical Research: Biogeosciences, **118**, 741-751.

Stocker TF, Qin D, Plattner GK *et al.* (2013) IPCC, 2013: climate change 2013: the physical science basis. Contribution of working group I to the fifth assessment report of the intergovernmental panel on climate change.

Tao B, Tian HQ, Chen GS *et al.* (2013) Terrestrial carbon balance in tropical Asia: Contribution from cropland expansion and land management. Global and Planetary Change, **100**, 85-98.

Tian HQ, Banger K, Bo T, Dadhwal VK (2014) History of land use in India during 1880-2010: Large-scale land transformations reconstructed from satellite data and historical archives. Global and Planetary Change, **121**, 78-88.

Tian HQ, Chen GS, Lu CQ *et al.* (2015a) Global methane and nitrous oxide emissions from terrestrial ecosystems due to multiple environmental changes. Ecosystem Health and Sustainability, **1**, art4.

Tian HQ, Lu CQ, Ciais P *et al.* (2016a) The terrestrial biosphere as a net source of greenhouse gases to the atmosphere. Nature, **531**, 225-228.

Tian HQ, Lu CQ, Melillo J *et al.* (2012) Food benefit and climate warming potential of nitrogen fertilizer uses in China. Environmental Research Letters, **7**.

Tian HQ, Ren W, Tao B *et al.* (2016b) Climate extremes and ozone pollution: a growing threat to China's food security. Ecosystem Health and Sustainability, **2**.

Tian HQ, Xu XF, Liu ML, Ren W, Zhang C, Chen GS, Lu CQ (2010) Spatial and temporal patterns of CH4 and N2O fluxes in terrestrial ecosystems of North America during 1979-2008: application of a global biogeochemistry model. Biogeosciences, **7**, 2673-2694.

Tian HQ, Xu XF, Lu CQ *et al.* (2011) Net exchanges of CO2, CH4, and N2O between China's terrestrial ecosystems and the atmosphere and their contributions to global climate warming. Journal of Geophysical Research-Biogeosciences, **116**.

Tian HQ, Yang QC, Najjar RG, Ren W, Friedrichs MaM, Hopkinson CS, Pan SF (2015b) Anthropogenic and climatic influences on carbon fluxes from eastern North America to

the Atlantic Ocean: A process-based modeling study. Journal of Geophysical Research: Biogeosciences, **120**, 757-772.

Tokida T, Adachi M, Cheng WG *et al.* (2011) Methane and soil CO2 production from current-season photosynthates in a rice paddy exposed to elevated CO2 concentration and soil temperature. Global Change Biology, **17**, 3327-3337.

Us-Epa (2012) Global Anthropogenic Non-CO2 Greenhouse Gas Emissions: 1990 - 2030.

Van Bodegom PM, Verburg PH, Van Der Gon D, Hugo AC (2002) Upscaling methane emissions from rice paddies: problems and possibilities. Global Biogeochemical Cycles, **16**.

Van Groenigen KJ, Osenberg CW, Hungate BA (2011) Increased soil emissions of potent greenhouse gases under increased atmospheric CO2. Nature, **475**, 214-U121.

Wang P, Wei L, Du X, Zhang W, Huang Y, Sun W, Liu W (2008) Simulating changes of methane emission from rice paddies of China, 1990~2000. Geo-Information Science, **10**, 573-577.

Wang ZY, Xu YC, Li Z *et al.* (2000) A four-year record of methane emissions from irrigated rice fields in the Beijing region of China. Nutrient Cycling in Agroecosystems, **58**, 55-63.

Wania R, Melton JR, Hodson EL *et al.* (2013) Present state of global wetland extent and wetland methane modelling: methodology of a model inter-comparison project (WETCHIMP). Geoscientific Model Development, **6**, 617-641.

Wassmann R, Buendia L, Lantin R *et al.* (2000) Mechanisms of crop management impact on methane emissions from rice fields in Los Baños, Philippines. Nutrient Cycling in Agroecosystems, **58**, 107-119.

Wei Y, Liu S, Huntzinger DN *et al.* (2014) The North American Carbon Program Multi-scale Synthesis and Terrestrial Model Intercomparison Project - Part 2: Environmental driver data. Geoscientific Model Development, **7**, 2875-2893.

Wieder WR, Boehnert J, Bonan GB, Langseth M (2014) Regridded Harmonized World Soil Database v1.2. Data set. Available on-line [http://daac.ornl.gov] from Oak Ridge National Laboratory Distributed Active Archive Center, Oak Ridge, Tennessee, USA.

Xiao XM, Boles S, Liu JY *et al.* (2005) Mapping paddy rice agriculture in southern China using multi-temporal MODIS images. Remote Sensing of Environment, **95**, 480-492.

Xu XF, Tian HQ, Zhang C *et al.* (2010) Attribution of spatial and temporal variations in terrestrial methane flux over North America. Biogeosciences, **7**, 3637-3655.

Yan HM, Cao MK, Liu JY, Zhuang DF, Guo JK, Liu ML (2005) Characterizing spatial patterns of multiple cropping system in China from multi-temporal remote sensing images. Transactions of the CSAE, **21**, 85-90.

Yan XY, Akiyama H, Yagi K, Akimoto H (2009) Global estimations of the inventory and mitigation potential of methane emissions from rice cultivation conducted using the 2006 Intergovernmental Panel on Climate Change Guidelines. Global Biogeochemical Cycles, **23**.

Yang QC, Tian HQ, Li X *et al.* (2014) Spatiotemporal patterns of evapotranspiration along the North American east coast as influenced by multiple environmental changes. Ecohydrology, **8**, 714-725.

Zak DR, Pregitzer KS, King JS, Holmes WE (2000) Elevated atmospheric CO2, fine roots and the response of soil microorganisms: a review and hypothesis. New Phytologist, **147**, 201-222.

Zhang B, Chen GQ (2014) China's CH4 and CO2 emissions: Bottom-up estimation and comparative analysis. Ecological Indicators, **47**, 112-122.

Zhang W, Yu YQ, Huang Y, Li TT, Wang P (2011a) Modeling methane emissions from irrigated rice cultivation in China from 1960 to 2050. Global Change Biology, **17**, 3511-3523.

Zhang W, Zhang Q, Huang Y, Li TT, Bian JY, Han PF (2014) Uncertainties in estimating regional methane emissions from rice paddies due to data scarcity in the modeling approach. Geoscientific Model Development, **7**, 1211-1224.

Zhang Y, Wang YY, Su SL, Li CS (2011b) Quantifying methane emissions from rice paddies in Northeast China by integrating remote sensing mapping with a biogeochemical model. Biogeosciences, **8**, 1225-1235.

Zheng FX, Wang XK, Lu F *et al.* (2011) Effects of elevated ozone concentration on methane emission from a rice paddy in Yangtze River Delta, China. Global Change Biology, **17**, 898-910.

Table 3.1. Experimental Design

	Climate (CLM)	CO_2	Ozone (O_3)	Nitrogen deposition (Ndep)	LCLUC			
					Land conversion	Nitrogen fertilizer (Nfer)	Irrigation	Other practices
Initial Simulation	Averaged (1901-1930)	1900	1900	1900	1900	1900	Averaged GIEMS (1993-2007)	1900
All-combined (SC1)	1901-2010	1901-2010	1901-2010	1901-2010	1901-2010	1901-2010	GIEMS (1993-2007)	1901-2010
All-combined (SC2)	1901-2010	1901-2010	1901-2010	1901-2010	1901-2010	1901-2010	MIRCA2000	1901-2010
All-combined (SC3)	1901-2010	1901-2010	1901-2010	1901-2010	1901-2010	1901-2010	Continuously flooding	1901-2010
Without CLM	Averaged (1901-1930)	1901-2010	1901-2010	1901-2010	1901-2010	1901-2010	GIEMS (1993-2007)	1901-2010
Without CO_2	1901-2010	1900	1901-2010	1901-2010	1901-2010	1901-2010	GIEMS (1993-2007)	1901-2010
Without O_3	1901-2010	1901-2010	1900	1901-2010	1901-2010	1901-2010	GIEMS (1993-2007)	1901-2010
Without Ndep	1901-2010	1901-2010	1901-2010	1900	1901-2010	1901-2010	GIEMS (1993-2007)	1901-2010
Without LC	1901-2010	1901-2010	1901-2010	1901-2010	1900	1901-2010	GIEMS (1993-2007)	1901-2010
Without Nfer	1901-2010	1901-2010	1901-2010	1901-2010	1901-2010	1900	GIEMS (1993-2007)	1901-2010

Notes: CLM, CO_2, O_3, LC, Ndep, and Nfer are abbreviations for climate, atmospheric CO_2 concentration, atmospheric O_3 concentration, land cover change, N deposition, and N fertilization, respectively. The time period indicates that driver data (e.g. climatic data, atmospheric chemistry data, etc.) are being used in those periods. In all-combined simulation, the averaged inundation datasets during 1993-2007 was used to represent the inundation extent of rice field before 1993.

Table 3.2 The major parameters for simulating the CH_4 emission from rice field in the DLEM

Parameter	Value	Observed Range	Location	Reference
Maximum rate of CH_4 production ($gC/m^3/d$)	0.65	0.51-1.82	China	(Chen *et al.*, 1993, Wassmann *et al.*, 1993)
		0.65-0.73	India	(Mitra *et al.*, 1999)
		0.64-1.14	Indonesia	(Nugroho *et al.*, 1994)
		0.28-0.59	Japan	(Yagi & Minami, 1990)
		0.43-1.16	Thailand	(Yagi & Minami, 1990)
		0.64-0.85	USA	(Lindau *et al.*, 1991, Sass *et al.*, 1992)
Half-saturation coefficient of CH_4 production (gC/m^3)	2	1.68-9.8		(Law *et al.*, 1993, Lokshina *et al.*, 2001)
Maximum rate of CH_4 oxidation ($gC/m^3/d$)	0.2	0.18		(Wang *et al.*, 1997)
Half-saturation coefficient of CH_4 oxidation (gC/m^3)	10	4.8-81.1	India	(Dubey, 2003, Dubey *et al.*, 2002)

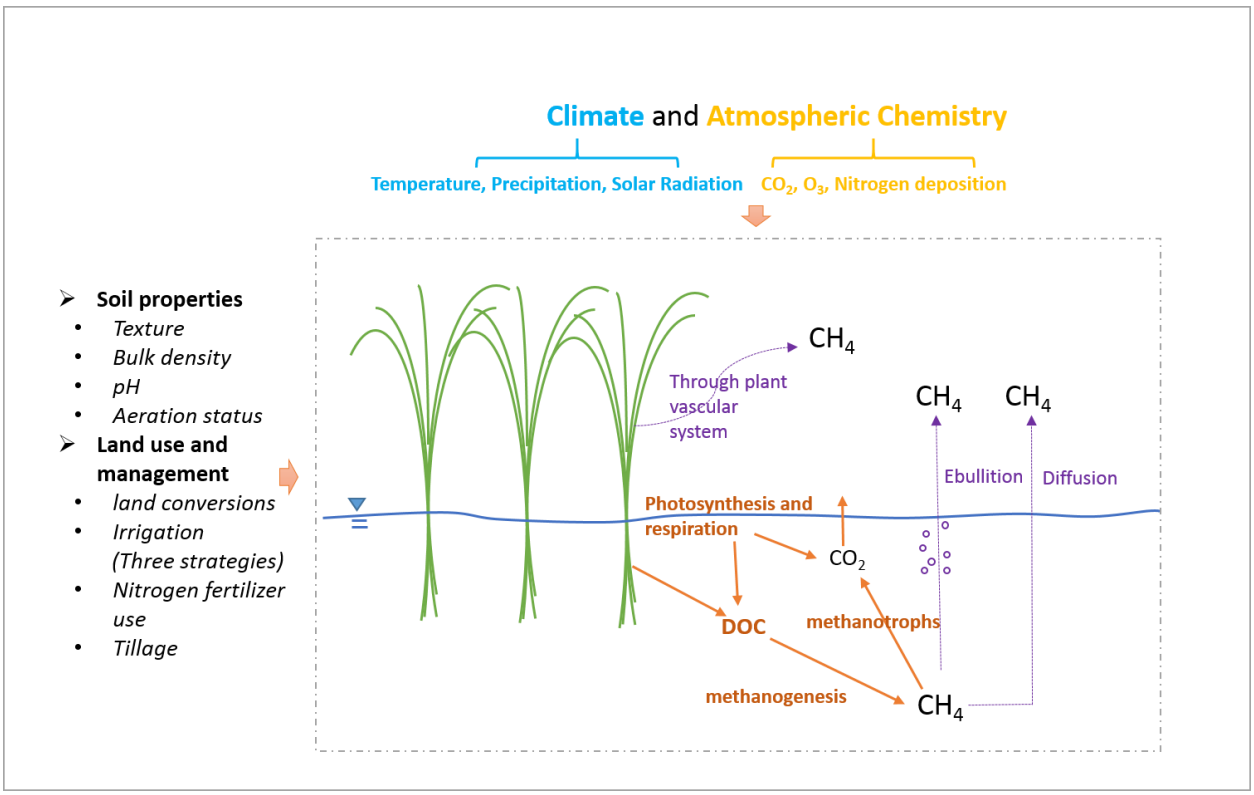

Figure 3.1 Framework of key biological processes controlling CH_4 fluxes in rice fields, including direct and indirect drivers

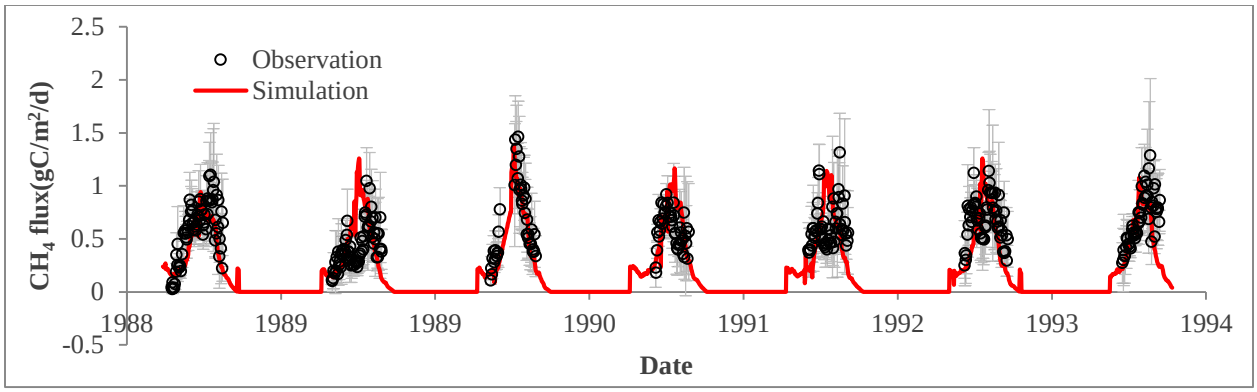

Figure 3.2 Evaluation of DLEM-estimated daily CH_4 emissions against observed data at Tuzu, Sichuan, China

Note: n=365, Modeled = 0.8475 * Observed, R^2 = 2878, $p < 0.0001$ [*Khalil et al.*, 1998]

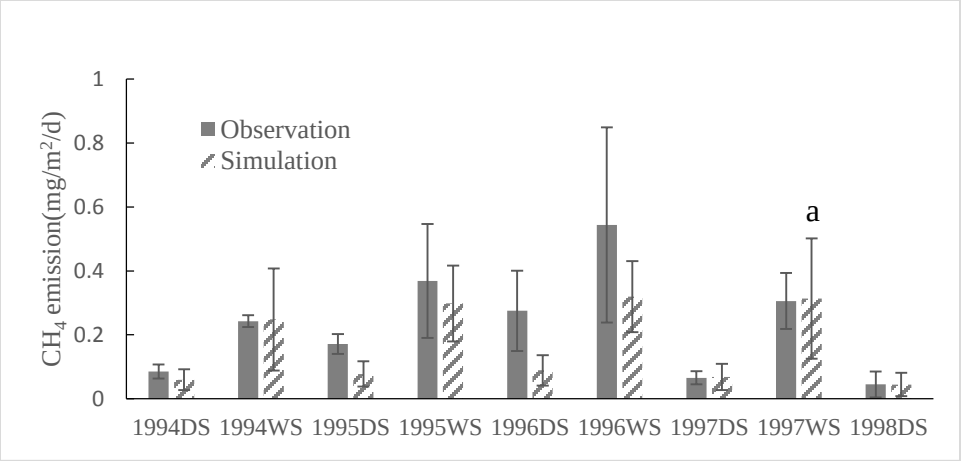

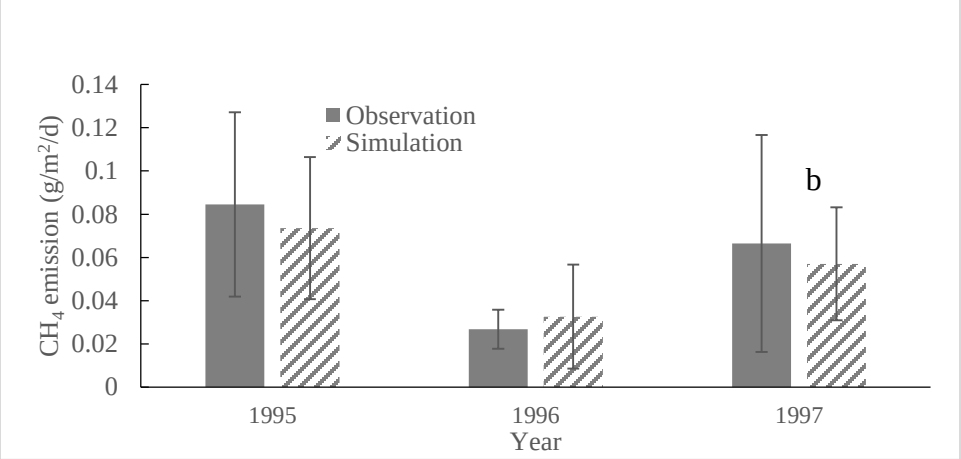

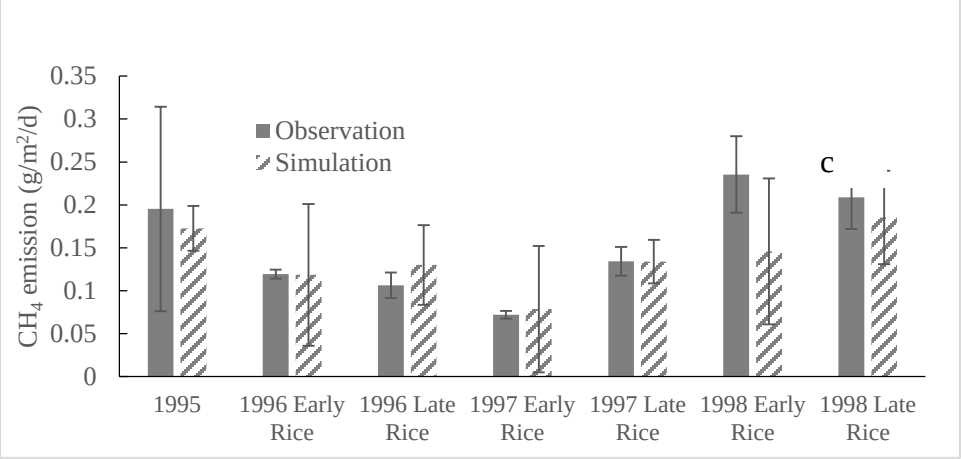

Figure 3.3 Evaluation of DLEM-estimated seasonal CH_4 emissions against observed data at multiple sites

Note: (a) CH_4 emissions at PhilRice Central Experiment Station in Maligaya, Muñoz, Nueva Ecija, Philippines (15.6725°N, 120.8906°E) [*Corton et al.*, 2000] (DS and WS are abbreviations for dry season and wet season); (b) CH_4 emissions at the experimental farm of the Institute of Crop Breeding and Cultivation, Beijing, China (39.9611°N, 116.3681°E) [*Wang et al.*, 2000]; (c) CH_4 emissions at the experimental farm of the China National Rice Research Institute in Hangzhou, China (30.2700°N, 120.1597°E) [*Lu et al.*, 2000].

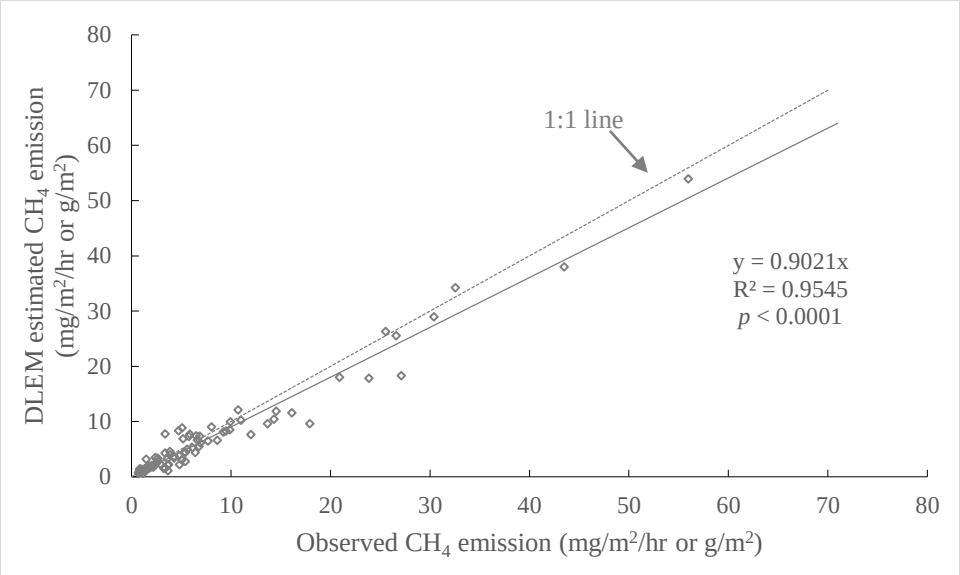

Figure 3.4 Comparison of DLEM-estimated CH_4 emissions from rice field with observed data at 28 sites

Note: n = 31, Modeled = 0.9021 * Observed, $R^2 = 0.9545$, $p < 0.0001$ (More detailed information could be found in Table S1). The error bars indicate the standard deviation.

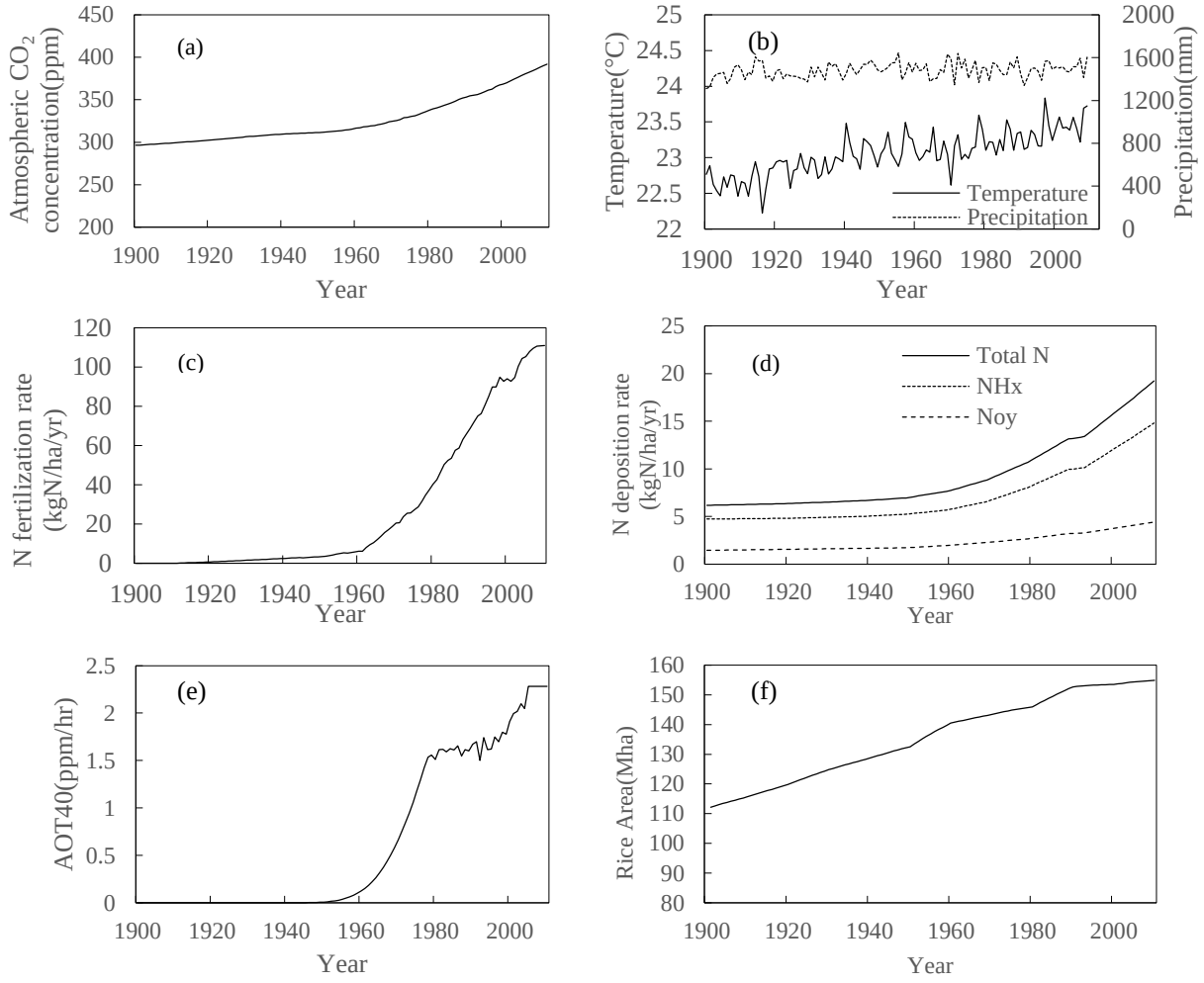

Figure 3.5 Multiple environmental changes over global rice fields. (a). annual atmospheric CO_2 concentration; (b). annual mean temperature and precipitation; (c). Nitrogen fertilizer use; (d). Nitrogen deposition; (e). AOT40 (Note: AOT40 is a cumulative O_3 index, the accumulated hourly O_3 dose over a threshold of 40 ppb in ppb per hour); (f). Rice area.

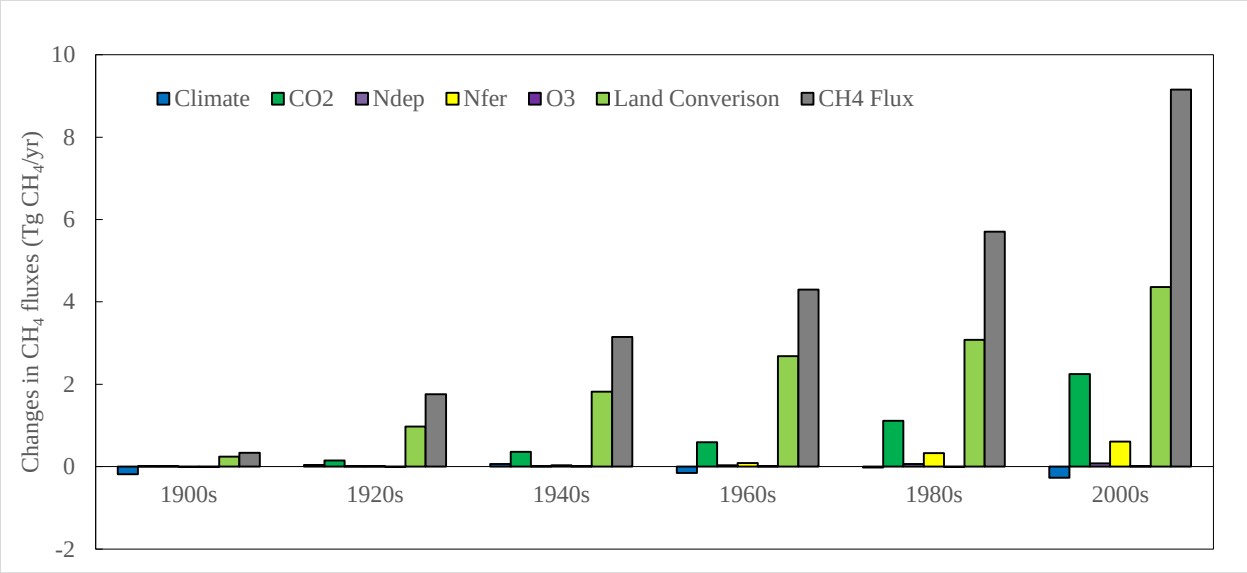

Figure 3.6 Relative contributions of land conversion, O_3, nitrogen fertilizer use, nitrogen deposition, atmospheric CO_2 concentration and climate to decadal changes in CH_4 fluxes from global rice fields during 1901-2010.

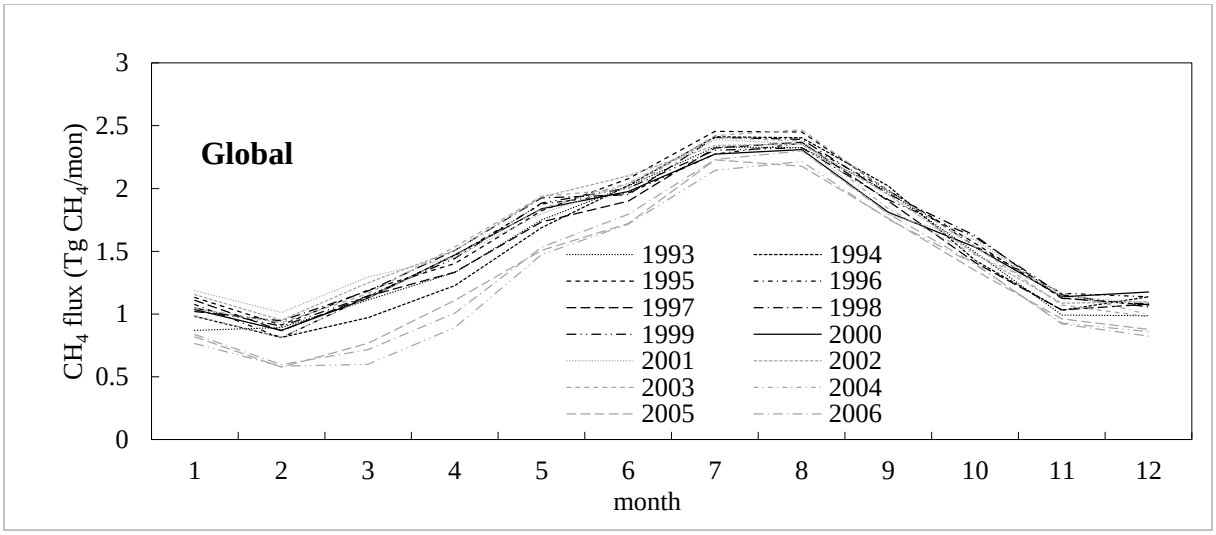

Figure 3.7 Simulated monthly CH_4 emissions for the time period 1993–2007 (Tg CH_4/mon)

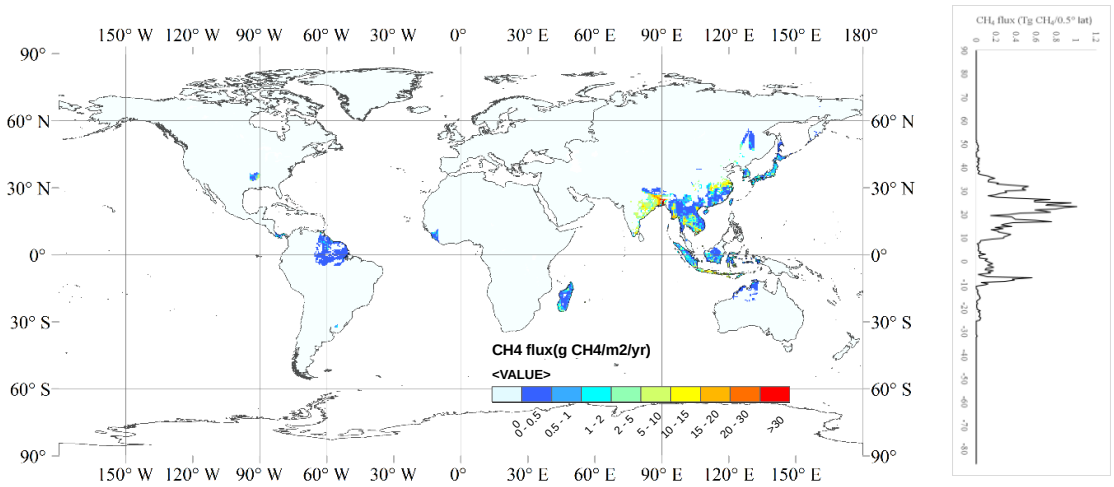

Figure 3.8 Spatial distribution of estimated mean annual CH_4 emissions (1993-2007) from global rice field

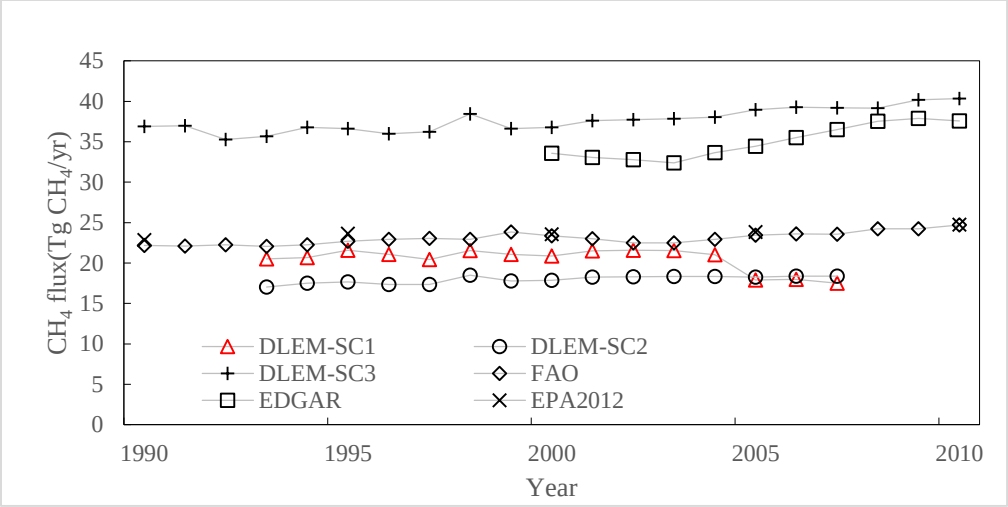

Figure 3.9 Comparison of temporal variation in estimated CH_4 emissions from global rice fields among three scenarios of water regime scheme (DLEM-SC1, DLEM-SC2 and DLEM-SC3) and three previous estimates (FAO, EDGAR and EPA2012)

3.8 Supporting Information for Chapter 3

Table S3.1 Comparison of DLEM-estimated CH_4 emission from rice field with observed data

Location	country	Water regimes	Observation ($g/m^2/hr$)	DLEM estimation ($g/m^2/hr$)	Reference
Ahmedabad, Gujarat	India	CF	12.00	7.65	(Gupta *et al.*, 1994)
IARI, New Delhi	India	CF	2.06	2.11	(Debnath *et al.*, 1996)
IARI, New Delhi	India	CF	1.55	1.51	(Jain *et al.*, 2000)
IARI, New Delhi	India	CF	1.00	1.41	(Jain *et al.*, 2000)
IARI, New Delhi	India	CF	0.83	1.45	(Jain *et al.*, 2000)
IARI, New Delhi	India	II	1.35	1.50	(Jain *et al.*, 2000)
IARI, New Delhi	India	CF	0.97	0.90	(Ghosh *et al.*, 2003)
IARI, New Delhi	India	CF	1.17	1.12	(Ghosh *et al.*, 2003)
IARI, New Delhi	India	CF	1.13	0.63	(Pathak *et al.*, 2003)
IARI, New Delhi	India	II	0.70	0.58	(Pathak *et al.*, 2003)
Varanasi	India	CF	3.59	3.28	(Singh *et al.*, 1996)
Varanasi	India	CF	6.40	4.39	(Singh *et al.*, 1996)
Varanasi	India	CF	5.38*	4.40*	(Singh *et al.*, 1999)
Cuttack, Orissa	India	CF	14.53*	11.85*	(Satpathy *et al.*, 1998)
Cuttack, Orissa	India	CF	9.49	8.31	(Bharati *et al.*, 2000)
Cuttack, Orissa	India	CF	1.64	1.80	(Adhya *et al.*, 2000)
Cuttack, Orissa	India	CF	6.09	5.28	(Adhya *et al.*, 2000)
CRRI, Cuttack	India	CF	2.38	2.29	(Mohanty *et al.*, 2001)
AAU,Jorhat, Assam	India	Unknown	1.57*	1.42*	(Bharati *et al.*, 2000)
Chongqing	China	CF	23.85*	17.82*	(Cai *et al.*, 2000)
Chongqing	China	CF	43.50	38.00	(Cai *et al.*, 2000)
Chongqing	China	CF	6.91	6.16	(Cai *et al.*, 2003)
Chongqing	China	CF	55.97	53.96	(Cai *et al.*, 2003)
Taoyuan, Hunan	China	CF	32.55	34.26	(Wassmann *et al.*, 1993)
Taoyuan, Hunan	China	CF	6.50	7.39	(Wassmann *et al.*, 1993)
Taoyuan, Hunan	China	CF	14.30	10.44	(Wassmann *et al.*, 1993)
Taoyuan, Hunan	China	CF	6.83	7.35	(Wassmann *et al.*, 1996)
Taoyuan, Hunan	China	CF	11.00	10.23	(Wassmann *et al.*, 1996)
Guangzhou	China	CF	5.83	7.68	(Tao, 1998)
Changsha, Hunan	China	II	9.86	8.49	(Cai *et al.*, 2000)
Changsha, Hunan	China	II	9.93	9.95	(Cai *et al.*, 2000)
Changsha, Hunan	China	II	13.66	9.64	(Cai *et al.*, 2000)
Changsha, Hunan	China	II	17.91	9.59	(Cai *et al.*, 2000)
Wuhan	China	CF	8.03	9.03	(Lin *et al.*, 2000)
Wuhan	China	CF	10.70	12.08	(Lin *et al.*, 2000)
Fenqiu, Henan	China	II	0.71	0.78	(Cai *et al.*, 2000)
Beijing	China	II	0.79	1.16	(Wang *et al.*, 2000a)
Beijing	China	II	1.11*	1.08*	(Wang *et al.*, 2000a)
Yintan, Jiangxi	China	II	20.89*	18.00*	(Cai *et al.*, 2000)
Yintan, Jiangxi	China	II	27.10	18.29	(Cai *et al.*, 2000)
Yancheng, Jiangsu	China	CF	1.83	1.61	(Xu *et al.*, 2004)
Hangzhou	China	II	9.22	8.13	(Lu *et al.*, 2000)
Hangzhou	China	II	2.90	2.32	(Lu *et al.*, 2000)
Hangzhou	China	II	3.62	2.13	(Lu *et al.*, 2000)

Hangzhou	China	II	4.83	2.23	(Lu *et al.*, 2000)
Suzhou, Jiangsu	China	II	4.26	3.68	(Cai *et al.*, 2000)
Shenyang	China	CF	3.40	1.58	(Chen *et al.*, 1995)
Xinlicheng, Liaoning	China	II	0.71	0.68	(Yan *et al.*, 2000)
Wanchang, Liaoning	China	CF	16.10	11.60	(Yan *et al.*, 2000)
Kyoto	Japan	II	26.60	25.57	(Matsumoto *et al.*, 2002)
Kyoto	Japan	II	25.55	26.33	(Matsumoto *et al.*, 2002)
Kyoto	Japan	II	30.40	28.95	(Matsumoto *et al.*, 2002)
Ryugasaki, Ibraki	Japan	II	4.78	3.83	(Yagi & Minami, 1990)
Ryugasaki, Ibraki	Japan	CF	3.84	4.00	(Yagi *et al.*, 1996)
Ryugasaki, Ibraki	Japan	CF	2.64	3.34	(Yagi *et al.*, 1996)
Mito, Ibaraki	Japan	II	2.36	3.49	(Yagi & Minami, 1990)
Yamagata	Japan	II	2.51	2.48	(Kumagai *et al.*, 2000)
Yamagata	Japan	II	3.72	2.20	(Kumagai *et al.*, 2000)
Yamagata	Japan	II	1.46	3.20	(Kumagai *et al.*, 2000)
Kamikawa, Hokkaido	Japan	CF	3.22	1.51	(Goto *et al.*, 2004)
Kamikawa, Hokkaido	Japan	CF	1.91	1.73	(Goto *et al.*, 2004)
Kamikawa, Hokkaido	Japan	CF	1.77	1.99	(Goto *et al.*, 2004)
Kamikawa, Hokkaido	Japan	CF	1.42	1.60	(Goto *et al.*, 2004)
Kamikawa, Hokkaido	Japan	CF	2.19	1.73	(Goto *et al.*, 2004)
Shizukuishi, Iwate	Japan	CF	5.41	2.80	(Inubushi *et al.*, 2003a)
Shizukuishi, Iwate	Japan	CF	2.67	2.82	(Inubushi *et al.*, 2003a)
Jakenan, Cental Java	Indonesia	CF	6.63	6.64	(Setyanto *et al.*, 2000)
Jakenan, Cental Java	Indonesia	CF	5.58	4.96	(Setyanto *et al.*, 2000)
Jakenan, Cental Java	Indonesia	CF	6.79	5.49	(Setyanto *et al.*, 2000)
Jakenan, Cental Java	Indonesia	CF	5.17	6.89	(Setyanto *et al.*, 2000)
Jakenan, Cental Java	Indonesia	CF	3.38	7.77	(Setyanto *et al.*, 2000)
Jakenan, Cental Java	Indonesia	CF	7.67	6.51	(Setyanto *et al.*, 2000)
Jakenan, Cental Java	Indonesia	CF	5.75	7.31	(Setyanto *et al.*, 2000)
Jakenan, Cental Java	Indonesia	CF	8.63	6.59	(Setyanto *et al.*, 2000)
Jakenan, Cental Java	Indonesia	CF	5.08	8.86	(Setyanto *et al.*, 2000)
Jakenan, Cental Java	Indonesia	CF	4.71	8.35	(Setyanto *et al.*, 2000)
Jakenan, Cental Java	Indonesia	CF	4.27	3.40	(Setyanto *et al.*, 2000)
Jakenan, Cental Java	Indonesia	CF	5.04	3.05	(Setyanto *et al.*, 2000)
Tabanan, Bali	Indonesia	CF	5.33	4.54	(Subadiyasa *et al.*, 1997)
Gianyar, Bali	Indonesia	CF	3.37	4.30	(Subadiyasa *et al.*, 1997)
Ratchaburi	Thailand	CF	3.84	4.60	(Jermsawatdipong *et al.*, 1994)
Prachinburi	Thailand	Unknown	3.65	1.13	(Chareonsilp *et al.*, 2000)
Prachinburi	Thailand	Unknown	1.19	1.15	(Chareonsilp *et al.*, 2000)
Prachinburi	Thailand	Unknown	1.46	1.15	(Chareonsilp *et al.*, 2000)
Prachinburi	Thailand	Unknown	1.33	1.21	(Chareonsilp *et al.*, 2000)

Note: * denotes that the unit of the CH_4 emission is g/m^2. ($n = 31$, $R^2 = 0.9545$, $p < 0.0001$). CF indicates continuous flooding. II indicates intermittent irrigation.

Table S3.2 Comparison of CH_4 fluxes from the rice field from multiple sources

	CH_4 fluxes (Tg CH_4/yr)			
Region	This study	Other studies	Method	Sources
Global	20.45	25.6-41.7	Inventory	(Yan *et al.*, 2009)
		24.8-44.9	Process-based modeling	(Ito & Inatomi, 2012, Spahni *et al.*, 2011)
		44-115	Top down approach	(Bergamaschi *et al.*, 2007, Bloom *et al.*, 2010, Chen & Prinn, 2006, Spahni *et al.*, 2011)
Asia				
China	3.61	5.2-11.4	Inventory	(Chen & Prinn, 2006, FAOSTAT, 2014, SNCCCC, 2012, Yan *et al.*, 2009, Zhang & Chen, 2014, Zhang *et al.*, 2014)
		4.1-7.5	Process-based modeling	(Kai *et al.*, 2010, Wang *et al.*, 2008b, Zhang *et al.*, 2011a)
India	4.99	3.4-6.1	Inventory	(Bhatia *et al.*, 2013, FAOSTAT, 2014, Garg *et al.*, 2011, Yan *et al.*, 2009)
Indonesia	2.68	1.7-2.5	Inventory	(FAOSTAT, 2014, Yan *et al.*, 2009)
Myanmar	1.31	1-1.2	Inventory	(FAOSTAT, 2014, Yan *et al.*, 2009)
Thailand	1.54	1.1-1.6	Inventory	(FAOSTAT, 2014, Yan *et al.*, 2009)

Representation of Environmental Controls on the CH_4 Fluxes in the DLEM

The DLEM assumes that the CH_4 production and oxidation is a function of soil pH, soil moisture, and temperature (Cao *et al.*, 1995, Huang *et al.*, 1998, Zhuang *et al.*, 2004). Most previous studies suggested that CH_4 production and oxidation mostly occurred when pH ranges from 5 to 9 (Amaral *et al.*, 1998, Sorokin *et al.*, 2000). Thus, the DLEM assumed that the CH_4 production and oxidation won't happen when soil pH < 4 or pH > 10, which is different from Zhuang et al. (2004) and Cao et al. (1995).

$$f(pH) = \begin{cases} 0 & pH \leq 4.0 \; or \; pH \geq 10.0 \\ \frac{1.02}{1+1{,}000{,}000*e^{(-2.5*pH)}} & 4.0 < pH < 7.0 \\ \frac{1.02}{1+1{,}000{,}000*e^{(-2.5*(14.0-pH))}} & 7.0 < pH < 10.0 \end{cases},$$

where pH is the pH value of the soil profile.

The effect of temperature on CH_4 processes ($f(T)$) was described by Q_{10} response curve, the similar method as used by Huang et al. (1998). We assumed that Q_{10} = 2.5 (Song *et al.*, 2009).

$$f(T) = \begin{cases} 0.0 & T < -5 \\ Q_{10}{}^{\frac{T-30}{10}} & 30 > T \geq -5 \\ 1 & T \geq 30 \end{cases}$$

where Q_{10} is a scalar for the temperature sensitivity; T is the temperature of soil or air.

We assumed that the CH_4 processes only happen in the top 50cm. The effect of CH_4 production and CH_4 oxidation could be described through the following equation.

$$f_{prod}(vwc) = \begin{cases} 0 & vwc \leq vwc_{fc} \\ (\frac{vwc - vwc_{fc}}{vwc_{sat} - vwc_{fc}})^2 * 0.368 * e^{\left(\frac{vwc - vwc_{fc}}{vwc_{sat} - vwc_{fc}}\right)} & vwc_{fc} < vwc < vwc_{sat} \\ 1 & vwc \geq vwc_{sat} \end{cases}$$

$$f_{oxid}(vwc) = 1 - f_{prod}(vwc)$$

where vwc is the volumetric water content of the top soil layer; vwc_{fc} is the field capacity and vwc_{sat} is the saturated water content.

Representation of Hydrological Processes in the DLEM

The DLEM considers the hydrological processes in the top 3 m of the soil surface, and is discretized into ten layers of which the thicknesses (Δz_i) from top to bottom are 0.1 m, 0.1 m, 0.1 m, 0.2 m, 0.2 m, 0.2 m, 0.3 m, 0.4 m, 0.4 m, 1 m, respectively. The hydraulic conductivity and the soil matric potential is affected by soil physical properties, such as moisture content and soil texture. The saturated hydraulic is determined by the sand content of the soil (Cosby *et al.*, 1984). The DLEM assumes that if the effective porosity of either layer is less than the impermeable liquid water content or if the volumetric liquid water content of layer i is less than 0.001, then there is no flow.

The soil matric potential (mm) is defined as

$$\Psi_i = \Psi_{sat,i}\left(\frac{\theta_{liq,i}}{\theta_{sat,i}}\right)^{-B_i} \geq -1 \times 10^8 \qquad 0.01 \leq \frac{\theta_{liq,i}}{\theta_{sat,i}} \leq 1$$

Where $\theta_{sat,i}$ is the volume water content at saturation, $\Psi_{sat,i}$ is the saturated soil matric potential, $\theta_{liq,i}$ is the liquid water content of of layer i

where the saturated soil matric potential is

$$\Psi_{sat,i} = -10 \times 10^{1.88-0.0131(\%sand)}$$

Precipitation is either intercepted by the canopy or falls to the ground as throughfall. The soil evaporation is calculated by using Penman-Monteith equation, and then further regulated by soil moisture status.

Surface runoff consists of overland flow due to saturation excess (Dunne runoff) and infiltration excess (Hortonian runoff). Soil water flux for soil layer i can be approximated through Darcy's law.

Soil water flux q (mm/s) for soil layer i can be approximated as

$$q_i = -k\left[z_{h,i}\right]\left[\frac{(\Psi_i - \Psi_{i+1}) + (z_{i+1} - z_i)}{(z_{i+1} - z_i)}\right]$$

where $k\left[z_{h,i}\right]$ is the hydraulic conductivity at the depth of the interface of two adjacent layer ($z_{h,i}$), and z_i is the node depth of layer i, Ψ_i is the soil matric potential (mm).

Applying the law of mass conservation for each soil layer, the soil water content in each soil layer is calculated as,

$$\frac{\partial \theta_{liq}}{\partial t} = (-q_{i-1} + q_i - Eroot_i)/\nabla z$$

where $Eroot_i$ is the water absorbed by roots, q_{i-1} and q_i are the water flux cross the soil layer's upper and lower boundary. For the first soil layer, q_{i-1} is the upper boundary condition, and set to be infiltration rate. For the tenth soil layer, q_i is the lower boundary condition, and equal to the recharge rate between soil column and groundwater. Similar to the method used in CLM (Oleson *et al.*, 2004), the change of water content ($\nabla\theta_{liq}$) is solved according to a tridiagonal equation set. Drainage (q_{drain}) is calculated according to SIMTOP scheme (Niu *et al.*, 2005),

$$q_{drain} = q_{drain,max} e^{-f_{drain}\nabla z}$$

where $q_{drain,max}$ (=5.5× 10^{-3}) is the maximum drainage when water table is at soil surface, f_{drain}=2.5 m-1 is the decay factor. ∇z is the water table depth (m).The recharge rate ($q_{recharge}$) is defined as positive when water enters the aquifer. In case water table is below soil column, It is calculated according to Darcy's law (Oleson *et al.*, 2008).

3.9 References for Supporting Information

Adhya, T., S. Mishra, A. Rath, K. Bharati, S. Mohanty, B. Ramakrishnan, V. Rao, and N. Sethunathan (2000), Methane efflux from rice-based cropping systems under humid tropical conditions of eastern India, Agriculture, Ecosystems & Environment, 79(1), 85-90.

Amaral, J. A., T. Ren, and R. Knowles (1998), Atmospheric methane consumption by forest soils and extracted bacteria at different pH values, Applied and environmental microbiology, 64(7), 2397-2402.

Bergamaschi, P., et al. (2007), Satellite chartography of atmospheric methane from SCIAMACHYon board ENVISAT: 2. Evaluation based on inverse model simulations, J Geophys Res-Atmos, 112(D2).

Bharati, K., S. R. Mohanty, D. P. Singh, V. R. Rao, and T. K. Adhya (2000), Influence of incorporation or dual cropping of Azolla on methane emission from a flooded alluvial soil planted to rice in eastern India, Agr Ecosyst Environ, 79(1), 73-83.

Bhatia, A., N. Jain, and H. Pathak (2013), Methane and nitrous oxide emissions from Indian rice paddies, agricultural soils and crop residue burning, Greenh Gases, 3(3), 196-211.

Bloom, A. A., P. I. Palmer, A. Fraser, D. S. Reay, and C. Frankenberg (2010), Large-Scale Controls of Methanogenesis Inferred from Methane and Gravity Spaceborne Data, Science, 327(5963), 322-325.

Cai, Z., H. Tsuruta, and K. Minami (2000), Methane emission from rice fields in China: measurements and influencing factors, Journal of Geophysical Research: Atmospheres (1984–2012), 105(D13), 17231-17242.

Cai, Z., H. Tsuruta, M. Gao, H. Xu, and C. Wei (2003), Options for mitigating methane emission from a permanently flooded rice field, Global Change Biol, 9(1), 37-45.

Cao, M., J. Dent, and O. Heal (1995), Modeling methane emissions from rice paddies, Global Biogeochem Cy, 9(2), 183-195.

Chareonsilp, N., C. Buddhaboon, P. Promnart, R. Wassmann, and R. Lantin (2000), Methane emission from deepwater rice fields in Thailand, in Methane Emissions from Major Rice Ecosystems in Asia, edited, pp. 121-130, Springer.

Chen, G., G. Huang, B. Huang, J. Wu, K. Yu, H. Xu, H. Xie, and Z. Wang (1995), CH4 and N2O emission from a rice field and effect of Azolla and fertilization on them, Chinese J. Appl. Ecol., 6, 378-382.

Chen, Y. H., and R. G. Prinn (2006), Estimation of atmospheric methane emissions between 1996 and 2001 using a three-dimensional global chemical transport model, J Geophys Res-Atmos, 111(D10).

Cosby, B., G. Hornberger, R. Clapp, and T. Ginn (1984), A statistical exploration of the relationships of soil moisture characteristics to the physical properties of soils, Water Resources Research, 20(6), 682-690.

Debnath, G., M. Jain, S. Kumar, K. Sarkar, and S. K. Sinha (1996), Methane emissions from rice fields amended with biogas slurry and farm yard manure, Climatic Change, 33(1), 97-109.

FAOSTAT (2014), FOOD AND AGRICULTURE ORGANIZATION OF THE UNITED NATIONS STATISTICS DIVISION.

Garg, A., B. Kankal, and P. R. Shukla (2011), Methane emissions in India: Sub-regional and sectoral trends, Atmos Environ, 45(28), 4922-4929.

Ghosh, S., D. Majumdar, and M. C. Jain (2003), Methane and nitrous oxide emissions from an irrigated rice of North India, Chemosphere, 51(3), 181-195.

Goto, E., Y. Miyamori, S. Hasegawa, and O. Inatsu (2004), Reduction effects of accelerating rice straw decomposition and water management on methane emission from paddy fields in a cold district [ofJapan], Japanese Journal of Soil Science and Plant Nutrition (Japan).

Gupta, M., S. Verma, D. Parashar, and P. K. Gupta (1994), Temporal variation of methane emission from rice paddy fields of Gujarat, Indian Journal of Radio & Space Physics, 23(4), 265-268.

Huang, Y., R. L. Sass, and F. M. Fisher Jr (1998), A semi‐empirical model of methane emission from flooded rice paddy soils, Global Change Biol, 4(3), 247-268.

Inubushi, K., W. Cheng, S. Aonuma, M. M. Hoque, K. Kobayashi, S. Miura, H. Y. Kim, and M. Okada (2003), Effects of free‐air CO2 enrichment (FACE) on CH4 emission from a rice paddy field, Global Change Biol, 9(10), 1458-1464.

Ito, A., and M. Inatomi (2012), Use of a process-based model for assessing the methane budgets of global terrestrial ecosystems and evaluation of uncertainty, Biogeosciences, 9(2), 759-773.

Jain, M. C., S. Kumar, R. Wassmann, S. Mitra, S. D. Singh, J. P. Singh, R. Singh, A. K. Yadav, and S. Gupta (2000), Methane emissions from irrigated rice fields in northern India (New Delhi), Nutr Cycl Agroecosys, 58(1-3), 75-83.

Jermsawatdipong, P., J. Murase, P. Prabuddham, Y. Hasathon, N. Khomthong, K. Naklang, A. Watanabe, H. Haraguchi, and M. Kimura (1994), Methane emission from plots with differences in fertilizer application in Thai paddy fields, Soil Sci Plant Nutr, 40(1), 63-71.

Kai, F. M., S. C. Tyler, and J. T. Randerson (2010), Modeling methane emissions from rice agriculture in China during 1961-2007, J Integr Environ Sci, 7, 49-60.

Kumagai, K., Y. Konno, and M. Togashi (2000), Effect of water management and rice plant growth on methane emission from rice paddy fields in a cold district of Japan, Japanese Journal of Soil Science and Plant Nutrition (Japan).

Lin, K., Y. Xiang, D. Jiang, Q. Hu, Z. Li, D. Du, and Z. Tao (2000), Methane emission flux from paddy fields in its control in Hubei, Agro-environment Protection, 19, 257-270.

Lu, W. F., W. Chen, B. W. Duan, W. M. Guo, Y. Lu, R. S. Lantin, R. Wassmann, and H. U. Neue (2000), Methane emissions and mitigation options in irrigated rice fields in southeast China, Nutr Cycl Agroecosys, 58(1-3), 65-73.

Matsumoto, J., Y. Minamiyama, S. Akahori, and K. Takahashi (2002), Suppression of methane emission from paddy field supplemented with organic matter, Japanese Journal of Soil Science and Plant Nutrition (Japan).

Mohanty, S., K. Bharati, B. Moorthy, B. Ramakrishnan, V. Rao, N. Sethunathan, and T. Adhya (2001), Effect of the herbicide butachlor on methane emission and ebullition flux from a direct-seeded flooded rice field, Biology and fertility of soils, 33(3), 175-180.

Niu, G.-Y., Z.-L. Yang, R. E. Dickinson, and L. E. Gulden (2005), A simple TOPMODEL-based runoff parameterization (SIMTOP) for use in global climate models, J. Geophys. Res., 110(D21), D21106.

Oleson, K. W., Y. J. Dai, G. Bonan, M. Bosilovich, R. Dickinson, P. Dirmeyer, F. Hoffman, P. Houser, S. Levis, and G. Y. Niu (2004), Technical description of the community land model (CLM), Tech. Note NCAR/TN-461+ STR.

Oleson, K. W., et al. (2008), Improvements to the Community Land Model and their impact on the hydrological cycle, J. Geophys. Res., 113(G1), G01021.

Pathak, H., S. Prasad, A. Bhatia, S. Singh, S. Kumar, J. Singh, and M. C. Jain (2003), Methane emission from rice-wheat cropping system in the Indo-Gangetic plain in relation to irrigation, farmyard manure and dicyandiamide application, Agr Ecosyst Environ, 97(1-3), 309-316.

Satpathy, S. N., S. Mishra, T. K. Adhya, B. Ramakrishnan, V. R. Rao, and N. Sethunathan (1998), Cultivar variation in methane efflux from tropical rice, Plant and Soil, 202(2), 223-229.

Setyanto, P., A. Makarim, A. Fagi, R. Wassmann, and L. Buendia (2000), Crop management affecting methane emissions from irrigated and rainfed rice in Central Java (Indonesia), in Methane Emissions from Major Rice Ecosystems in Asia, edited, pp. 85-93, Springer.

Singh, J. S., S. Singh, A. S. Raghubanshi, S. Singh, and A. K. Kashyap (1996), Methane flux from rice/wheat agroecosystem as affected by crop phenology, fertilization and water level, Plant and Soil, 183(2), 323-327.

Singh, S., J. S. Singh, and A. K. Kashyap (1999), Methane flux from irrigated rice fields in relation to crop growth and N-fertilization, Soil Biol Biochem, 31(9), 1219-1228.

SNCCCC (2012), Second National Communication on Climate Change of The People's Republic of China.

Song, C., X. Xu, H. Tian, and Y. Wang (2009), Ecosystem–atmosphere exchange of CH4 and N2O and ecosystem respiration in wetlands in the Sanjiang Plain, Northeastern China, Global Change Biol, 15(3), 692-705.

Sorokin, D. Y., B. E. Jones, and J. G. Kuenen (2000), An obligate methylotrophic, methane-oxidizing Methylomicrobium species from a highly alkaline environment, Extremophiles, 4(3), 145-155.

Spahni, R., et al. (2011), Constraining global methane emissions and uptake by ecosystems, Biogeosciences, 8(6), 1643-1665.

Subadiyasa, N., N. Arya, and M. Kimura (1997), Methane emissions from paddy fields in Bali Island, Indonesia, Soil Sci Plant Nutr, 43(2), 387-394.

Tao, Z. (1998), Methane emission from rice fields in difference regions of China and mitigation options, Agro-environment Protection, 17, 1-7.

Wang, Y. F., W. Chen, Z. Zhao, and J. Gu (2008), Charatceristics and estimation of CH4, N2O emission from cold paddy field in the Sanjiang Plain, Transcations of the CSAE, 24, 170-176.

Wang, Z., Y. Xu, Z. Li, Y. Guo, R. Wassmann, H. Neue, R. Lantin, L. Buendia, Y. Ding, and Z. Wang (2000), A four-year record of methane emissions from irrigated rice fields in the Beijing region of China, in Methane Emissions from Major Rice Ecosystems in Asia, edited, pp. 55-63, Springer.

Wassmann, R., X. J. Shangguan, D. X. Cheng, M. X. Wang, H. Papen, H. Rennenberg, and W. Seiler (1996), Spatial and seasonal distribution of organic amendments affecting methane emission from Chinese rice fields, Biology and Fertility of Soils, 22(3), 191-195.

Wassmann, R., M. Wang, X. Shangguan, X. Xie, R. Shen, Y. Wang, H. Papen, H. Rennenberg, and W. Seiler (1993), First records of a field experiment on fertilizer effects on methane emission from rice fields in Hunan ‐ Province (PR China), Geophys Res Lett, 20(19), 2071-2074.

Xu, Y. C., Q. R. Shen, M. L. Li, K. Dittert, and B. Sattelmacher (2004), Effect of soil water status and mulching on N2O and CH4 emission from lowland rice field in China, Biology and Fertility of Soils, 39(3), 215-217.

Yagi, K., and K. Minami (1990), Effect of organic matter application on methane emission from some Japanese paddy fields, Soil Sci Plant Nutr, 36(4), 599-610.

Yagi, K., H. Tsuruta, K. i. Kanda, and K. Minami (1996), Effect of water management on methane emission from a Japanese rice paddy field: Automated methane monitoring, Global Biogeochem Cy, 10(2), 255-267.

Yan, M., R. Hua, D. Wang, and X. Ma (2000), Study on estimation of methane emission from rice fields in Changchun area, Scientia Geographica Sinica, 20, 386-390.

Yan, X. Y., H. Akiyama, K. Yagi, and H. Akimoto (2009), Global estimations of the inventory and mitigation potential of methane emissions from rice cultivation conducted using the 2006 Intergovernmental Panel on Climate Change Guidelines, Global Biogeochem Cy, 23.

Zhang, B., and G. Q. Chen (2014), China's CH4 and CO2 emissions: Bottom-up estimation and comparative analysis, Ecol Indic, 47, 112-122.

Zhang, W., Y. Q. Yu, Y. Huang, T. T. Li, and P. Wang (2011), Modeling methane emissions from irrigated rice cultivation in China from 1960 to 2050, Global Change Biol, 17(12), 3511-3523.

Zhang, W., Q. Zhang, Y. Huang, T. T. Li, J. Y. Bian, and P. F. Han (2014), Uncertainties in estimating regional methane emissions from rice paddies due to data scarcity in the modeling approach, Geosci Model Dev, 7(3), 1211-1224.

Zhuang, Q., J. M. Melillo, D. W. Kicklighter, R. G. Prinn, A. D. McGuire, P. A. Steudler, B. S. Felzer, and S. Hu (2004), Methane fluxes between terrestrial ecosystems and the atmosphere at northern high latitudes during the past century: A retrospective analysis with a process‐based biogeochemistry model, Global Biogeochem Cy, 18(3).

Chapter 4

Methane Emissions from Global Wetland: Magnitude, Spatio-Temporal Patterns and Climatic Controls

4.1 Abstract

Wetlands have long been recognized as the dominant contributor for the inter-annual variation in atmospheric methane (CH_4) concentration over the past two decades. A further question would be which factors dominate the variation of wetland CH_4 emissions? Here, we examined the magnitude, spatial and temporal distribution of CH_4 emission from wetlands during 1993 -2014 by employing a process-based biogeochemical model, the Dynamic Land Ecosystem Model (DLEM). Wetlands experienced significant climatic changes during the study period. Temperature increased significantly across the globe, whereas shortwave radiation increased significantly in the southern hemisphere. The estimated wetland CH_4 emission was around 92.9±4.2 (Avg. ± 1 std. dev., same hereafter) Tg C/yr during 1993-2014, with ~ 64.3% originated from the tropical region. Among six continents, South America shared the largest portion of estimated CH_4 emission. The estimated CH_4 emission from wetland exhibited clear seasonal trend over the entire globe during 1993-2014, with the most apparent trend being found in autumn. Our study indicated that the variation of wetland extent was important and needs to be considered for quantifying the inter-annual and intra-annual variation of estimated CH_4 emissions from wetland. Further analyses have revealed that 20% and 16% of the global inundation extent showed a significant correlation with precipitation and temperature,

respectively. Inundation extent in most parts of the globe was found to have positive correlation with annual precipitation amount. However, when considering direct and indirect impacts of climate variability on the DLEM estimated CH_4 fluxes, temperature had a greater effect than precipitation on anomalous CH_4 estimation.

4.2 Introduction

Methane (CH_4), the most abundant non-carbon dioxide (CO_2) greenhouse gas (GHG) in the atmosphere, has 28 times higher global warming potential than CO_2 on a 100-year time horizon (Montzka *et al.*, 2011a, Stocker *et al.*, 2013b). Changes in CH_4 fluxes could have a quick response to GHG-induced radiative forcing, especially in a short time frame (Tian *et al.*, 2016a). The atmospheric concentration of CH_4 has reached an unprecedentedly high level over the past 800,000 years partly owing to the intense anthropogenic activities (Montzka *et al.*, 2011a). Wetlands, the single largest CH_4 source, contributed 40%-50% of the total CH_4 emission during the 2000s (Kirschke *et al.*, 2013, Tian *et al.*, 2016a). Methane emission from wetlands has been proposed to explain the inter-annual variation in atmospheric CH_4 concentration over the past two decades (Bousquet *et al.*, 2006, Bousquet *et al.*, 2011, Kirschke *et al.*, 2013, Schaefer *et al.*, 2016).

A further question would be which factors dominate the variation of wetland CH_4 emissions? Wetland CH_4 emission encompasses a natural component (background emissions) as well as human-induced perturbations, such as climate change (Tian *et al.*, 2016a). Although it has been well documented that wetland emissions are substantially influenced by climatic variability (Melton *et al.*, 2013, Pison *et al.*, 2013), understanding of the feedback between wetland emissions and climate change remains unclear. Both wetland extent and CH_4 producing capability were found to be regulated by inter-annual and intra-annual variations of temperature and precipitation (Pison *et al.*, 2013). A warming climate could enhance the CH_4 producing capability via accelerating the microbial breakdown of organic substrate (Schuur *et al.*, 2015), but may reduce CH_4 production by drying out the inundation area. Variations in precipitation could determine water availability, which directly regulates the activities of methanogenic and

methanotrophic bacteria. Although substantial progress has been made in addressing CH_4 flux at regional, continental and global levels, reasons for observed CH_4 anomalies, especially how temperature and precipitation affect CH_4 flux, are still poorly understood (Nisbet *et al.*, 2014).

Given its importance of regulating the CH_4 budget from the terrestrial ecosystems and inter-annual variability of atmospheric CH_4 concentration, bottom-up (BU) and top-down (TD) approaches have been extensively used to examine the CH_4 emission from wetlands at both regional and global scales (Bohn *et al.*, 2015, Kirschke *et al.*, 2013, Melton *et al.*, 2013). A previous synthesis study suggested that BU approaches tend to overestimate wetland CH_4 emission (Kirschke *et al.*, 2013). Uncertainty in current wetland extent has restricted the understanding of the estimated CH_4 emission from wetland. The estimation of CH_4 emission from TD approaches was restricted by the sparse observation in the tropical region, which has been suggested to account for 70% of the total wetland CH_4 emission (Montzka *et al.*, 2011a). Thus, further efforts need to be made to improve the accuracy of estimated CH_4 from wetlands and the understanding of feedback with climatic factors.

Herein, we apply an improved process-based biogeochemical model with multiple-satellite observed inundation area to examine the magnitude, spatio-temporal variations and climatic controls of CH_4 emission from wetlands. Our major objectives were to 1) examine the spatial and temporal patterns of climatic factors during 1993-2014; 2) identify the impacts of precipitation and temperature on wetland extent change over time; 3) estimate the magnitude, spatial and temporal patterns of the estimated CH_4 fluxes from global wetlands.

4.3 Method

4.3.1 Dynamic Land Ecosystem Model

Same as described in Chapter 3

4.3.2 Description of the CH_4 Module in the DLEM

Same as described in Chapter 3

4.3.3 Input Data

Same as described in Chapter 3

4.3.4 Model Calibration and Validation

Same as described in Chapter 3

The DLEM-estimated CH_4 fluxes have been extensively validated against field observations in previous studies (Tian *et al*., 2010, Xu *et al*., 2010). Here, we further compared the estimated daily/seasonal CH_4 fluxes with observations at 5 wetland sites (**Fig. 4.1**). The DLEM-estimated CH_4 fluxes followed the same variation as the site-level observation. However, at some sites, it was difficult to track the extreme or abrupt high or low CH_4 flux, which may be related to the sub-daily CH_4 fluxes variation. The current version of the DLEM-CH_4 module is at a daily time step.

4.3.5 Experimental Design

Same as described in Chapter 3

4.3.6 Relationship between Inundation Extent and Climatic Factors

To investigate the relationship between the year-to-year changes in maximum inundation extent and climatic factors of temperature and precipitation, we used the Global Inundation Extent from Multi-Satellites (GIEMS) (Prigent *et al.*, 2012) from 1993 to 2007 to calculate the 15-year monthly mean inundation extents and then determine the month with peak inundation extent in each grid cell (**Fig. 4.2**). Climatic variables from CRUNCEP_v6, including precipitation and temperature were adopted. The Pearson's correlations between year-to-year

changes in maximum inundation extent and climatic factors of temperature and precipitation were calculated in each grid cell.

4.4 Results and discussion

4.4.1 Spatial and Temporal Patterns of Climatic Factors during 1993-2014

In this study, Mann-Kendall trend analysis was used to examine the short-term trends of climatic variables. Global average temperature greatly fluctuated during the study period, with a significant increasing trend (0.2°C/decade, $p < 0.001$). 2005 was identified as the warmest year and 1993 was the coolest year during 1993-2014. The change in average temperature from different latitudinal regions exhibited substantial spatial variations (**Fig. 4.3**). Average temperature in the northern high latitude region (NH, 60°N -90°N), and tropical regions (30°S-30°N), and southern hemisphere (SM, 30°S-60°S) showed a significant increasing trend (0.5°C/decade, 0.2°C/decade and 0.2°C/decade, $p < 0.001$), while average temperature in the northern hemisphere (NM, 30°N-60°N) showed a non-significant increasing trend. It is noteworthy that the anomalous average temperature started to increase from almost all the latitude bands after 2000. The temperature increase in the NH was found to be ahead of other places especially after 2005. The anomalous high temperature was found during 2009-2010 in the tropical region and in the SM in 2014. Global annual precipitation showed a non-significant increasing trend at a rate of 9 mm/decade during 1993-2014. The change in anomalous precipitation was more evident in the southern hemisphere than that in the northern hemisphere (**Fig. 4.3**). The positive anomalous precipitation was found in the most area of the globe after 2006. There is no obvious trend for the change of shortwave solar radiation at the global scale. However, a signification increasing trend was found in the SM at a rate of 3.2 W/m^2/decade

during 1993-2014. The temporal variation of anomalous shortwave radiation was much stronger in the southern hemisphere than that in the northern hemisphere.

4.4.2 Spatial and Temporal Patterns of Wetland CH_4 Emissions

In this study, we quantified the CH_4 emissions from global wetlands during 1993-2014, which was 92.9±4.2 (Avg. ± 1 std. dev., same hereafter) Tg C/yr, with great inter-annual variation. The peak CH_4 emission occurred in 1993, followed by 1998 and 2002, and the lowest annual CH_4 emission occurred in 2000. For the intra-annual variation, estimated CH_4 emission from wetlands gradually increased from January to April, and then increased rapidly to reach the peak emission around July or August, and leveled off until the end of year.

When investigating CH_4 emissions from wetlands along the latitudinal gradient, tropical regions (30°N-30°S) contributed 64.3% of the estimated global wetland emission, followed by northern mid-latitude (30°N-60°N) (~22.8%) and northern high-latitude (60°N-90°N) (~9.0%), and southern mid-latitude (30°S-60°S) (~3.9%) shared the least portion. The dominant contribution of tropics in the global wetland CH_4 emissions were consistent with previous findings (Bousquet *et al.*, 2011, Ito & Inatomi, 2012, Melton *et al.*, 2013, Tian *et al.*, 2015a). From the continental perspective, South America was the primary emitter, which contributed around 33.1% of the total wetland emissions, followed by Asia (~29.3%). North America together with Africa contributed to another one-third of the global total emission, and Europe and Oceania share the least portion. Previous study (Chapter 2) has compared the DLEM-estimated CH_4 emission from wetland with estimation from atmospheric inversion model and other process-based models, and indicated the DLEM estimates fall well within the range of other estimations (Kirschke *et al.*, 2013).

The estimated CH_4 emission from wetlands exhibited significant seasonal variability over the entire globe during 1993-2014 (Fig. 4.4). The estimated CH_4 emissions from wetland in summer (June, July and August) accounts for the largest portion (~37.9%) of the annual emission, followed by autumn (September, October and November; ~23.0%), spring (March, April and May; ~21.9%), and winter (December, January and February; ~17.1%). Largest seasonal trend of CH_4 emissions from wetlands were found in autumn and seasonal trend was relatively small in spring, summer, and winter. The largest increase in CH_4 emissions during autumn was found in high latitude region, especially in the Hudson Bay Lowland (HBL) and larges area in Canada during 1993-2014. Both increasing and decreasing trend were found in tropical South America and Africa in autumn. An apparent decreasing trend was found in east Asia, northwest India and northern Quebec (Fig. 4.4).

4.4.3 Impacts of Precipitation and Temperature on Wetland Extent Change over Time

At the global scale, maximum inundation extent decreased by 6% during 1993-2007. From long-term perspective, agricultural development driven by population growth and economic development dominated the wetland conversion since the pre-industrial times (Prigent *et al.*, 2012, Van Asselen *et al.*, 2013). If focusing on the short-term (1993-2007), 20% of the wetland extent showed a significant correlation with change in precipitation (**Fig. 4.5**). Among those areas, over 86% showed a significant positive correlation with precipitation. In the northeast United States, parts of the Amazon plain in South America, the vast area in Europe, Northwest India as well as Southeast China, the peak inundation extent showed a significant positive correlation with precipitation. At the global level, over 16% of the wetland extent showed a significant correlation with temperature. Among those areas, 63% of the tropical region had a significant negative correlation with temperature, 58%, 31% and 43% of the NH,

NM and SM regions showed a significant positive correlation with temperature. At the global scale, in most areas, like South Asia, most parts of South America and the Southeast United States, peak inundation extent showed a significant negative correlation with temperature. The decrease in inundation extent in the tropical region should be partly owing to the great reduction of precipitation in that region from 2001 to 2004 (**Fig. 4.3**). At the global scale, anomalous temperature showed an increasing trend from 1993 to 2007, which may also result in a reduction in the inundation extent. Especially, in the tropical region, the vast area of wetland showed a negative correlation with the change of temperature. A regional study in Amazon basin showed that the severe drought during 2005 resulted in a great reduction of water storage, with 70% below 2003-2007 average (Frappart *et al.*, 2012), which was consistent with our findings that in 2005 global anomalous temperature and precipitation was above and below 1993-2007 average, respectively. The decreases in wetland extent could lead to the reduction of global wetland CH_4 emissions.

Temperature and precipitation not only affect the variation in wetland extent but also influence the CH_4 producing capability (Paudel *et al.*, 2016). Our results showed that when considering the effect of climatic variables on DLEM estimated CH_4 fluxes, temperature had a greater effect than precipitation on the CH_4 estimation. At global scale, the change in temperature during 1993-2014 increased the estimated CH_4 fluxes from wetlands. The change in CH_4 fluxes was largest at the tropical regions, followed by NM, NH and SM regions and exhibited great inter-annual variation. Temperature posed both positive and negative effect on the estimated CH_4 fluxes at the NH during the study period. For the NM regions in most of the years during the study period the variation of temperature increased the estimated CH_4 fluxes, with an abrupt high CH_4 estimation occurred in 1998. In DLEM, CH_4 processes are affected by

soil temperature with a Q10 response curve (Tian *et al.*, 2010b, Xu *et al.*, 2010). While, precipitation had no direct effect on CH_4 processes, but it could affect the soil water content which further affected the CH_4 producing and oxidation processes. In the DLEM, wetlands were assumed to be inundated and increase in precipitation would not have further impact on the estimated CH_4 processes in those regions.

4.5 Conclusion

Wetlands, the single largest CH_4 source, dominated the inter-annual variation of the recent global atmospheric CH_4 anomalies. During the past two decades, wetlands experienced significant climatic changes. Temperature over the globe and shortwave solar radiation in the southern hemisphere was found to increase significantly. The change of precipitation showed a non-significant increasing trend. The estimated CH_4 emissions from wetland was 92.9±4.2 Tg C/yr during 1993-2014 and exhibited great inter-annual and intra-annual variation. The CH_4 emissions in summer shared the largest portion of annual emission, and the largest seasonal trend of estimated CH_4 emissions was found in autumn. Climatic factors of temperature and precipitation greatly affect both wetland extent and CH_4 producing capability. 20% and 16% of the global inundation extent showed a significant correlation with precipitation and temperature, respectively. When considering the individual effect of DLEM estimated CH_4 fluxes, temperature had a greater effect than precipitation on CH_4 estimation. In the 21st century, temperature is expected to increase globally, with the Arctic region increasing most. Precipitation is also expected to increase in high latitude. The change in precipitation and temperature could affect both wetland extent and CH_4 emissions in high latitude. The warming climate could lead to the changes in seasonal melt cycle, and may trigger the wetting or drying of

the permafrost regions in the high latitude. Therefore, the feedback of CH_4 emissions and climate change should be investigated in this region.

4.6 References

Bohn TJ, Melton JR, Ito A et al. (2015) WETCHIMP-WSL: intercomparison of wetland methane emissions models over West Siberia. Biogeosciences, 12, 3321-3349.

Bousquet P, Ciais P, Miller JB et al. (2006) Contribution of anthropogenic and natural sources to atmospheric methane variability. Nature, 443, 439-443.

Bousquet P, Ringeval B, Pison I et al. (2011) Source attribution of the changes in atmospheric methane for 2006–2008. Atmospheric Chemistry and Physics, 11, 3689-3700.

Frappart F, Papa F, Da Silva JS, Ramillien G, Prigent C, Seyler F, Calmant S (2012) Surface freshwater storage and dynamics in the Amazon basin during the 2005 exceptional drought. Environmental Research Letters, 7, 044010.

Ito A, Inatomi M (2012) Use of a process-based model for assessing the methane budgets of global terrestrial ecosystems and evaluation of uncertainty. Biogeosciences, 9, 759-773.

Kirschke S, Bousquet P, Ciais P et al. (2013) Three decades of global methane sources and sinks. Nature Geoscience, 6, 813-823.

Melton JR, Wania R, Hodson EL et al. (2013) Present state of global wetland extent and wetland methane modelling: conclusions from a model inter-comparison project (WETCHIMP). Biogeosciences, 10, 753-788.

Montzka SA, Dlugokencky EJ, Butler JH (2011) Non-CO2 greenhouse gases and climate change. Nature, 476(7358), 43-50.

Nisbet EG, Dlugokencky EJ, Bousquet P (2014) Methane on the Rise-Again. Science, 343, 493-495.

Paudel R, Mahowald NM, Hess PG, Meng L, Riley WJ (2016) Attribution of changes in global wetland methane emissions from pre-industrial to present using CLM4. 5-BGC. Environmental Research Letters, 11, 034020.

Pison I, Ringeval B, Bousquet P, Prigent C, Papa F (2013) Stable atmospheric methane in the 2000s: key-role of emissions from natural wetlands. Atmospheric Chemistry and Physics, 13, 11609-11623.

Prigent C, Papa F, Aires F, Jimenez C, Rossow WB, Matthews E (2012) Changes in land surface water dynamics since the 1990s and relation to population pressure. Geophysical Research Letters, 39.

Schaefer H, Fletcher SEM, Veidt C et al. (2016) A 21st-century shift from fossil-fuel to biogenic methane emissions indicated by 13CH4. Science, 352, 80-84.

Schuur E, Mcguire A, Schädel C et al. (2015) Climate change and the permafrost carbon feedback. Nature, 520, 171-179.

Stocker TF, Qin D, Plattner GK et al. (2013) IPCC, 2013: climate change 2013: the physical science basis. Contribution of working group I to the fifth assessment report of the intergovernmental panel on climate change.

Tian HQ, Chen GS, Lu CQ et al. (2015) Global methane and nitrous oxide emissions from terrestrial ecosystems due to multiple environmental changes. Ecosystem Health and Sustainability, 1, art4.

Tian HQ, Lu CQ, Ciais P et al. (2016) The terrestrial biosphere as a net source of greenhouse gases to the atmosphere. Nature, 531, 225-228.

Tian HQ, Xu XF, Liu ML, Ren W, Zhang C, Chen GS, Lu CQ (2010) Spatial and temporal patterns of CH4 and N2O fluxes in terrestrial ecosystems of North America during 1979-2008: application of a global biogeochemistry model. Biogeosciences, 7, 2673-2694.

Van Asselen S, Verburg PH, Vermaat JE, Janse JH (2013) Drivers of wetland conversion: A global meta-analysis. Plos One, 8, e81292.

Xu XF, Tian HQ, Zhang C et al. (2010) Attribution of spatial and temporal variations in terrestrial methane flux over North America. Biogeosciences, 7, 3637-3655.

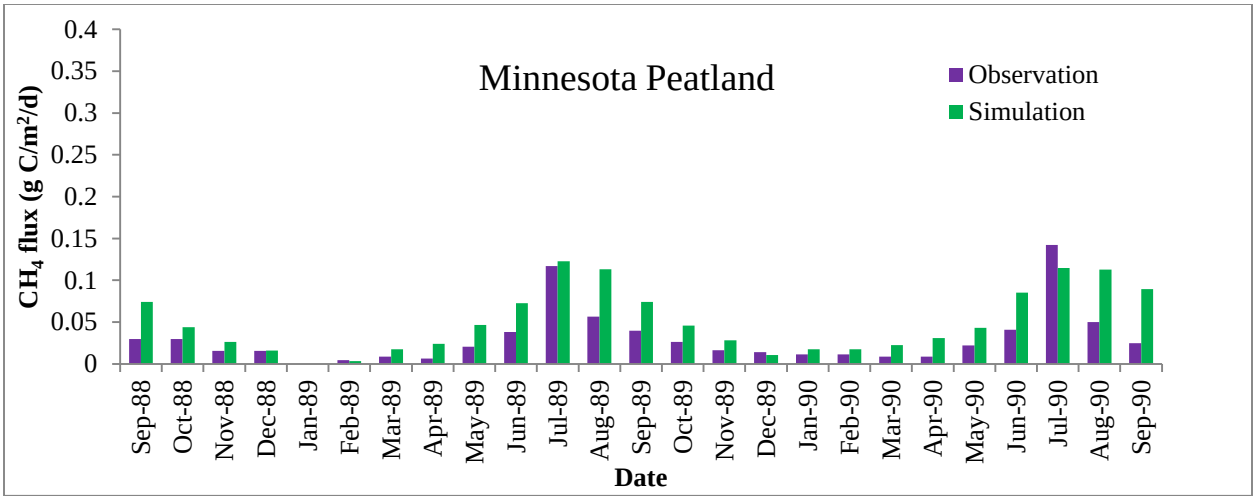
Minnesota Peatland
Observation
Simulation
CH4 flux (g C/m2/d)
0.4
0.35
0.3
0.25
0.2
0.15
0.1
0.05
0
Sep-88
Oct-88
Nov-88
Dec-88
Jan-89
Feb-89
Mar-89
Apr-89
May-89
Jun-89
Jul-89
Aug-89
Sep-89
Oct-89
Nov-89
Dec-89
Jan-90
Feb-90
Mar-90
Apr-90
May-90
Jun-90
Jul-90
Aug-90
Sep-90
Date

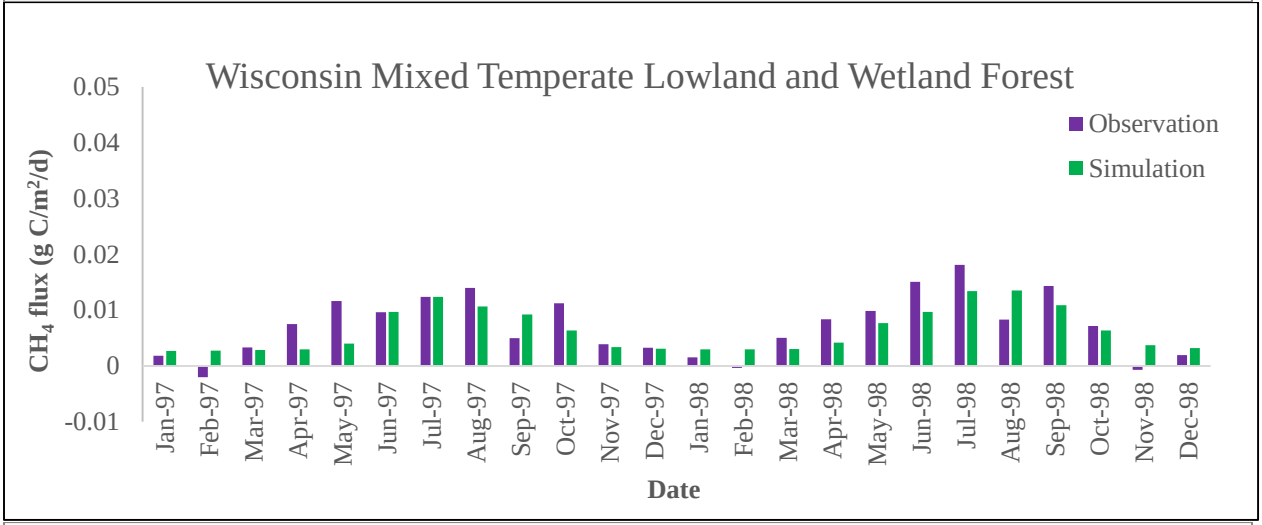
Wisconsin Mixed Temperate Lowland and Wetland Forest
Observation
Simulation
CH4 flux (g C/m2/d)
0.05
0.04
0.03
0.02
0.01
0
-0.01
Jan-97
Feb-97
Mar-97
Apr-97
May-97
Jun-97
Jul-97
Aug-97
Sep-97
Oct-97
Nov-97
Dec-97
Jan-98
Feb-98
Mar-98
Apr-98
May-98
Jun-98
Jul-98
Aug-98
Sep-98
Oct-98
Nov-98
Dec-98
Date

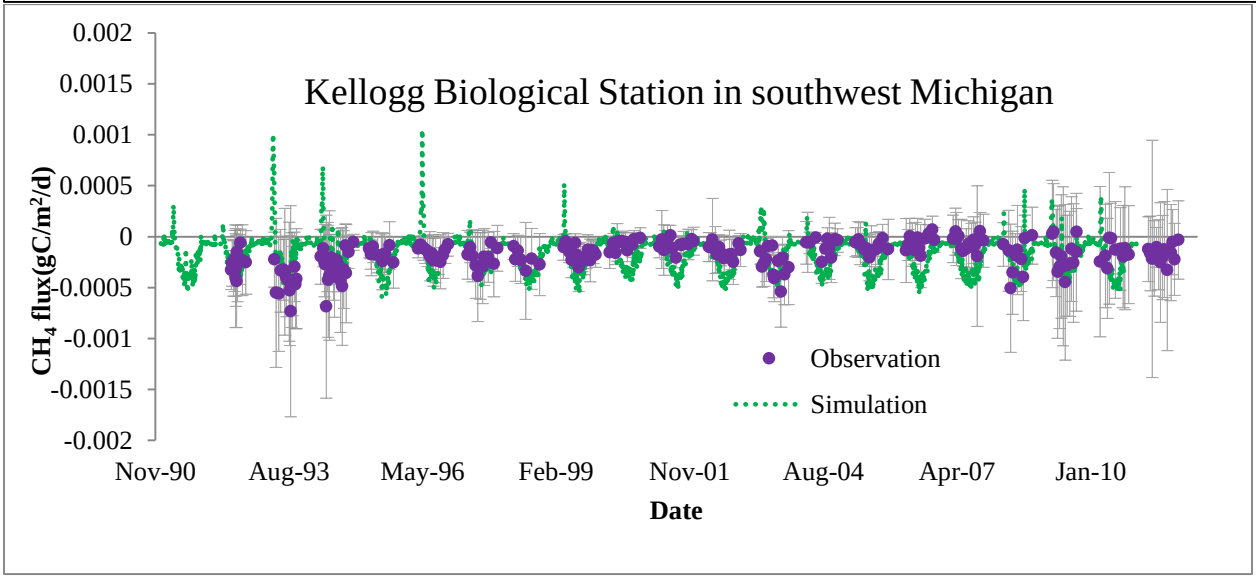
Kellogg Biological Station in southwest Michigan
CH4 flux(gC/m2/d)
0.002
0.0015
0.001
0.0005
0
-0.0005
-0.001
-0.0015
-0.002
Observation
Simulation
Nov-90
Aug-93
May-96
Feb-99
Nov-01
Aug-04
Apr-07
Jan-10
Date

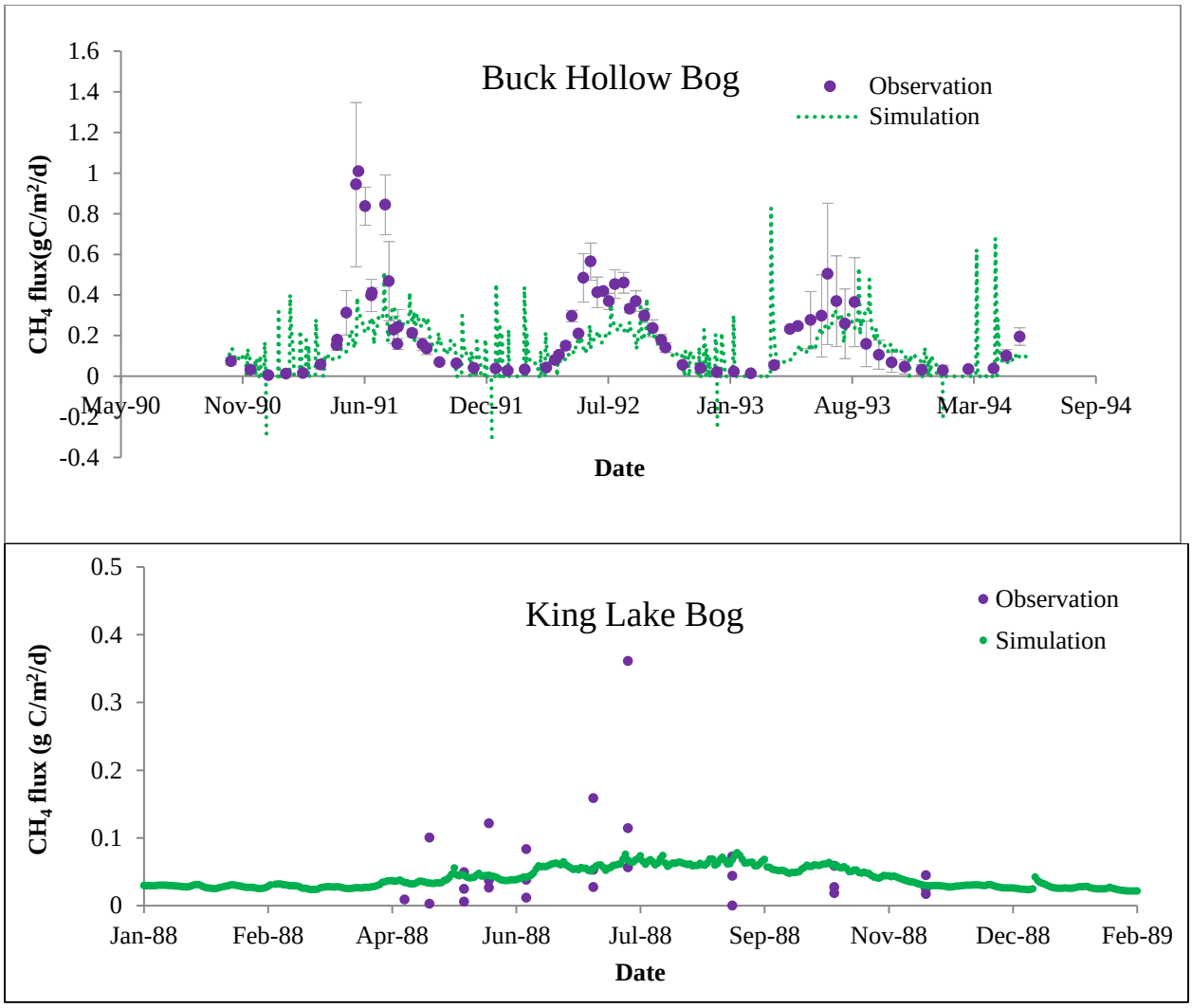

Figure 4.1 Comparison of DLEM-estimated CH_4 flux with field observations at 5 sites

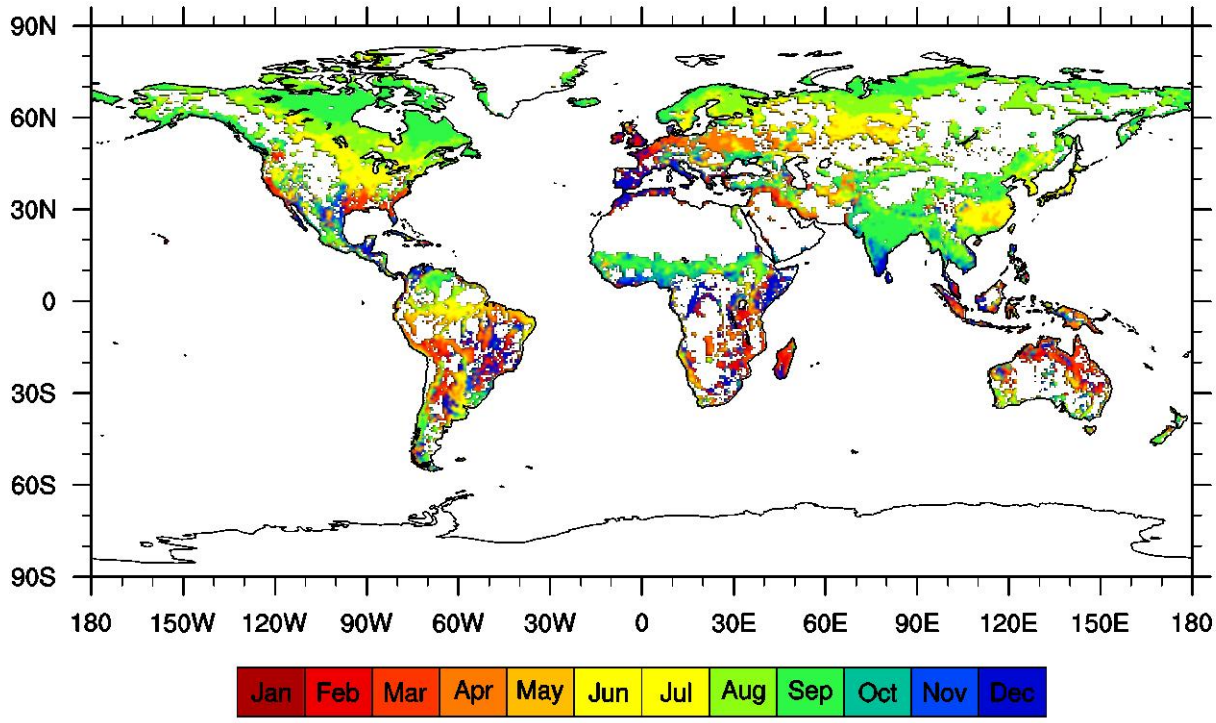

Figure 4.2 Spatial distribution of month with peak inundation from global wetlands

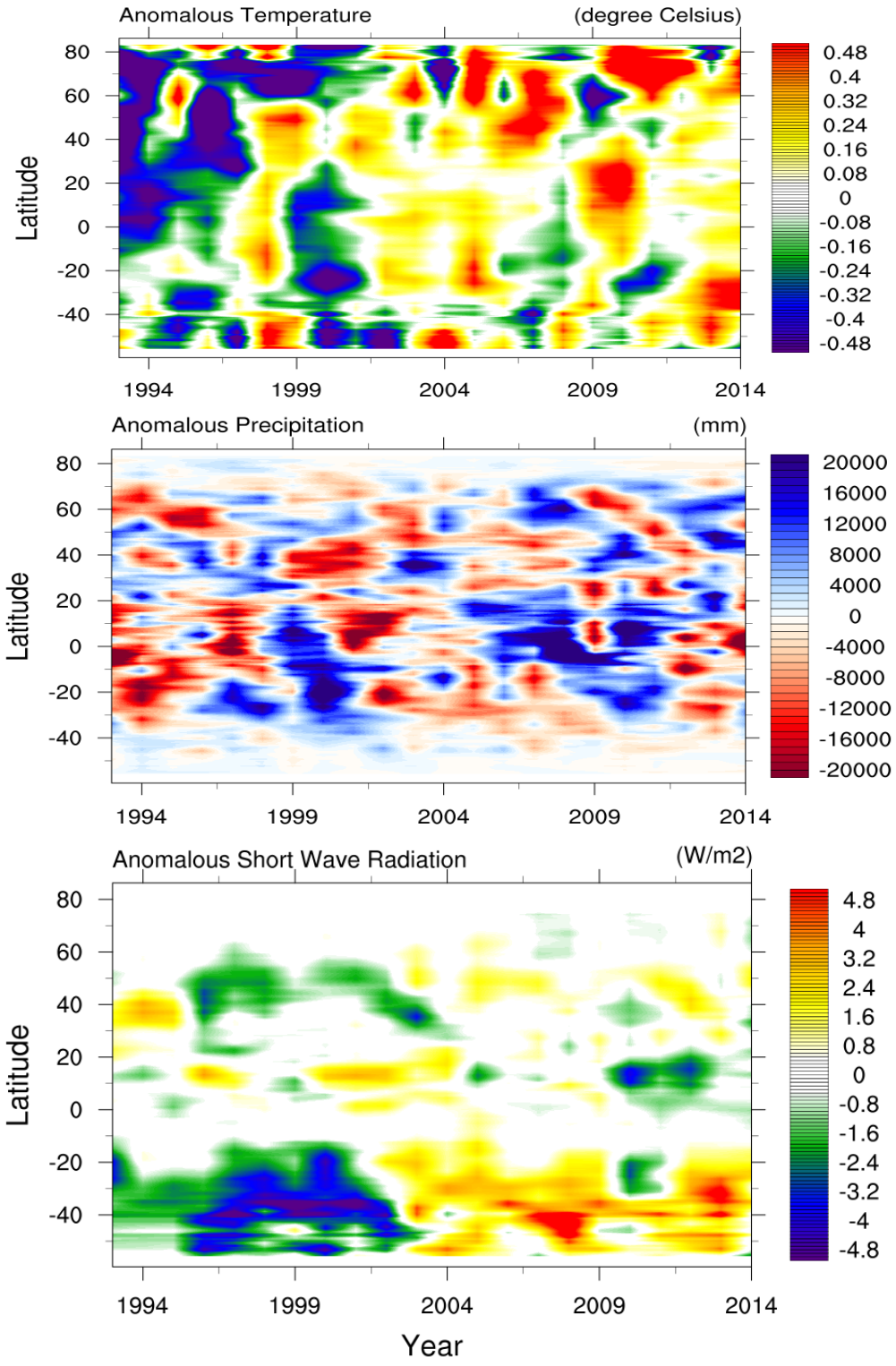

Figure 4.3 Temporal dynamics of climatic factors anomalies: temperature (°C), precipitation (mm) and short-wave radiation (W/m^2) (relative to 1993-2014 annual mean)

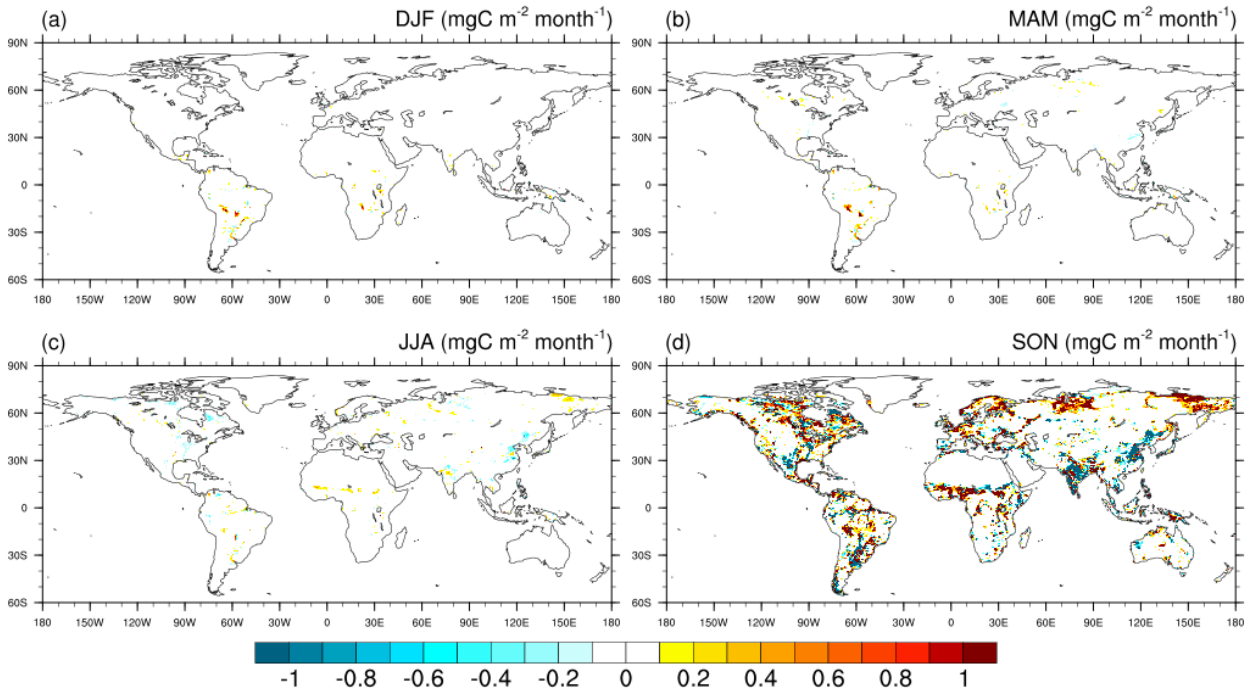

Figure 4.4 Seasonal variation of estimated CH_4 emission from wetland

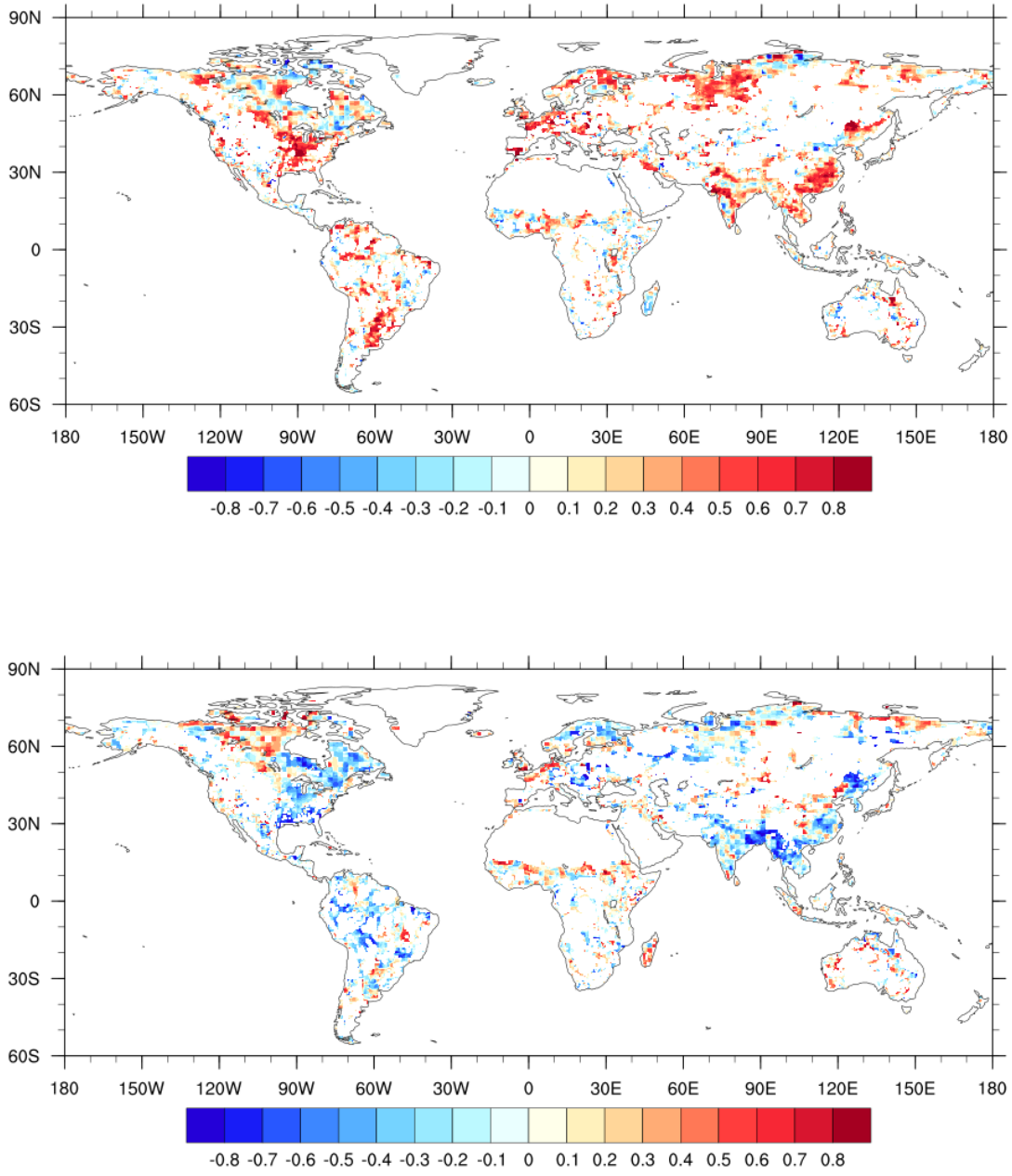

Figure 4.5 a. Pearson correlation coefficient of year-to-year changes in maximum inundation extent and precipitation (top) and b. Pearson correlation coefficient of year-to-year changes in maximum inundation extent and temperature (bottom)

Chapter 5

Net Exchange of Methane Fluxes between Terrestrial Ecosystem and the Atmosphere in the Arctic-Boreal Regions under Future Climate Change Scenarios

5.1 Abstract

Due to a large portion of wetland and permafrost distribution as well as soil carbon storage, arctic and boreal terrestrial ecosystems have long been recognized as a potentially huge methane (CH_4) source in the future. In the 21st century, temperature is expected to increase globally, with the largest increase in this region. Precipitation is expected to vary substantially across the globe, with an increase in the arctic and boreal region. However, the question of how future climate change might influence the CH_4 fluxes remains unclear. Increasing disturbances, like permafrost-thaw and climate extreme, would greatly change the patterns and variations of CH_4 emission and further affect the feedback between terrestrial ecosystem and climate change. In this study, we used a process-based model (Dynamic Land Ecosystem Model) driven by temperature, precipitation and nitrogen deposition projections under the RCP 2.6 and RCP 8.5 scenarios, to quantify the magnitude, spatial and temporal variation of CH_4 fluxes across the arctic and boreal regions. We further quantified the sub-regional differences of CH_4 fluxes within study area. Our results indicated that the estimated CH_4 emission from wetland showed an increasing trend from 2006-2099. The magnitude of CH_4 emission from wetland was projected to increase 2%~65% by the end of 21st century compared with the contemporary level. Seasonal analyses indicated that the change of CH_4 fluxes exhibited great spatial variability over time. The

projected CH_4 emissions in summer accounted for the largest portion of annual emission and showed the largest increase during the 21st century. Climate variability was the dominant factor for the projected increase of CH_4 emission. Given the importance of the potential positive feedback between CH_4 emission and climate change, it is vital to have a reasonable estimation of CH_4 emission before developing the adaptation strategies.

5.2 Introduction

Despite only covering ~20% of the global land surface area, over one-third of the world's wetlands, including peatlands, and more than ~50% of the global carbon storage are located in the arctic and boreal regions (Lehner & Döll, 2004, Schuur *et al.*, 2015, Tian *et al.*, 2015b). The vast portion of soil organic carbon (~900 – 1700 petagrams) stored in this region is susceptible to future environmental changes (Hugelius *et al.*, 2014, Koven *et al.*, 2011, Schneider von Deimling *et al.*, 2015). The warming climate may liberate currently frozen and inert old carbon to be accessible for microbial decay (Burke *et al.*, 2012, Schneider von Deimling *et al.*, 2015). During the past three decades, the temperature in the arctic and boreal region has risen two times faster than the global average (O'Shea *et al.*, 2014, Stocker *et al.*, 2013b), with the high confidence that temperature will likely further increase compared to other places under the future scenarios.

A warming climate can accelerate the release of methane (CH_4) emission to the atmosphere (Schuur *et al.*, 2015). Methane is a potent greenhouse gas which has 28 and 84 times higher global warming potential than carbon dioxide (CO_2) on 100-year and 20-year time horizons, respectively (Stocker *et al.*, 2013b). Therefore, the change of CH_4 emissions could have a rapid response to the GHG-induced radiative forcing as well as the rate of climate warming especially in a short time frame (Tian *et al.*, 2016). It has been suggested that CH_4 is likely to contribute almost half of the future carbon emissions on climate forcing in the permafrost regions (Schuur & Abbott, 2011).

The magnitude of CH_4 fluxes from the terrestrial ecosystems are influenced by the multiple environmental factors, such as climate variability and nitrogen addition (Xu *et al.*, 2010). More specifically, climate variability, especially temperature, and precipitation could influence the

CH_4 fluxes through direct and indirect pathways. From the direct pathway, the increase in temperature usually has a positive feedback to the microbial activities, such as methanogens and methanotrophs, which accelerate the release and uptake of CH_4 fluxes from the terrestrial ecosystems. The variation of precipitation usually affects the water availability of the ecosystems and has a direct influence on the CH_4 producing and oxidizing processes. On the other hand, changes in climate variables could affect plant growth, such as gross primary production (GPP), root exudate etc., which is a source of the carbon substrate for the microbial activities. The response of nitrogen (N) addition to the CH_4 fluxes may vary in magnitude and direction depending on ecosystem types and local environmental conditions (Liu & Greaver, 2009). In the arctic and boreal region, most ecosystems are N-limited and the change in N addition might lead to the positive feedback of the CH_4 fluxes. Long-term incubation study suggested that the C:N in permafrost soil should be used to interpret potential C loss from this region (Schädel *et al.*, 2014). It is also important to note that, the response of multifactorial interaction to the CH_4 fluxes from terrestrial ecosystem might be distinct compared to simply adding up the response of single factorial interaction to the CH_4 fluxes (Van Groenigen *et al.*, 2011). Thus, it is important to quantify the projected CH_4 fluxes by simultaneously considering the multiple environmental factors under the future scenarios.

Fortunately, awareness of the importance of CH_4 release from the permafrost region is increasing; however, large uncertainties still persists in estimating the response of CH_4 fluxes to future climate change. Process-based model is an increasingly important tool to examine the feedback between the CH_4 fluxes and the projected future scenarios with consideration of multiple environmental changing factors. Previous studies have enhanced our understanding of the current and potential future carbon budget and identified gaps and uncertainties in restricting

the assessment of regional C budget in the arctic and boreal region (Stocker *et al.*, 2013a, Zhu *et al.*, 2013, Zhuang *et al.*, 2006).

The critical questions centered on the magnitude and timing of the projected CH_4 fluxes to atmosphere in response to multiple environmental factors and potential feedback to future climate change. Thus, the purpose of this paper were: (i) to examine the future changes in multiple environmental factors; (ii) to quantify the projected CH_4 fluxes under future environmental changes; (iii) to identify the seasonal variation in the projected CH_4 fluxes; and (iv) to assess the sub-regional differences of the projected CH_4 fluxes.

5.3 Materials and Methods

5.3.1 Dynamic Land Ecosystem Model

The Dynamic Land Ecosystem Model (DLEM) is an integrated processed-based model which extensively couples the basic biophysical features, a series of soil biogeochemical processes, plant physiological characteristics and different land use, land management practices and fire disturbance. The current version of DLEM is able to make daily, spatially-explicit estimation for the exchange of water, carbon and nitrogen fluxes between land and the atmosphere and at the land-ocean interface (Tian *et al.*, 2015a, Tian *et al.*, 2015c). The major components and related processes have been extensively evaluated at the site and regional observations and estimates from other studies (Tian *et al.*, 2010a, Tian *et al.*, 2015a, Tian *et al.*, 2012, Tian *et al.*, 2015c).

5.3.2 The CH_4 Module

In the DLEM, the CH_4-related processes were calculated through soil biogeochemical component. The DLEM assumed that CH_4 production, oxidation, and transportation only occurred in the top 50 cm of the soil column. Methane was produced under anaerobic conditions

and mainly derived from dissolved organic carbon (DOC). The DLEM assumes that DOC was produced through the decomposition of litterfall and soil organic matter and the byproduct of gross primary production (GPP). The net CH_4 fluxes were determined by CH_4 production, oxidation, and transportation from soil pore water to the atmosphere, and between land and the atmosphere. CH_4 production is described by using the Michaelis–Menten equation in the DLEM and indirectly controlled by multiple environmental factors including soil pH, temperature and soil moisture content. There are three pathways involved in the calculation of CH_4 oxidation, including (1) Atmospheric CH_4 oxidation, (2) CH_4 oxidation in the soil pore water, and (3) CH_4 oxidation during plant-mediated transport. CH_4 can be transported from soil pore water to the atmosphere through ebullition, diffusion, and plant-mediated transport. More detailed information about the calculation of net CH_4 fluxes in the DLEM could be found in Tian *et al.* (2010b). The CH_4 module in the DLEM has already been extensively validated and applied at various scales, from site, to regional and global level (Banger *et al.*, 2015, Ren *et al.*, 2011, Tian *et al.*, 2015a, Tian *et al.*, 2010b).

We improved the permafrost control of the CH_4 fluxes in the current version of DLEM. The freezing and thawing of soil water were determined according to energy excess/deficit during the phase change. The DLEM assumed that CH_4 production and oxidation only occurred when soil water was in liquid phase. The process of freezing and thawing also influenced the CH_4 transportation through ebullition and diffusion. Once the ice was formed in the soil layer, it would impede the CH_4 transportation. The accumulated CH_4 will be further released once ice thawed.

5.3.3 Data and Simulation Experiments Design

The DLEM 2.0 was used to project future changes of CH_4 fluxes in the arctic and boreal region (North of 50°N) using eight sets of climate projections derived from General Circulation Models (GCMs) run under two emission scenarios (Representative Concentration Pathways, RCP2.6, and RCP8.5). RCP2.6, a climate mitigation scenario, targets to maintain the temperature increase within 2 °C. On the other hand, RCP8.5 is considered as business-as-usual scenario (Stocker *et al.*, 2013a, Stocker *et al.*, 2013b). The climate projections from four GCMs (the Community Climate System Model Version 3 (CCSM3), the HADley center Global Environment Model Version 2 – Earth System Model (hadgem2-es), the Max-Planck-Institute (mpi_lr), and the CANadian Earth System Model (canesm2) are selected, which represent a broad range of uncertainties raised by the climate model. The downscaled CMIP5 climate data were obtained from http://gdo-dcp.ucllnl.org/downscaled_cmip_projections/dcpInterface.html. The climate variables, including daily average temperature, daily maximum temperature, daily minimum temperature, and daily precipitation were processed to drive the DLEM model. The projected atmospheric nitrogen deposition during the 21st century was derived from the Atmospheric Chemistry and Climate Model Intercomparison Project (Lamarque *et al.*, 2013). The data for basic soil physical and chemical properties, including bulk density, soil texture, soil pH were obtained from Harmonized World Soil Database and assumed unchanged during the study period (Hurtt *et al.*, 2011). The prescribed wetland extent with seasonal variations was derived from multi-satellite observation (Surface WAter Microwave Product Series Version 2.0, SWAMP) together with an inventory based wetland dataset (Global Lakes and Wetlands Database, GLWD) (Lehner & Döll, 2004).

To address the projected CH_4 fluxes from the terrestrial ecosystems in response to the future climate change in the arctic and boreal region, we conducted two sets (S1 and S2) of

simulations (twenty simulations in total) (Table 1). In the S1, the simulations were conducted by considering all the environmental changing factors, such as climatic variables and nitrogen deposition under the specific scenarios (RCP2.6 or RCP8.5). In the S2, only one single factor would change throughout the study period and the rest of environmental factors would keep the level in 2006.

5.4 Results and discussion

5.4.1 Future Changes in Multiple Environmental Factors

In the 21st century, the arctic and boreal regions will experience substantial environmental changes, such as climate change and shifts in the atmospheric composition according to the RCP2.6 and RCP8.5 scenarios (Fig. 5.1). Both temperature and precipitation are expected to increase in varying degrees under different scenarios. Temperature is projected to increase at a rate of 0.13 ± 0.06°C/decade (Avg. ± Std., thereafter), and 0.81 ± 0.14°C/decade under the RCP2.6 and RCP8.5 scenarios, respectively, with the largest increase under hadgem2-es\RCP8.5 scenario (~0.98°C/decade) and the smallest increase under ccsm4\RCP2.6 scenario (~0.07°C/decade). Using the recent decade (2001-2010) as a baseline, precipitation is projected to increase 8% (18%) at the end of 21st century under the RCP2.6 (RCP8.5) scenarios, respectively, with the largest increase under canesm2\RCP8.5 scenario (~31%) and the smallest increase under mpi_lr\RCP2.6 scenario (~5%). The atmospheric nitrogen deposition is projected to decrease significantly at a rate of 9.67 mgN/m2/decade under the RCP2.6 and fluctuate greatly with no significant trend under the RCP8.5.

5.4.2 Projected Changes in CH_4 Flux under Future Environmental Changes.

The DLEM estimated CH_4 emission from wetlands is projected to increase from 31.90 Tg C in the 2000s to 33.41±1.87 Tg C/yr and 49.82±5.32 Tg C/yr in 2099 under RCP2.6 and

RCP8.5, respectively (Fig. 5.2). Compared with the 2000s, the projected CH_4 emission is expected to increase from 2%~65% in the 2090s. The Mann-Kendall trend test was used to examine the trend of estimated CH_4 emission during 2001-2099. The estimated CH_4 emission showed a significant increasing trend ($p < 0.0001$) under almost all the scenarios, except under the ccsm4\RCP2.6 and mpi_lr\RCP2.6 scenarios ($p < 0.05$). The largest increase in projected CH_4 emission during the study period was found under the hadgem2-es\RCP8.5 scenario (~2.62 Tg C/decade) and the smallest increase occurred under the mpi_lr \RCP2.6 scenario (~0.12 Tg C/decade).

The DLEM-estimated CH_4 fluxes from uplands are projected to increase from -1.94 Tg C in the 2000s to -2.10 ±0.19 Tg C/yr and -3.40±0.33 Tg C/yr in 2099 under RCP2.6 and RCP8.5, respectively (Here, negative indicates the CH_4 uptake from the soil). The Mann-Kendall trend test indicates that the CH_4 uptake is projected increase significantly ($p < 0.0001$) under almost all the scenarios, except under the ccsm4\RCP2.6 and mpi_lr\RCP2.6 scenarios ($p < 0.05$). The largest increase in projected CH_4 uptake during the study period was found under the hadgem2-es\RCP8.5 scenario (~0.24 Tg C/decade, ~98% increase in the 2090s compared with 2000s) and the smallest increase was under the ccsm4 \RCP2.6 scenario (~0.01 Tg C/decade, ~11% increase in the 2090s compared with 2000s).

The relative increase in the DLEM-estimated CH_4 uptake from uplands is larger than that in the CH_4 emissions from wetland under each scenario in the 2090s compared with the 2000s, but the amount of increase in the estimated CH_4 uptake is much smaller than that in the estimated CH_4 emissions. Therefore, net balance of the projected CH_4 fluxes showed an increasing trend and contributed to global warming.

The magnitude of the DLEM estimated net CH_4 fluxes during the 2000s was comparable with previous studies, ranging from 25.5~42 Tg C/yr in this region (Chen *et al.*, 2015, Walter *et al.*, 2001, Zhu *et al.*, 2013). Stocker *et al.* (2013a) and Zhuang *et al.* (2006) suggested that the projected CH_4 emission showed an increasing trend from wetlands over the 21_{st} century, which was identical to our results. Chen *et al.* (2015) implied that the potential impact of warming temperature on CH_4 emissions might be weakened in the Pan-arctic region by the end of 21^{st} century. Under the policy and no-policy scenarios, Zhu *et al.* (2013) suggested that the annual changing rate of CH_4 fluxes was around 0.08 and 0.29 Tg C/yr, respectively, which was similar to our estimation (~0.02 and 0.21 Tg C/yr under the RCP2.6 and RCP8.5 scenarios).

5.4.3 Seasonal Variation in Projected CH_4 Fluxes

The projected CH_4 fluxes exhibit significant seasonal variability in the arctic and boreal region. The projected CH_4 emissions from wetland in summer (June, July and August) accounts for the largest portion (62% ~ 69%) of annual emission, followed by autumn (September, October and November;18% ~ 26%), spring (March, April and May; 10%~18%), and winter (December, January and February) under all scenarios. Meanwhile, around half (44%~55%) of the projected CH_4 uptake occur in summer, followed by autumn (23%~28%), spring (15%~21%) and winter (7%~12%). Using the general circulation model (GCM), Shindell *et al.* (2004) projected that CH_4 emissions are dramatically enhanced in summer, which is consistent with the estimation from this study.

The projected trend of CH_4 fluxes from both wetlands and uplands exhibit great spatial variability among four seasons and eight scenarios (Fig. 5.3). Our simulations suggest that the significant increasing trend of CH_4 emissions from wetland was found in summer, autumn and spring. The Hudson Bay Lowland (HBL), north and northeast Alaska, and the West Siberian

Lowland (WSL) are identified as the hotspot for the projected CH_4 emissions with the largest increase during the study period, especially in summer. Previous studies also confirmed that the WSL and the HBL acted as strong CH_4 sources in the northern high latitudes (Stocker *et al.*, 2013a, Zhu *et al.*, 2013). At the same time, an apparent decreasing trend of the projected CH_4 emissions from wetland was found in the HBL and WSL in spring and HBL near Quebec in summer. In general, the projected CH_4 uptake exhibit the increasing trend over almost the entire study region, except in the east Nunavut and north Quebec in Canada and northeast Central Siberian Plain and north Khabarovsk in Russia where the decreasing trend was found (Fig. 5.3).

5.4.4 Sub-Regional Differences

Regional analyses indicate that northern North America dominates the projected net CH_4 emissions over the entire study domain (67%~72%), followed by northern Asia (20%~26%) and northern Europe (6%~8%) under different scenarios. The projected net CH_4 emissions increase under the RCP8.5 scenarios is much greater than under the RCP2.6 scenarios and exhibits large spatial heterogeneity. The net CH_4 emissions are projected to increase most in the northern North America, ranging from 5±5% ~ 59±17% under the RCP2.6~RCP8.5. For the northern Asia and northern Europe, the projected CH_4 emissions were found to increase slightly with large uncertainties under different RCP2.6 scenarios (~2±14% and 1±6%), and increase dramatically under the RCP8.5 scenarios (~45±14% and 30±15%).

5.5 Conclusion and Future Research Needs

The CH_4 emissions from the arctic and boreal region with high carbon storage are considered a potentially large positive feedback in the future climate-carbon system and are irreversible on a human timescale. However, due to complex interactions of carbon and nitrogen cycles as well as large uncertainties of the hydrological response to climate change, our

understanding of the magnitude and timing of CH_4 fluxes in the 21st century remain limited. Here, we used a process-based land ecosystem model driven by downscaled climate data derived from a number of GCMs and N deposition to examine the CH_4 fluxes over the arctic and boreal region in the 21st century. Our results indicate both the CH_4 emission and uptake are projected to increase under the future scenarios. The projected CH_4 emission increase is larger under the RCP85 than RCP26 scenarios and exhibits the great spatial heterogeneity. The projected CH_4 emissions in summer account for the largest portion of annual emission and show the largest increase during the 21st century. The change in climate factors is the dominant contributor to an increase in the projected CH_4 fluxes.

Despite improved representation of the permafrost control on the CH_4 related processes, the DLEM still lacks some features which are important in the arctic and boreal region, such as the absence of insulating effect of organic carbon (Chen *et al.*, 2015), the vegetation successional processes in response to the future climate change and hydrological variation (Lawrence *et al.*, 2015). In addition, the current version of the DLEM only considered the CH_4 related processes happened in the top 50 cm, which may underestimate the CH_4 emission since field studies suggested that permafrost thawing could be active in deeper soil layers associated with warming climate (Schneider von Deimling *et al.*, 2015, Shiklomanov *et al.*, 2010, Wu & Zhang, 2010). In this study, the wetland extent was prescribed over the 21st century. One recent study indicated that the warming climate may dry out wetland and reduce wetland extent (Lawrence *et al.*, 2015). On the contrary, other studies indicated that additional amount of CH_4 (~11Tg CH4/y) could be released due to the expansion of wetland in summer (Shindell *et al.*, 2004). Thus, future studies need to incorporate better hydrological processes to improving our understanding of the response of CH_4 fluxes to future climate in the arctic and boreal region.

5.6 References

Banger K, Tian HQ, Zhang BW, Lu CQ, Ren W, Tao B (2015) Biosphere-atmosphere exchange of methane in India as influenced by multiple environmental changes during 1901-2010. Atmospheric Environment, 192-200.

Burke EJ, Hartley IP, Jones CD (2012) Uncertainties in the global temperature change caused by carbon release from permafrost thawing. The Cryosphere, **6**, 1063-1076.

Chen X, Bohn T, Lettenmaier D (2015) Model estimates of climate controls on pan-Arctic wetland methane emissions. Biogeosciences, **12**, 6259-6277.

Dijkstra FA, Prior SA, Runion GB, Torbert HA, Tian H, Lu C, Venterea RT (2012) Effects of elevated carbon dioxide and increased temperature on methane and nitrous oxide fluxes: evidence from field experiments. Frontiers in Ecology and the Environment, **10**, 520-527.

Frolking S, Talbot J, Jones MC, Treat CC, Kauffman JB, Tuittila E-S, Roulet N (2011) Peatlands in the Earth's 21st century climate system. Environmental Reviews, **19**, 371-396.

Hugelius G, Strauss J, Zubrzycki S *et al.* (2014) Estimated stocks of circumpolar permafrost carbon with quantified uncertainty ranges and identified data gaps. Biogeosciences, **11**, 6573-6593.

Hungate BA, Van Groenigen KJ, Six J *et al.* (2009) Assessing the effect of elevated carbon dioxide on soil carbon: a comparison of four meta- analyses. Global Change Biology, **15**, 2020-2034.

Hurtt GC, Chini LP, Frolking S *et al.* (2011) Harmonization of land-use scenarios for the period 1500-2100: 600 years of global gridded annual land-use transitions, wood harvest, and resulting secondary lands. Climatic Change, **109**, 117-161.

Kang H, Freeman C, Ashendon TW (2001) Effects of elevated CO 2 on fen peat biogeochemistry. Science of The Total Environment, **279**, 45-50.

Kimball B, Kobayashi K, Bindi M (2002) Responses of agricultural crops to free-air CO 2 enrichment. Advances in Agronomy, **77**, 293-368.

Koven CD, Ringeval B, Friedlingstein P *et al.* (2011) Permafrost carbon-climate feedbacks accelerate global warming. Proceedings of the National Academy of Sciences, **108**, 14769-14774.

Lamarque J-F, Dentener F, Mcconnell J *et al.* (2013) Multi-model mean nitrogen and sulfur deposition from the Atmospheric Chemistry and Climate Model Intercomparison Project (ACCMIP): evaluation historical and projected changes.

Lawrence D, Koven C, Swenson S, Riley W, Slater A (2015) Permafrost thaw and resulting soil moisture changes regulate projected high-latitude CO2 and CH4 emissions. Environmental Research Letters, **10**, 094011.

Lehner B, Döll P (2004) Development and validation of a global database of lakes, reservoirs and wetlands. Journal of Hydrology, **296**, 1-22.

Liu L, Greaver TL (2009) A review of nitrogen enrichment effects on three biogenic GHGs: the CO2 sink may be largely offset by stimulated N2O and CH4 emission. Ecology Letters, **12**, 1103-1117.

O'shea S, Allen G, Gallagher M *et al.* (2014) Methane and carbon dioxide fluxes and their regional scalability for the European Arctic wetlands during the MAMM project in summer 2012. Atmospheric Chemistry and Physics, **14**, 13159-13174.

Ren W, Tian HQ, Xu XF *et al.* (2011) Spatial and temporal patterns of CO2 and CH4 fluxes in China's croplands in response to multifactor environmental changes. Tellus Series B-Chemical and Physical Meteorology, **63**, 222-240.

Saarnio S, Alm J, Martikainen PJ, Silvola J (1998) Effects of raised CO2 on potential CH4 production and oxidation in, and CH4 emission from, a boreal mire. Journal of Ecology, **86**, 261-268.

Saarnio S, Saarinen T, Vasander H, Silvola J (2000) A moderate increase in the annual CH4 efflux by raised CO2 or NH4NO3 supply in a boreal oligotrophic mire. Global Change Biology, **6**, 137-144.

Saarnio S, Silvola J (1999) Effects of increased CO2 and N on CH4 efflux from a boreal mire: a growth chamber experiment. Oecologia, **119**, 349-356.

Schädel C, Schuur EA, Bracho R *et al.* (2014) Circumpolar assessment of permafrost C quality and its vulnerability over time using long- term incubation data. Global Change Biology, **20**, 641-652.

Schneider Von Deimling T, Grosse G, Strauss J *et al.* (2015) Observation-based modelling of permafrost carbon fluxes with accounting for deep carbon deposits and thermokarst activity. Biogeosciences, **12**, 3469-3488.

Schuur E, Mcguire A, Schädel C *et al.* (2015) Climate change and the permafrost carbon feedback. Nature, **520**, 171-179.

Schuur EA, Abbott B (2011) Climate change: High risk of permafrost thaw. Nature, **480**, 32-33.

Shiklomanov NI, Streletskiy DA, Nelson FE *et al.* (2010) Decadal variations of active- layer thickness in moisture- controlled landscapes, Barrow, Alaska. Journal of Geophysical Research: Biogeosciences, **115**.

Shindell DT, Walter BP, Faluvegi G (2004) Impacts of climate change on methane emissions from wetlands. Geophysical Research Letters, **31**.

Stocker BD, Roth R, Joos F *et al.* (2013a) Multiple greenhouse-gas feedbacks from the land biosphere under future climate change scenarios. Nature Climate Change, **3**, 666-672.

Stocker TF, Qin D, Plattner GK *et al.* (2013b) IPCC, 2013: climate change 2013: the physical science basis. Contribution of working group I to the fifth assessment report of the intergovernmental panel on climate change.

Tian HQ, Chen GS, Liu ML *et al.* (2010a) Model estimates of net primary productivity, evapotranspiration, and water use efficiency in the terrestrial ecosystems of the southern United States during 1895-2007. Forest Ecology and Management, **259**, 1311-1327.

Tian HQ, Chen GS, Lu CQ *et al.* (2015a) Global methane and nitrous oxide emissions from terrestrial ecosystems due to multiple environmental changes. Ecosystem Health and Sustainability, **1**, art4.

Tian HQ, Lu CQ, Ciais P *et al.* (2016) The terrestrial biosphere as a net source of greenhouse gases to the atmosphere. Nature, **531**, 225-228.

Tian HQ, Lu CQ, Melillo J *et al.* (2012) Food benefit and climate warming potential of nitrogen fertilizer uses in China. Environmental Research Letters, **7**.

Tian HQ, Lu CQ, Yang J *et al.* (2015b) Global patterns and controls of soil organic carbon dynamics as simulated by multiple terrestrial biosphere models: Current status and future directions. Global Biogeochemical Cycles, **29**, 775-792.

Tian HQ, Xu XF, Liu ML, Ren W, Zhang C, Chen GS, Lu CQ (2010b) Spatial and temporal patterns of CH4 and N2O fluxes in terrestrial ecosystems of North America during 1979-2008: application of a global biogeochemistry model. Biogeosciences, **7**, 2673-2694.

Tian HQ, Yang QC, Najjar RG, Ren W, Friedrichs MaM, Hopkinson CS, Pan SF (2015c) Anthropogenic and climatic influences on carbon fluxes from eastern North America to the Atlantic Ocean: A process-based modeling study. Journal of Geophysical Research: Biogeosciences, **120**, 757-772.

Van Groenigen KJ, Osenberg CW, Hungate BA (2011) Increased soil emissions of potent greenhouse gases under increased atmospheric CO2. Nature, **475**, 214-216.

Walter BP, Heimann M, Matthews E (2001) Modeling modern methane emissions from natural wetlands: 1. Model description and results. Journal of Geophysical Research: Atmospheres, **106**, 34189-34206.

Wu Q, Zhang T (2010) Changes in active layer thickness over the Qinghai- Tibetan Plateau from 1995 to 2007. Journal of Geophysical Research: Atmospheres, **115**.

Xu XF, Tian HQ, Zhang C *et al.* (2010) Attribution of spatial and temporal variations in terrestrial methane flux over North America. Biogeosciences, **7**, 3637-3655.

Zhu X, Zhuang Q, Gao X, Sokolov A, Schlosser CA (2013) Pan-Arctic land–atmospheric fluxes of methane and carbon dioxide in response to climate change over the 21st century. Environmental Research Letters, **8**, 045003.

Zhuang Q, Melillo JM, Sarofim MC *et al.* (2006) CO2 and CH4 exchanges between land ecosystems and the atmosphere in northern high latitudes over the 21st century. Geophysical Research Letters, **33**.

Table 5.1 Experimental design

	Simulation Experiments	Temperature and Precipitation (4 GCMs)								Nitrogen Deposition	
		CCSM3		HADGEM2-ES		MPI-LR		CANESM2		RCP2.6	RCP8.5
		RCP2.6	RCP8.5	RCP2.6	RCP8.5	RCP2.6	RCP8.5	RCP2.6	RCP8.5		
S1	S1_CCSM3_RCP2.6	●	○	○	○	○	○	○	○	●	○
	S1_CCSM3_RCP8.5	○	●	○	○	○	○	○	○	○	●
	S1_HADGEM2-ES_RCP2.6	○	○	●	○	○	○	○	○	●	○
	S1_HADGEM2-ES_RCP8.5	○	○	○	●	○	○	○	○	○	●
	S1_MPI-LR_RCP2.6	○	○	○	○	●	○	○	○	●	○
	S1_MPI-LR_RCP8.5	○	○	○	○	○	●	○	○	○	●
	S1_CANESM2_RCP 2.6	○	○	○	○	○	○	●	○	●	○
	S1_CANESM2_RCP 8.5	○	○	○	○	○	○	○	●	○	●
S2	S2_CCSM3_RCP2.6	●	○	○	○	○	○	○	○	○	○
	S2_CCSM3_RCP8.5	○	●	○	○	○	○	○	○	○	○
	S2_HADGEM2-ES_RCP2.6	○	○	●	○	○	○	○	○	○	○
	S2_HADGEM2-ES_RCP8.5	○	○	○	●	○	○	○	○	○	○
	S2_MPI-LR_RCP2.6	○	○	○	○	●	○	○	○	○	○
	S2_MPI-LR_RCP8.5	○	○	○	○	○	●	○	○	○	○
	S2_CANESM2_RCP 2.6	○	○	○	○	○	○	●	○	○	○
	S2_CANESM2_RCP 8.5	○	○	○	○	○	○	○	●	○	○
	S2_Ndep_RCP 2.6	○	○	○	○	○	○	○	○	●	○
	S2_Ndep_RCP 8.5	○	○	○	○	○	○	○	○	○	●

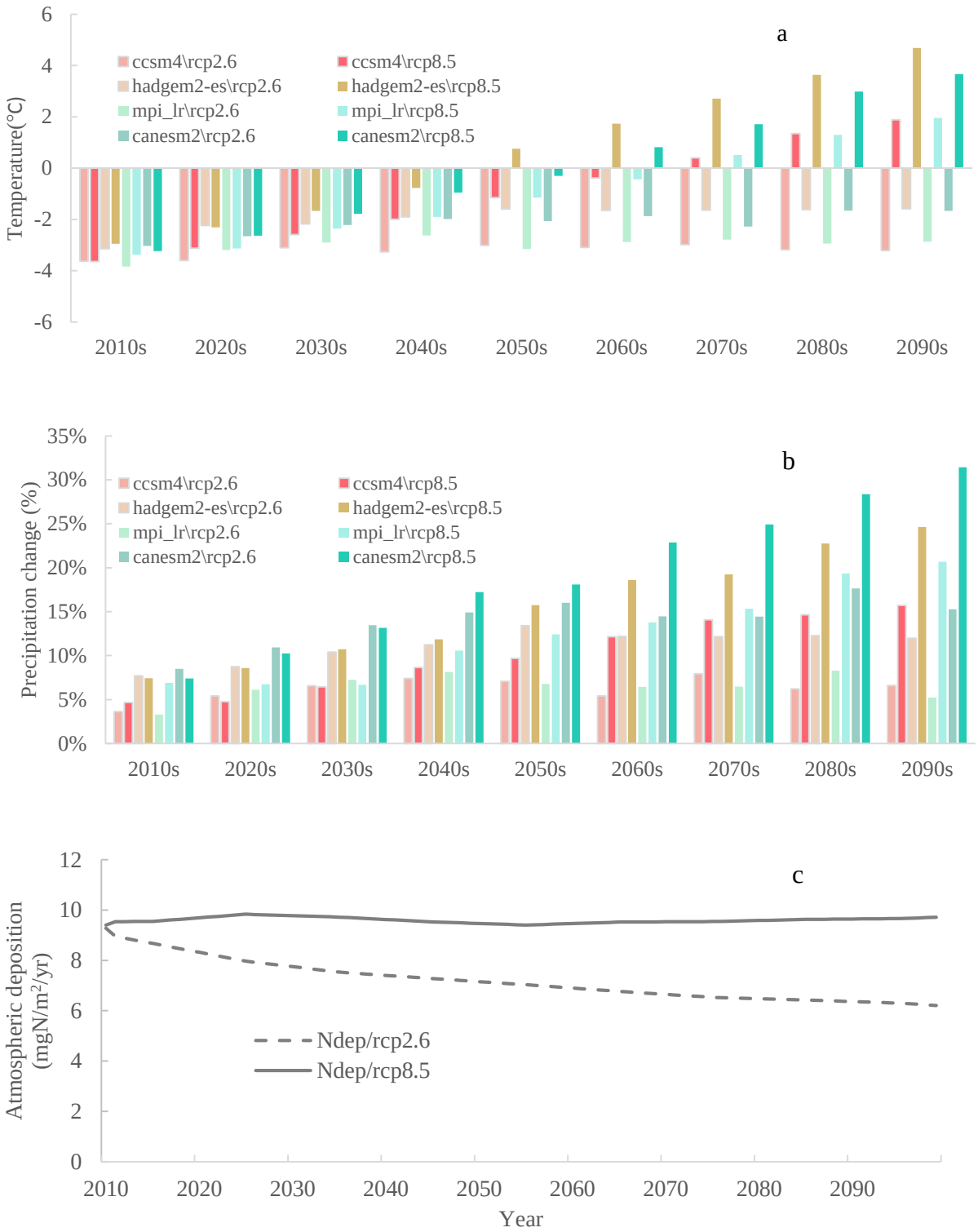

Figure 5.1 Projected changes in 10-year averages of temperature (^{o}C) (a) and precipitation (%) (b) during 2011-2099 relative to the 10-year average of 2001-2010; and (c) projected atmospheric nitrogen deposition under the RCP2.6 and RCP8.5 scenarios

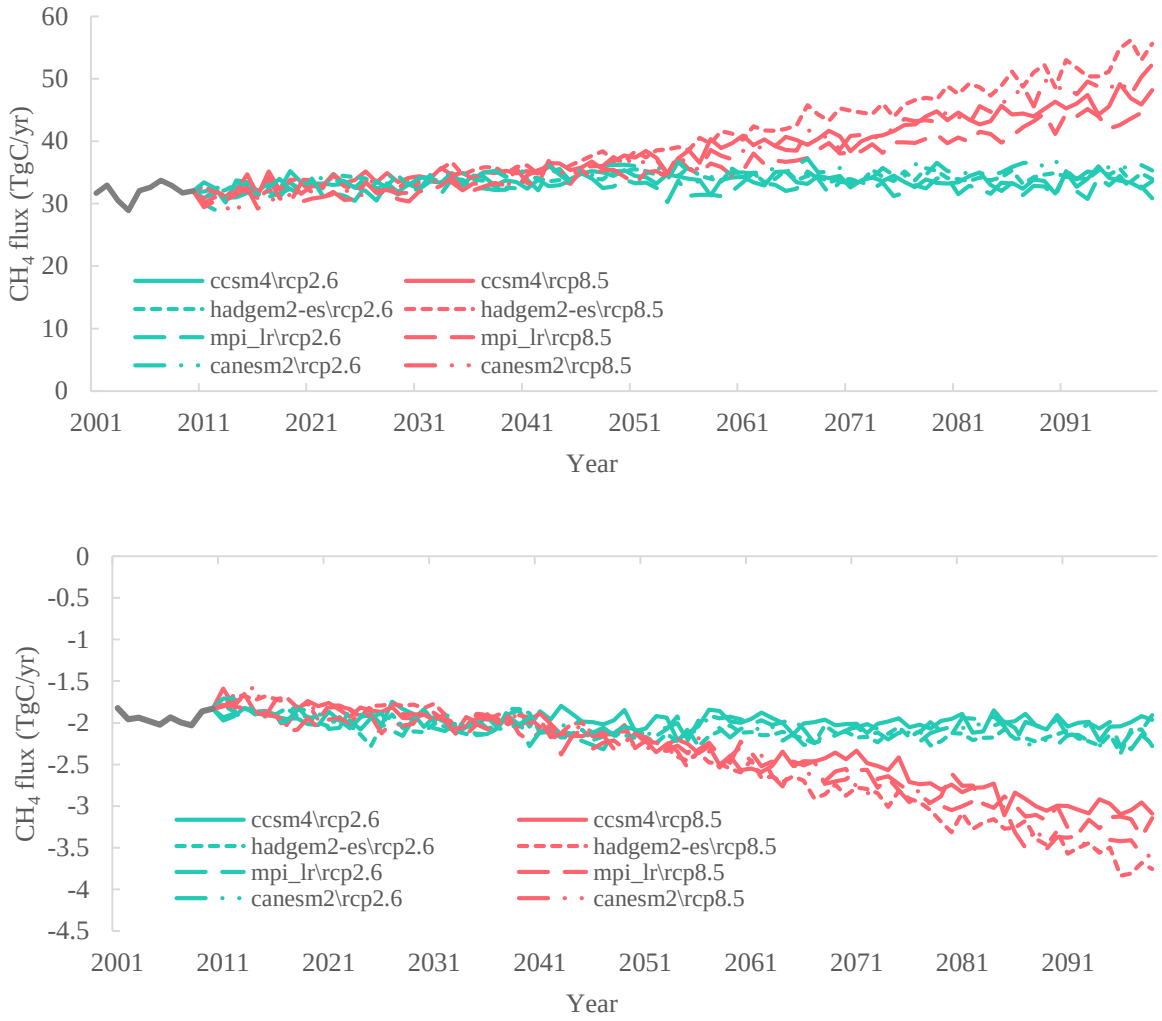

Figure 5.2 Projected interannual variations of CH_4 fluxes from (a) wetlands and (b) uplands in the arctic-boreal region during 2001-2099

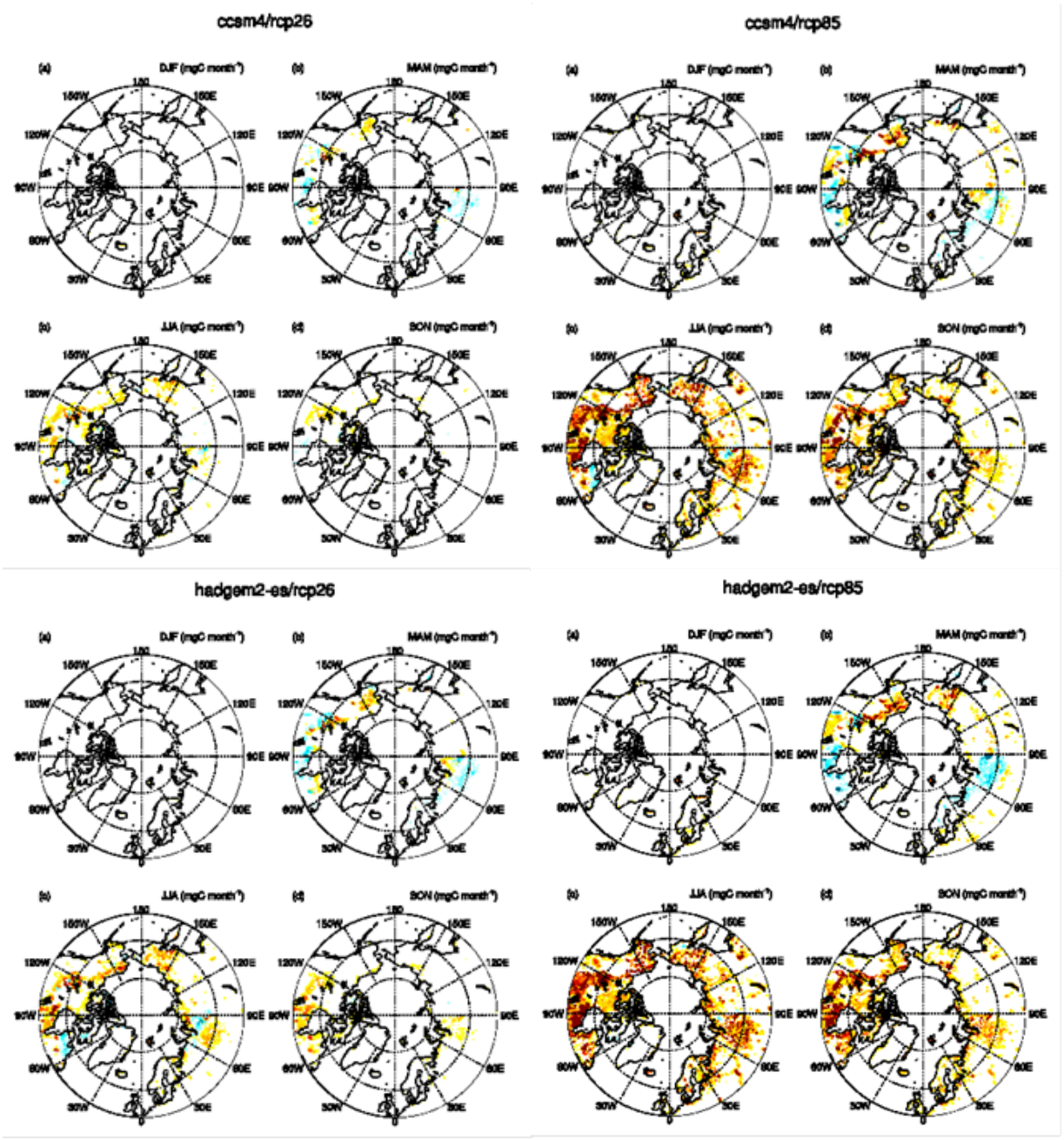
ccsm4/rcp26
ccsm4/rcp85
hadgem2-es/rcp26
hadgem2-es/rcp85
(a) DJF (mgC month⁻¹)
(b) MAM (mgC month⁻¹)
(c) JJA (mgC month⁻¹)
(d) SON (mgC month⁻¹)

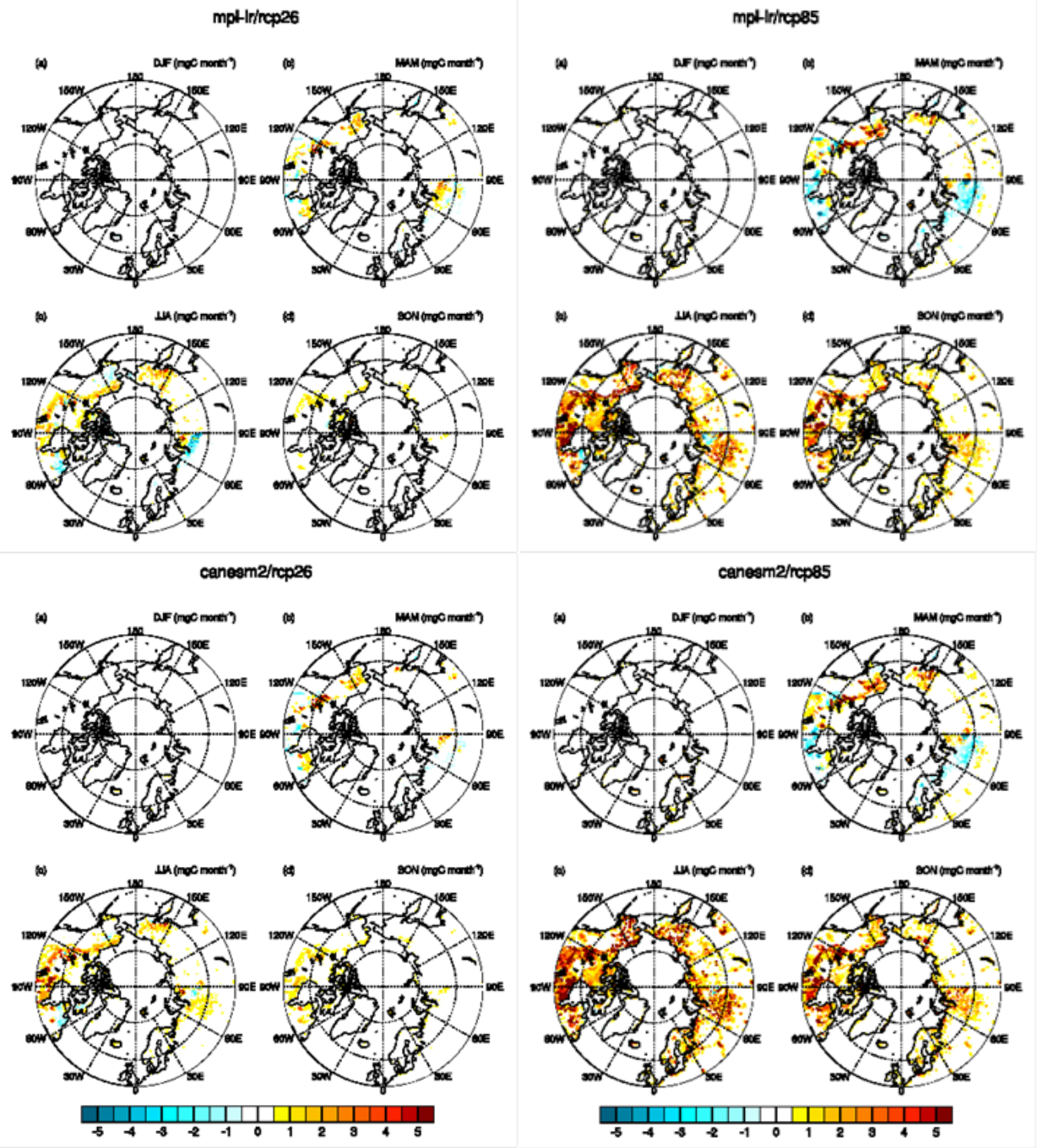
mpi-lr/rcp26
mpi-lr/rcp85
canesm2/rcp26
canesm2/rcp85
(a) DJF (mgC month⁻¹)
(b) MAM (mgC month⁻¹)
(c) JJA (mgC month⁻¹)
(d) SON (mgC month⁻¹)
-5 -4 -3 -2 -1 0 1 2 3 4 5

ccsm4/rcp26

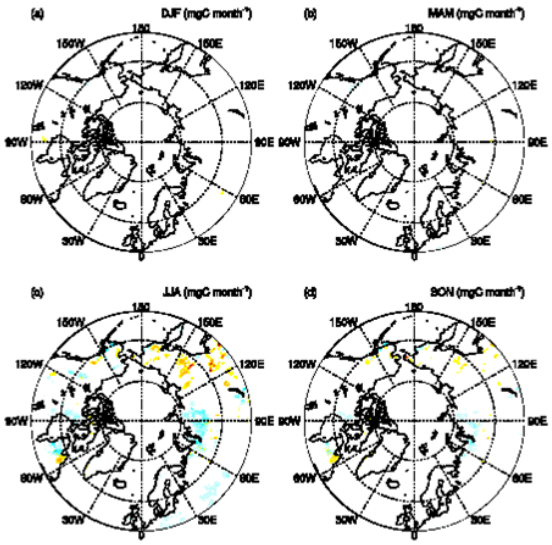

ccsm4/rcp85

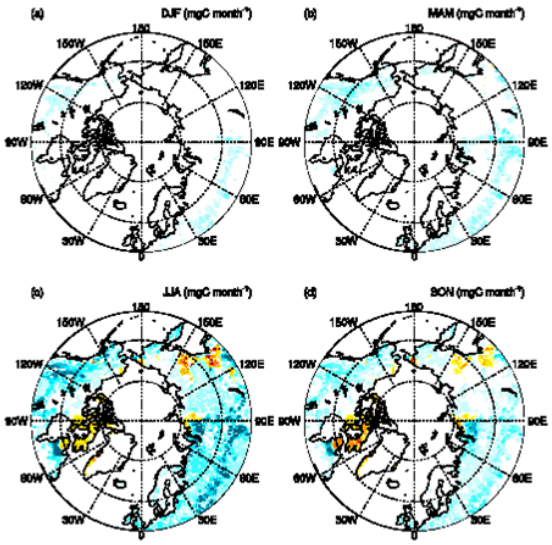

hadgem2/rcp26

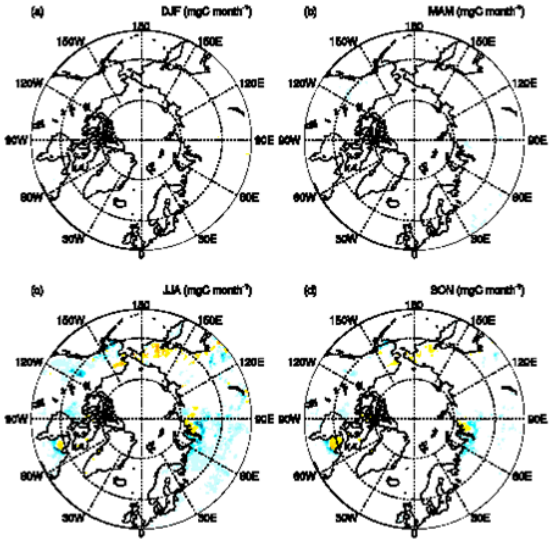

hadgem2/rcp85

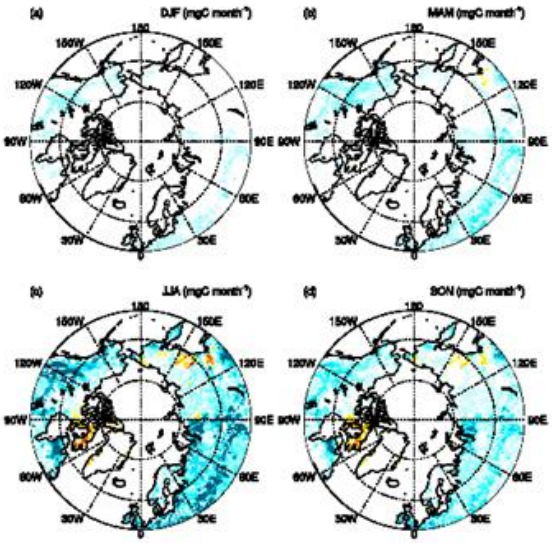

mpi-lr/rcp26

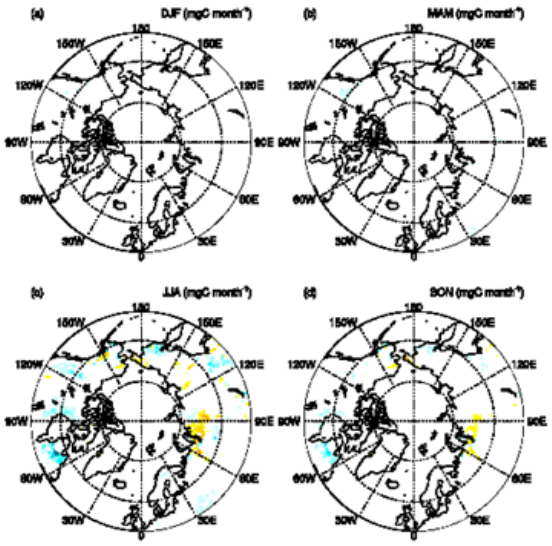

mpi-lr/rcp85

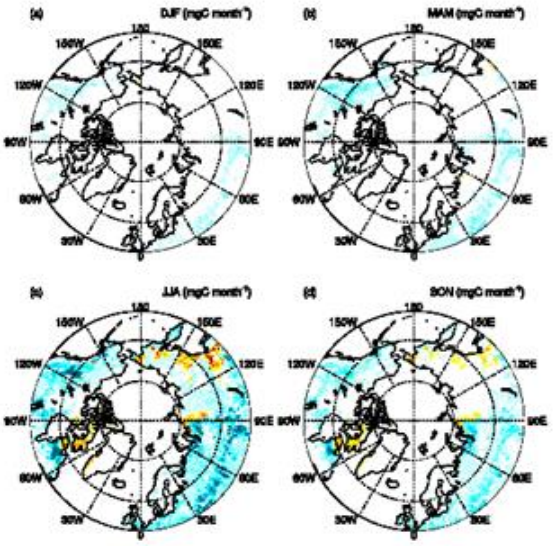

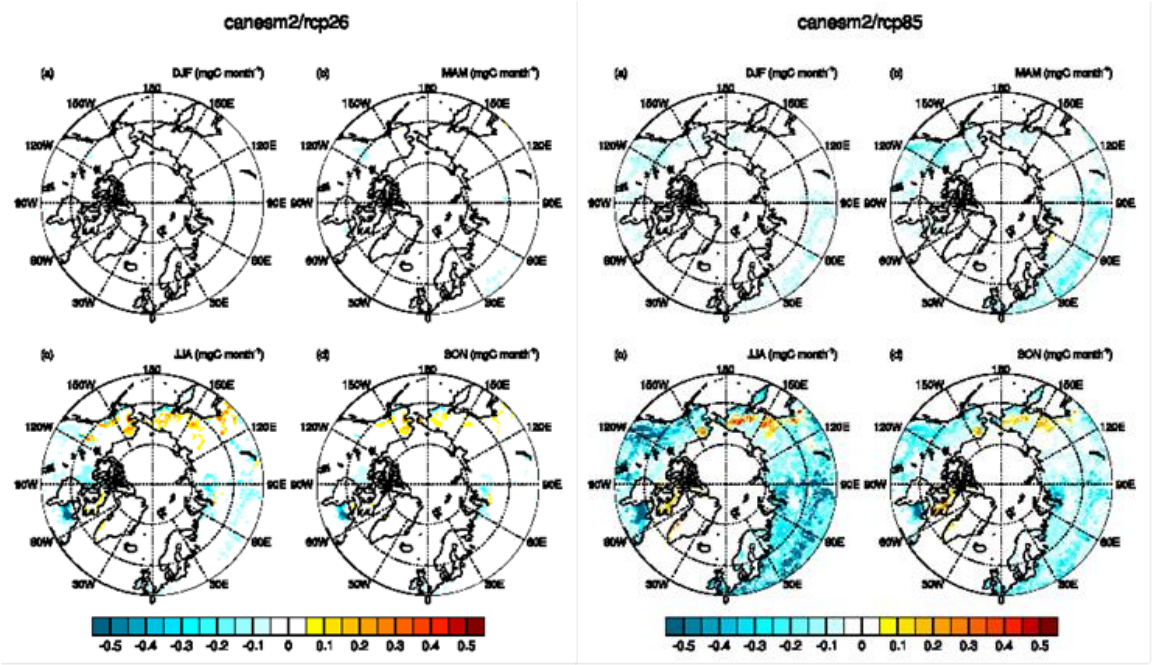

Figure 5.3 Projected seasonal trend of CH_4 fluxes from (i) wetland and (ii) upland in the arctic-boreal region during 2001-2099 under different scenarios.

Chapter 6

Methane Emissions from Global Wetlands: Assessing the Estimation Uncertainty from Various Wetland Extent Datasets

6.1 Abstract

Reliable estimation of methane (CH_4) fluxes in terrestrial ecosystems relies on the accuracy of wetland extent data. However, it remains uncertain to what extent different wetland data explain the modeling divergence in the global CH_4 estimation. In this study, we adopted five wetland datasets that are extensively used in modeling and statistical extrapolation of global CH_4 emission. Among them, three were one-phase static wetland datasets (GISS, GLWD, and Kaplan) and two were time-series dynamic datasets (GIEMS and SWAMP). Large differences in the magnitude and spatial distribution of wetlands existed among these datasets. There was a large uncertainty range in the wetland area (7.8 ± 2.2 million km^2, Avg. ± 1 std. dev.), ranging from 5.3 million km^2 (GISS) to 10.2 million km^2 (SWAMP), with the largest discrepancy in the tropical region. By feeding these datasets into a dynamic land ecosystem model (DLEM), we further examined how different wetland datasets could bias model-estimated CH_4 emissions from global wetlands. The DLEM-estimated CH_4 emission from global wetland was 132.9 ± 37.2 Tg C/yr during 2000~2007, ranging from 106.0 Tg C/yr (GIEMS) to 197.6 Tg C/yr (GLWD). Low latitude regions accounted for the largest portion (~72 ± 7%) of the estimated CH_4 emission from wetlands and also had the largest uncertainty. Among 6 continents, the largest uncertainties were found in South America while the least in Europe and Australia. Tropics dominated the inter-

annual variations of global CH_4 emissions from wetlands. Methane emissions derived from static wetland datasets and GIEMS showed an opposite trend during 1993-2005. The intra-annual variation patterns in estimated CH_4 emissions agreed well, with the peak emissions in July and August. To reduce uncertainty in estimating CH_4 emission from global wetlands, it is critical to developing a robust dataset delineating dynamic wetland extent and the inter-annual and intra-annual variation of inundation patterns, particularly in the tropical region.

6.2 Introduction

Carbon dioxide (CO_2), methane (CH_4) and nitrous oxide (N_2O) account for more than 87% of the radioactive forcing (RF) due to long-lived greenhouse gases (LLGHGs) (WMO, 2015). Among them, methane ranks as the second largest RF (Ciais *et al.*, 2014). The global warming potential (GWP) of CH_4 is 28 times higher than that of CO_2 at 100-year time horizon (Myhre *et al.*, 2013). In 2014, the global abundance (as mole fractions) of CH_4 had already reached 1833±1 ppb, increased by 254% since pre-industrial time (WMO, 2015). The relative increase of CH_4 is 1.8 and 2.1 times higher than that of CO_2 and N_2O, respectively. The shorter lifetime (~9 years) and higher GWP make CH_4 a good candidate to reduce the human-induced climate warming (Dlugokencky *et al.*, 2011, Tian *et al.*, 2016). Although CH_4 is considered as an important GHG, it also determines the oxidizing capacity of troposphere by removing hydroxyl radical and subsequently changing the level of water vapor through CH_4 oxidation and the climate influence of HFCs and HCFCs in the stratosphere (Ciais *et al.*, 2014, Montzka *et al.*, 2011). Thus, the change of atmospheric CH_4 concentration could cause a quick response to the climate (Tian *et al.*, 2016).

Among all natural and anthropogenic sources, wetlands are considered to be the single largest CH_4 source, and contribute 40%-50% of the total CH_4 emission (Bohn *et al.*, 2015, Kirschke *et al.*, 2013). Despite the crucial role of anthropogenic emission from a long-term perspective, CH_4 emission from wetlands likely dominated the inter-annual variability of CH_4 sources and determined the fluctuation of CH_4 growth rate in the recent two decades (Bousquet *et al.*, 2006, Pison *et al.*, 2013). Previous research has intensively examined CH_4 emission from wetland ecosystems through bottom-up (BU: e.g., inventory, statistical extrapolation of local flux measurements, process-based modeling) and top-down (TD: atmospheric inversions) approaches

(Kirschke *et al.*, 2013, Tian *et al.*, 2016), and an increasing number of site and regional observations derived from field experiments, eddy covariance from tall towers and aircraft data (Desai *et al.*, 2015, Zona *et al.*, 2016). However, there are still large discrepancies in the estimated magnitude and spatial-temporal variation of CH_4 emission (Kirschke *et al.*, 2013, Melton *et al.*, 2013). Recent reviews suggest that wetlands contribute the largest absolute uncertainty from all the CH_4 emission categories, with a min-max range of 107 Tg CH_4 yr^{-1}, approximately 49.3% of the global total estimate (Kirschke *et al.*, 2013). The large uncertainties of CH_4 emission mainly come from variations in estimated flux density and wetland spatial extent (Bohn *et al.*, 2015, Kirschke *et al.*, 2013, Melton *et al.*, 2013).

To determine the extent of global wetlands, terrestrial ecosystem models in general either simulate the extent through a hydrological module or use the wetland spatial data from inventory or remote sensing observations (Melton *et al.*, 2013). However, model-simulated wetland extent tends to overestimate the wetland area and shows distinct patterns in spatial and temporal distribution compared to observed datasets (Melton *et al.*, 2013, Stacke & Hagemann, 2012). Wetland extent datasets derived from inventory or satellite observations are broadly used in land ecosystem models to estimate CH_4 emission and other biogeochemical processes at regional scale (Banger *et al.*, 2015, Bohn *et al.*, 2015, Ito & Inatomi, 2012, Melton *et al.*, 2013, Pison *et al.*, 2013, Zhuang *et al.*, 2015). However, lack of accurate knowledge on the spatial and temporal variations of wetland extent has impeded the understanding of related biogeochemical processes, such as CH_4 fluxes (Mitra *et al.*, 2005) and the feedbacks between CH_4 fluxes and future climate change (Zhu *et al.*, 2013). These knowledge gaps likely resulted in significant uncertainties and errors in the large-scale estimation of CH_4 emission (Bridgham *et al.*, 2013).

In this study, we applied the Dynamic Land Ecosystem Model (DLEM), a process-based model, which is driven by multiple environmental factors and has been widely used to estimate multiple greenhouse gas fluxes (Tian *et al.*, 2015a), to quantify the uncertainties of global and regional-scale estimations of CH_4 emission due to multiple wetland datasets. Our major objectives were to 1) examine the difference in the magnitude, spatial and temporal patterns of wetland extent among different datasets; 2) estimate the magnitude of the uncertainty of estimated CH_4 fluxes induced by different wetland datasets; and 3) compare the differences in spatial and temporal variations of estimated CH_4 fluxes induced by different wetland datasets.

6.3 Methodology

6.3.1 Wetland Datasets

In this study, we chose five wetland datasets, which were well recognized and broadly used by different studies to estimate the CH_4 emission and related biogeochemical processes. Matthews and Fung (1987) developed the first global distribution of wetland datasets from Goddard Institute for Space Studies (GISS) and classified wetlands into five types (forested bog, nonforested bog, forested swamp, nonforested swamp, and alluvial formations) with a spatial resolution of 1°. Based on the existing data, maps, and information, Lehner and Döll (2004) developed the Global Lakes and Wetlands Database (GLWD) in three coordinated levels. The GLWD-Level 3 provides a global coverage of maximum wetland extent, with a spatial resolution of 30', and divided into 9 wetland classes, including: (1) freshwater marsh, floodplain, (2) swamp forest, flooded forest, (3) coastal wetland, (4) pan, brackish/saline wetland, (5) bog, fen, mire, (6) intermittent wetland/lake, (7) 50-100% wetland, (8) 25-50% wetland, and (9), wetland complex (0-25% wetland) (Lehner & Döll, 2004). By using five major data sources (the Canadian peatland database (Tarnocai *et al.*, 2000), the U. S. National Land Cover Dataset

(Vogelmann *et al.*, 2001), Global land Cover 2000 dataset (JRC, 2003), CORINE90 Land Cover dataset (ETCTE, 2000), and GLWD (Lehner & Döll, 2004)), Kaplan (2007) created a global wetland map for 2003-2007, with a spatial resolution of 0.5°. The above datasets are all static wetland datasets. With the development of a multi-satellite observation methodology, Prigent and Papa generated the Global Inundation Extent from Multi-Satellites (GIEMS) dataset (Papa *et al.*, 2010, Prigent *et al.*, 2012). GIEMS, for the first time, provided the global coverage and monthly change of inundation extent from 1993-2007, and was later used in the multi-model intercomparison projects (Melton *et al.*, 2013). Recently, global wetland area and inundation dynamics from 2000 - 2012 were estimated at monthly time-step by using remote sensing based observations from the Surface WAter Microwave Product Series Version 2.0 (SWAMPS; Schroeder *et al.*, In preparation) in combination with GLWD (Poulter et al., In preparation). In this study, all the five datasets were transformed to the same spatial resolution of 0.5°.

6.3.2 Dynamic Land Ecosystem Model

The DLEM is a highly integrated process-based land ecosystem model, which is comprised of five major components: (1) biophysics, (2) plant physiology, (3) soil biogeochemistry, (4) dynamic vegetation, and (5) land use, land management practices and disturbance. The DLEM is able to make daily, spatially-explicit estimations of the exchange of water, carbon and nitrogen fluxes between land and the atmosphere and at the land-ocean interface (Tian *et al.*, 2015a, Tian *et al.*, 2015b). The major components and related processes have been extensively validated against site and regional data and measured fluxes from other studies (Tian *et al.*, 2010a, Tian *et al.*, 2015a, Tian *et al.*, 2012, Tian *et al.*, 2015b).

6.3.3 CH_4 Module

In the DLEM, the CH_4-related processes are assumed to occur in the top 50 cm of soil. The DLEM only accounts for CH_4 produced from dissolved organic carbon (DOC), which comes from the decomposition of litters and soil organic matter, and the byproduct of gross primary production (GPP). In the DLEM, the net CH_4 fluxes were collectively determined by CH_4 production, oxidation, and transportation from soil pore to the atmosphere.

CH_4 production is calculated using the Michaelis–Menten equations in the DLEM and is a function of DOC, soil pH, temperature, and soil moisture content. Methane oxidation occurs through three pathways, including atmospheric CH_4 oxidation, CH_4 oxidation in the soil pore water, and CH_4 oxidation during plant-mediated transport. CH_4 is assumed to be transported from soil pore to the atmosphere via ebullition, diffusion, and plant-mediated transport. More detailed information about the simulation of CH_4 fluxes were described in Tian *et al.* (2010b). The CH_4 module in the DLEM has already been extensively validated and applied at various spatial scales, including site, regional, and global scales (Banger *et al.*, 2015, Lu & Tian, 2013, Pan *et al.*, 2014, Pan *et al.*, 2015, Ren *et al.*, 2011, Tian *et al.*, 2015a, Tian *et al.*, 2010b, Xu & Tian, 2012). DLEM's performance in simulating daily and annual CH_4 fluxes has been evaluated against estimates from field observational data, inventory studies, other process-based and inverse models (Banger *et al.*, 2015, Bohn *et al.*, 2015, Tian *et al.*, 2011, Xu *et al.*, 2010). These evaluations have indicated that DLEM can generally capture the magnitude and daily/seasonal/annual patterns of CH_4 fluxes.

6.3.4 Other Model Input Data

To run the DLEM, the geo-referenced data with spatial resolution of 0.5° are grouped into two broad categories, which includes (1) Dynamic data at daily time-step (e.g., climate data - maximum, minimum, and mean air temperature, precipitation, relative humidity, and shortwave

solar radiation) and at annual time-step (e.g., datasets of atmospheric chemical components - atmospheric CO_2 concentration, AOT40 O_3 index and nitrogen deposition; datasets of land use and land management practices), and (2) One phase static data (e.g., dataset of soil properties - soil texture, soil pH, and soil bulk density; and other ancillary data, such as river network and topographic data). More specifically, daily climate data is derived from CRUNCEP 6-hourly climate datasets (http://dods.extra.cea.fr/store/p529viov/cruncep/V4_1901_2012/readme.htm). Atmospheric CO_2 concentration is obtained from Ice core and NOAA observations (http://www.esrl.noaa.gov/gmd/ccgg/trends/global.html#global_data). Atmospheric ozone index (AOT40- Accumulated Ozone exposure over a Threshold of 40 ppb) is used to represent the change of atmospheric ozone concentration (Felzer *et al.*, 2005, Ren *et al.*, 2007). Atmospheric nitrogen deposition data is developed based on 3-phase global datasets (Dentener *et al.*, 2006). The geo-reference information for the soil physical properties is derived from Harmonized World Soil Database (http://webarchive.iiasa.ac.at/Research/LUC/External-World-soil-database/HTML/). The land use and land cover data are generated by using HYDE 3.1 (Goldewijk *et al.*, 2011). The detailed information of generating the data for land management practices could be found in (Ren *et al.*, 2012, Ren *et al.*, 2011).

6.3.5 Model Experimental Design

To address the uncertainties of global and regional-scale estimations of CH_4 emission due to different wetland extents, we conducted ten simulations in total. By using each wetland dataset, we conducted two simulations. We first have the model reach equilibrium state by using averaged climate data from 1901-1930 and keeping all other input variables constant at the level in 1900. After the initial run, the model was run another 900 years for the spin-up with de-trended climate data from 1901 to 2012 and followed by the transient simulation by

incorporating other environmental drivers during 1901-2012. For one-phase static wetland datasets (GISS, GLWD, and Kaplan), we assumed the wetland extent didn't change over the time. For time-series dynamic wetland datasets (GIEMS and SWAMP), we extracted the seasonal trend from long-term mean wetland extent and applied to the study period beyond the observation period.

6.3.6 Analysis and Statistical Method

To keep consistent, the period 2000-2007 (the overlapped period from all wetland datasets) was chosen to quantify the uncertainties in the estimated CH_4 emission among all wetland datasets. The cross-data standard deviation was determined when driven by multi-wetland datasets.

6.4 Results

6.4.1 Uncertainties in Wetland Datasets

Based on the five wetland datasets, we found that the global wetland area was 7.8±2.2 (Avg. ± 1 std. dev.) million km^2 varied from 5.3 million km^2 (GISS) to 10.2 million km^2 (SWAMP). All datasets agreed that low-latitude region (LLR, 30°S-30°N) had the largest wetland area (3.4±1.1 million km^2, Fig. 6.1a), which accounted for about 43±4% of the total wetland area. Among the five datasets, GISS had the smallest wetland area in the LLR (~1.9 million km^2, 37% of the global wetland area from GISS), while GIEMS had the largest area (~4.3 million km^2, 47% of the global wetland area from GIEMS). Middle-latitude region (MLR, 30° - 60°N and S) occupied around 36±1% of the global wetland area (~2.8±0.9 million km^2). The estimated wetland area for GISS and Kaplan matched well, which was around 1.8 ~2.0 million km^2 while the estimate was around 3.2~3.4 million km^2 in GLWD and GIEMS. SWAMP showed the largest estimation of 3.9 million km^2 in MLR, which was two times more than the

estimate from GISS. The high-latitude region (HLR, 60° - 90° N and S) accounted for 20±5% of the global total wetland area. GISS, GLWD, and GIEMS all suggested that the wetland area was around 1.4~1.5 million km^2, with Kaplan showed the least estimation (~1.1 million km^2) and SWAMP showed the largest estimation (~2.1 million km^2). If taking a close look at the latitudinal distribution, all the dataset except GIEMS showed a peak wetland distribution around 60°N-66°N, where large areas of peatland distributed (Fig. 6.2), GIEMS showed larger wetland extent in 20°N-33°N as compared to other four datasets, owing to the inclusion of the inundated rice paddy land.

At the continental scale, all datasets except GIEMS agreed that about one-third of wetland area is located in Asia, while GIEMS showed 43% of wetland area in this continent due to its inclusions of rice paddy land (Fig. 6.2b). North America accounted for about 28 ± 8% of the global wetland area. Africa and South America accounted for 14 ± 3% and 14 ± 1% of the total global wetland area, respectively. Europe and Oceania shared the least portion of the global wetland area.

The temporal variation in wetland extent could be observed from dynamic wetland datasets (GIEMS and SWAMP). The changing trend of wetland extent was negligible in North America and Europe in winter (December ~ February, DJF), with decreasing trend being found in South America from both datasets. GIEMS showed an apparently decreasing trend of the wetland extent in Canada, the West Siberian Lowland (WSL), India and East China in summer (June ~ August, JJA) during 1993-2007 (Fig. 6.3). SWAMP showed an apparent increase in wetland extent at northern high latitude, especially in the Hudson Bay Lowland (HBL) and the WSL in spring (March ~ May, MAM), summer and autumn (September ~ November, SON) during 2000-2012 (Fig. 6.3). The wetland extent in Alaska, Alberta, and Northwest Territories of

Canada was found to decline in summer and autumn. The wetland extent in swamp forest and floodplain extent in South America showed a decreasing trend all year round during 2000-2012. The inter-annual comparison indicated that wetland extent fluctuated from 1993 to 2007, with an overall decreasing rate of 67,700 km^2/yr from January 1993 to mid-2000 followed by a small increasing trend (Prigent *et al.*, 2012). For the SWAMP, a significant reduction of wetland area (~26,946 km^2/yr) was observed during June, July, and August during 2000~2012, which is mainly caused by the reduction of wetland area in the tropical area (Poulter et al., in preparation). For the intra-annual variations, both datasets agreed that wetland area reached the maximum extent in August, and the minimum extent in December.

6.4.2 Uncertainties in the Spatial Variation of CH_4 Emission

Poor agreements on the estimation of CH_4 emission were found at both global and regional scales, which was mainly due to the inconsistent estimation of wetland extent from different datasets (Fig. 6.4). The estimated CH_4 emission from global wetlands was around 132.9±37.2 Tg C/yr, with the maximum CH_4 emission from the GLWD (197.6 Tg C/yr) and the minimum emission from the GIEMS (106.0 Tg C/yr). LLR had the largest portion (~72±7%) of CH_4 emission, followed by MLR (~25 ±6 %) and HLR contributed the least (~9 ± 2%). The largest inconsistency was found in LLR, which was 96.3 ± 28.9 Tg C/yr, ranging from 68.3 Tg C/yr (GIEMS) to 140.9 Tg C/yr (GLWD). The mean CH_4 emission in MLR was 32.9 ± 10.2 Tg C/yr, with smaller estimation from GISS (23.7 Tg C/yr) and Kaplan (24.2 Tg C/yr) and higher estimation from SWAMP (42.7 Tg C/yr) and GLWD (44.9 Tg C/yr). For the HLR, CH_4 emission was 11.1 ± 2.6 Tg C/yr, ranging from 8.8 Tg C/yr (Kaplan and GIEMS) to 15.0 Tg C/yr (SWAMP).

Among the six continents, South America was the largest contributor to wetland CH_4 emission (~40.1 ±17.4 Tg C/yr), followed by Asia (~35.6 ±8.5 Tg C/yr), Africa (~26.2 ±10.3 Tg C/yr), and North America (~22.7 ±9.9 Tg C/yr) (Fig. 6.4). Europe and Oceania shared the least portion of the CH_4 emission, which was 4.8 ±2.3 and 3.6 ±1.2 Tg C/yr, respectively. The largest uncertainties in CH_4 emission were found in South America and Africa. In South America, CH_4 emission from GLWD (~69.7 Tg C/yr) was about two times larger than those from other datasets (24.8 Tg C/yr from GIEMS and 39.6 Tg C/yr from SWAMP). In Africa, the largest estimation was from GLWD, followed by Kaplan, GISS, SWAMP, and GIEMS. In Asia, lower estimations were found from GISS (26.1 Tg C/yr), Kaplan (31.1 Tg C/yr) and SWAMP (31.7 Tg C/yr), while higher estimations were from GLWD (42.8 Tg C/yr) and GIEMS (46.0 Tg C/yr). In North America, the highest estimation from GLWD (~38.3 Tg C/yr) was over three times higher than the estimation from GISS (~12.5 Tg C/yr). In contrast, in Europe, the highest estimation was from GISS (~8.7 Tg C/yr), which was over two times higher than those from GLWD (~3.2 Tg C/yr) and Kaplan (~3.1 Tg C/yr). In Oceania, CH_4 emission was similar from all datasets (3.6 ~ 4.9 Tg C/yr), except GIEMS (~1.6 Tg C/yr). We found that GLWD has larger wetland area in South America, Africa, Australia, and North America than other datasets, GIEMS has larger wetland area in Asia, while GISS has larger wetland area in Europe, which is roughly consistent with the model estimated divergence in CH_4 flux driven by these data.

6.4.3 Uncertainties in Temporal Variation of CH_4 Emission

To make the interannual variation pattern comparable, the estimated anomalous fluxes were determined by subtracting the averaged CH_4 emission during the overlapped period (2000-2007) from all simulations (Fig. 6.4). The CH_4 anomalies from all static wetland datasets (i.e., GISS, GLWD and Kaplan) showed similar inter-annual variations at all latitudinal bands since

wetland extents was not changed and the inter-annual variations was owing to the changing environmental factors.

The largest inter-annual variation in CH_4 emission occurred in the LLR (Fig. 6.5). The CH_4 fluxes from the three static wetland datasets showed a significant increasing trend with a mean rate of 0.24 Tg C/yr during 1993-2005. On the contrary, CH_4 fluxes from GIEMS demonstrated a significant decreasing trend with a rate of 0.69 Tg C/yr during1993-2005. After 2007, the patterns of interannual variation in CH_4 fluxes were similar among GISS, GLWD, Kaplan and SWAMP, but with different magnitudes. For the MLR, the experiment with GIEMS showed a higher and positive anomalous CH_4 fluxes before 1997, while the rest four datasets have similar interannual variations, decreasing before 1997 and keeping neutral or slightly increasing after that. For the HLR, all the simulation experiments agree that the estimated anomalous CH_4 fluxes showed a reduction from 1993 to 1997, and followed a small fluctuation, with an abrupt high positive anomaly in 2005, 2007 and 2012.

Although significant difference in CH_4 emission magnitudes were found based on all wetland datasets, the estimated CH_4 showed a similar intra-annual/seasonal variation (Fig. 6.6). Methane fluxes decreased slightly from January to February, and then started to increase and reached the peak emissions in July and August. After that, CH_4 emission began to decrease, in which around 60% of annual emission occurred during May-October. GLWD and SWAMP still led to the highest monthly estimations of CH_4 emission from global wetlands, compared to other datasets.

6.5 Discussion

6.5.1 Wetland Datasets

There are large discrepancies on both the magnitude and spatial distribution of wetland extents among different datasets (Zhu & Gong, 2014). The differences in wetland extents from different datasets may be partially due to the difference in the definition and classification of wetland types, the accuracy, limitations and computational uncertainties of methodologies, the duration, and time of the project. In this study, each dataset classified wetlands into different types. For example, in GISS, 5 types of wetlands (forested bog, forested swamp, alluvial formations, non-forested bog and non-forested swamp) were identified; while in GLWD, 9 types of wetlands (a. freshwater marsh, floodplain; b. swamp forest, flooded forest; c. coastal wetland; d. pan, brackish/saline wetland; e. bog, fen, mire; f. intermittent wetland/lake; g. 50-100% wetland; h. 25-50% wetland; and i. wetland complex (0-25% wetland)) were identified. Meanwhile, the wetland datasets were collected at different time periods. The wetland area may be different due to the wetland drainage, land conversion, freezing and thawing, etc. Here, we applied all the wetland datasets to estimate CH_4 emission during the same period, which could be used to quantify the data-driven modeling uncertainties in CH_4 estimation.

Due to the limitation of observational methodology, each dataset had its own weakness. The GISS was generated by using three independent datasets, including vegetation, soil properties, and fractional inundation maps (Matthews & Fung, 1987). The magnitude of estimated wetland extent from GISS was two times smaller than the estimation from other datasets in this study. The GLWD aimed to produce the maximum global wetland extent based on previous maps, data, and information (Lehner & Döll, 2004). Three classes (0-25% wetland; 25%-50% wetland; 50%-100% wetland) were provided as the fractional range, which led to large uncertainties in previous modeling studies using the GLWD. Here, we set the representative wetland class as 12.5%, 25% and 75% for 0-25% wetland, 25%-50% wetland and 50%-100%

wetland, respectively. However, this could lead to an overestimation of wetland extents in North America in GLWD (Lehner & Döll, 2004). It also has been suggested that the GLWD may overestimate the wetland extent in arid or semiarid regions (Lehner & Döll, 2004, Melton *et al.*, 2013). In addition, previous study conducted in the WSL suggested that the GLWD underestimate the wetland area in the tundra region while overestimate the wetland area in the northwest of WSL (Bohn *et al.*, 2015). However, GLWD still represents the best 1km global static water-related land cover dataset so far (Prigent et al., 2016). The static wetland datasets, in general, fail to capture the variation of wetland extents over time. GIEMS and SWAMP are the only datasets which considered the dynamic inundation extent with global coverage. However, quite a large area of wetlands was not inundated all the time. For example, in the HLR, some wetlands are frozen when soil temperature is lower than 0°C, which could only periodically or even never experience the inundated condition (Prigent *et al.*, 2007). The inundation datasets derived from multi-satellite observations could not accurately represent the wetland without standing water, but with the water table beneath the peatland surface, in which the soil is well saturated and could produce considerable amounts of CH_4 (Melton *et al.*, 2013). It has been suggested that GIEMS may underestimate the peatland area in the HBL. Meanwhile, it may also underestimate some small wetlands, which comprises less than 10% fractional coverage of a grid cell, and also the inundation area under dense forest canopy (Prigent *et al.*, 2007).

6.5.2 Estimated CH_4 Emissions Driven by Wetland Datasets

Existing wetland datasets were widely used for CH_4 flux estimation at both global and regional levels. Here, we identified large discrepancies of the wetland extent and quantified the resulting model estimation spread of wetland CH_4 emission by using the same model and various wetland datasets at both regional and global scale. Both wetland extent and distribution

determined the magnitude of CH_4 fluxes. For model-estimated CH_4 fluxes, larger wetland areas could lead to more CH_4 emission. The same magnitude of difference in wetland area could produce substantially different amounts of CH_4 emission at different locations due to different CH_4 producing capabilities per unit area. For example, CH_4 producing capability was greater in the tropical region than in the HLR. This was mainly due to enhanced microbial activity in a warmer climate throughout the year. In the HLR, large amounts of CH_4 emission mainly occurred during the growing season. Tropics contribute 50~70% of wetland emission (Bousquet *et al.*, 2006, Montzka *et al.*, 2011, Ringeval *et al.*, 2014). Here we found there was more than two times difference in wetland extents in the tropical region from five datasets, which could bring considerable uncertainties to the estimation of CH_4 emission. A series of more accurate and dynamic wetland distributions are needed for the estimation of CH_4 emission and other purposes.

Different wetland datasets were extensively used in previous studies, especially by process-based models to estimate the CH_4 emission from wetlands. At the global scale, the multi-model intercomparison project (WETCHIMP) used the GIEMS to estimate wetland emission, which was 143 ± 29 (106 ± 8~198 ± 9) Tg C/yr from different models. By applying the seasonal variation from GIEMS to the GISS derived annual mean inundation together with GLWD, VISIT showed that CH_4 emission from wetlands was around 127.2 ± 4.8 ~ 144.0 ± 6.2 Tg CH_4/yr (Ito & Inatomi, 2012). Ringeval *et al.*, (2011) tried to address the climate-CH_4 feedback from wetlands and its interaction with the climate-CO_2 feedback by using GIEMS during 1993-2000. Other studies estimated the regional CH_4 emissions by adopting wetland distribution from different datasets. An intercomparison of wetland CH_4 emissions models over West Siberian considered six wetland maps, including two regional wetland maps, the Northern Circumpolar Soil Carbon Database, GLWD, GIEMS, and SWAMP, which suggested that GISS and SWAMP

underestimated part of the peatland without inundation, but overestimated the wetland area by including permanent water body due to the polluted signal from remote sensed observation (Bohn *et al.*, 2015, Prigent *et al.*, 2007). The HBL, the second largest boreal wetland, covers approximately 10% of the Earth's total northern wetland (Pickett-Heaps *et al.*, 2011, Worthy *et al.*, 2000). In this region emission rates are dominated by temperature restricted thaw season (Kuhlmann *et al.*, 1998), which is particularly vulnerable to current and future climate change condition. By using the GEOS-Chem chemical transport model, the mean annual emission in HBL is estimated to be 2.3 Tg C/yr (Pickett-Heaps *et al.*, 2011). In WETCHIMP, eight models estimated the CH_4 flux in the HBL by using GIEMS datasets, which ranged from 1.7±0.2 to 8.5±5.9 Tg C/yr (Melton *et al.*, 2013). In this study, based on different wetland extent data and one model, we obtained a similar estimation range of CH_4 emission from 1.4±0.1 to 6.4±0.4 Tg C/yr in the HBL.

The CH_4 emission from wetlands has long been identified as the dominant contributor to the recent variation of global CH_4 burden. Here, we found contrasting inter-annual variation in CH_4 fluxes between static wetland datasets and two dynamic wetland datasets. Dynamic wetland datasets could provide more inter-annual and intra-annual information of the change in wetland extent compared with other datasets. It has been suggested that during 1993-2007, global inundation extent showed a decreasing trend and tropical regions contributed more than 50% of the decline (Prigent et al., 2012). To get an accurate estimation of inter-annual variation of CH_4 emission from wetland, changes of wetland extent should not be ignored, which was missing from the static wetland datasets.

6.5.3 Future Research Needs

The magnitude of CH_4 emission from wetland ecosystems is still far from certain owing to various sources of uncertainties. Poor delineation of wetland extent and distribution has restricted the accuracy of model-derived flux estimation. The current knowledge about the wetland extent from different datasets led to inconsistent results. There is an urgent need to have a dataset delineating global dynamic wetland extent which provides the information on the inter-annual and intra-annual variation of wetlands. Dynamic wetland data could be used to examine: (1) the large differences in CH_4 emission between the continuous flooded wetlands and seasonal flooded wetlands (Chen *et al.*, 2013), (2) the importance of extreme climate (e.g., drought and flooding) on CH_4 fluxes, and (3) the importance of CH_4 emission anomalies owing to wetland area change. All these components are unlikely to be fully addressed with a static wetland database. Therefore, it is critical to have a robust dynamic wetland extent dataset with high spatial/temporal resolution and large area coverage. Model structure and underrepresented mechanisms also contribute to the uncertainty of estimated CH_4 fluxes. For example, most previous studies showed that the wetland in high latitude had weak CH_4 flux during the winter and spring (Matthews & Fung, 1987, Tian *et al.*, 2011, Walter *et al.*, 2001). However, recent studies showed that during the spring thaw, large amounts of CH_4 may be released to the atmosphere, mainly through ebullition (Song *et al.*, 2012, Tarnocai *et al.*, 2000). The maximum hourly emission rate could even reach to 10~50,000 mg $C/m^2/h$, which may be even higher than the CH_4 emission rate in the growing season (Song *et al.*, 2012, Tarnocai *et al.*, 2000). However, it is hard to track these CH_4 spikes due to great temporal variability and uncertainties in their distribution.

6.6 Conclusion

This study quantified the uncertainty in estimating wetland CH_4 emission by using five well-recognized wetland datasets. The wetland extents derived from the different datasets have over two-fold differences. Compared with the static wetland datasets, the dynamic wetland datasets could provide information on the inter-annual and intra-annual variation of wetland extent. There were extensive disagreements on the wetland distribution from the tropical to the northern high latitude region. Poor knowledge of current wetland extents has already impeded the estimation of CH_4 emission from the global wetland. The tropical regions contributed the largest portion of estimated CH_4 emission from wetland, but the magnitude of estimated CH_4 emission showed the least agreement from different datasets. From a continental perspective, the estimated CH_4 emission in GLWD was two times larger than the estimation from all other datasets in South America. In Africa, there was no consistency in estimated CH_4 emission from the datasets. Tropical regions dominated the inter-annual variation of estimated global CH_4 emission. Similar trends of inter-annual variation of CH_4 fluxes were found in the static wetlands but their inter-annual variation were different from that derived from dynamic wetland dataset. This study suggests that there is a critical need for accurately estimating CH_4 emission to develop a well-validated data set on global dynamic wetland extent with information on the inter-annual and intra-annual variation of inundation patterns, particularly in the tropical region.

6.7 References

Banger K, Tian HQ, Zhang BW, Lu CQ, Ren W, Tao B (2015) Biosphere-atmosphere exchange of methane in India as influenced by multiple environmental changes during 1901-2010. Atmospheric Environment, 192-200.

Bohn TJ, Melton JR, Ito A *et al.* (2015) WETCHIMP-WSL: intercomparison of wetland methane emissions models over West Siberia. Biogeosciences, **12**, 3321-3349.

Bousquet P, Ciais P, Miller JB *et al.* (2006) Contribution of anthropogenic and natural sources to atmospheric methane variability. Nature, **443**, 439-443.

Bridgham SD, Cadillo-Quiroz H, Keller JK, Zhuang QL (2013) Methane emissions from wetlands: biogeochemical, microbial, and modeling perspectives from local to global scales. Global Change Biology, **19**, 1325-1346.

Chen Y, Huang C, Ticehurst C, Merrin L, Thew P (2013) An evaluation of MODIS daily and 8-day composite products for floodplain and wetland inundation mapping. Wetlands, **33**, 823-835.

Ciais P, Sabine C, Bala G *et al.* (2014) Carbon and other biogeochemical cycles. In: *Climate Change 2013: The Physical Science Basis. Contribution of Working Group I to the Fifth Assessment Report of the Intergovernmental Panel on Climate Change.* pp Page., Cambridge University Press.

Dentener F, Drevet J, Lamarque J *et al.* (2006) Nitrogen and sulfur deposition on regional and global scales: a multimodel evaluation. Global Biogeochemical Cycles, **20**.

Desai AR, Xu K, Tian H *et al.* (2015) Landscape-level terrestrial methane flux observed from a very tall tower. Agricultural and Forest Meteorology, **201**, 61-75.

Dlugokencky EJ, Nisbet EG, Fisher R, Lowry D (2011) Global atmospheric methane: budget, changes and dangers. Philosophical Transactions of the Royal Society a-Mathematical Physical and Engineering Sciences, **369**, 2058-2072.

Etcte (2000) Corine land cover database (Version 12/2000 extended coverage), The European Topic Centre on Terrestrial Environment, European Environment Agency,.

Felzer B, Reilly J, Melillo J *et al.* (2005) Future effects of ozone on carbon sequestration and climate change policy using a global biogeochemical model. Climatic Change, **73**, 345-373.

Goldewijk KK, Beusen A, Van Drecht G, De Vos M (2011) The HYDE 3.1 spatially explicit database of human-induced global land-use change over the past 12,000 years. Global Ecology and Biogeography, **20**, 73-86.

Ito A, Inatomi M (2012) Use of a process-based model for assessing the methane budgets of global terrestrial ecosystems and evaluation of uncertainty. Biogeosciences, **9**, 759-773.

Jrc (2003) Global Land Cover 2000 database. European Commission, Joint Research Centre, Ispra, Italy. http://www.gvm.jrc.it/glc2000.

Kirschke S, Bousquet P, Ciais P *et al.* (2013) Three decades of global methane sources and sinks. Nature Geoscience, **6**, 813-823.

Kuhlmann A, Worthy D, Trivett N, Levin I (1998) Methane emissions from a wetland region within the Hudson Bay Lowland: An atmospheric approach. Journal of Geophysical Research: Atmospheres, **103**, 16009-16016.

Lehner B, Döll P (2004) Development and validation of a global database of lakes, reservoirs and wetlands. Journal of Hydrology, **296**, 1-22.

Lu CQ, Tian HQ (2013) Net greenhouse gas balance in response to nitrogen enrichment: perspectives from a coupled biogeochemical model. Global Change Biology, **19**, 571-588.

Matthews E, Fung I (1987) Methane emission from natural wetlands: Global distribution, area, and environmental characteristics of sources. Global Biogeochemical Cycles, **1**, 61-86.

Melton JR, Wania R, Hodson EL *et al.* (2013) Present state of global wetland extent and wetland methane modelling: conclusions from a model inter-comparison project (WETCHIMP). Biogeosciences, **10**, 753-788.

Mitra S, Wassmann R, Vlek PL (2005) An appraisal of global wetland area and its organic carbon stock. Current Science, **88**, 25.

Montzka SA, Dlugokencky EJ, Butler JH (2011) Non-CO2 greenhouse gases and climate change. Nature, **476**, 43-50.

Myhre G, Shindell D, Bréon F *et al.* (2013) Anthropogenic and natural radiative forcing. Climate change, **423**.

Pan SF, Tian HQ, Dangal SRS *et al.* (2014) Modeling and monitoring terrestrial primary production in a changing global environment: toward a multiscale synthesis of observation and simulation. Advances in Meteorology, **2014**.

Pan SF, Tian HQ, Yang QC *et al.* (2015) Responses of global terrestrial evapotranspiration to climate change and increasing atmospheric CO2 in the 21st century. Earth's Future, **3**, 15-35.

Papa F, Prigent C, Aires F, Jimenez C, Rossow W, Matthews E (2010) Interannual variability of surface water extent at the global scale, 1993–2004. Journal of Geophysical Research: Atmospheres, **115**.

Pickett-Heaps C, Jacob DJ, Wecht K *et al.* (2011) Magnitude and seasonality of wetland methane emissions from the Hudson Bay Lowlands (Canada). Atmospheric Chemistry and Physics, **11**, 3773-3779.

Pison I, Ringeval B, Bousquet P, Prigent C, Papa F (2013) Stable atmospheric methane in the 2000s: key-role of emissions from natural wetlands. Atmospheric Chemistry and Physics, **13**, 11609-11623.

Prigent C, Papa F, Aires F, Jimenez C, Rossow WB, Matthews E (2012) Changes in land surface water dynamics since the 1990s and relation to population pressure. Geophysical Research Letters, **39**.

Prigent C, Papa F, Aires F, Rossow W, Matthews E (2007) Global inundation dynamics inferred from multiple satellite observations, 1993–2000. Journal of Geophysical Research: Atmospheres, **112**.

Ren W, Tian HQ, Liu ML *et al.* (2007) Effects of tropospheric ozone pollution on net primary productivity and carbon storage in terrestrial ecosystems of China. Journal of Geophysical Research-Atmospheres, **112**.

Ren W, Tian HQ, Tao B, Huang Y, Pan SF (2012) China's crop productivity and soil carbon storage as influenced by multifactor global change. Global Change Biology, **18**, 2945-2957.

Ren W, Tian HQ, Xu XF *et al.* (2011) Spatial and temporal patterns of CO2 and CH4 fluxes in China's croplands in response to multifactor environmental changes. Tellus Series B-Chemical and Physical Meteorology, **63**, 222-240.

Ringeval B, Houweling S, Van Bodegom P, Spahni R, Van Beek R, Joos F, Röckmann T (2014) Methane emissions from floodplains in the Amazon Basin: challenges in developing a process-based model for global applications. Biogeosciences, **11**, 1519-1558.

Schroeder R, Mcdonald K, Chan S *et al.* (In preparation) Development and evaluation of a multi-year global inundated area dataset derived from combined active/passive microwave remote sensing.

Song C, Xu X, Sun X *et al.* (2012) Large methane emission upon spring thaw from natural wetlands in the northern permafrost region. Environmental Research Letters, **7**, 034009.

Stacke T, Hagemann S (2012) Development and validation of a global dynamical wetlands extent scheme. Hydrology and Earth System Science, **16**, 2915-2933.

Tarnocai C, Kettles IM, Lacelle B (2000) Peatlands of Canada Database. Geological Survey of Canada Open File Report 3834.

Tian H, Lu C, Ciais P *et al.* (2016) The terrestrial biosphere as a net source of greenhouse gases to the atmosphere. Nature, **531**, 225-228.

Tian HQ, Chen GS, Liu ML *et al.* (2010a) Model estimates of net primary productivity, evapotranspiration, and water use efficiency in the terrestrial ecosystems of the southern United States during 1895-2007. Forest Ecology and Management, **259**, 1311-1327.

Tian HQ, Chen GS, Lu CQ *et al.* (2015a) Global methane and nitrous oxide emissions from terrestrial ecosystems due to multiple environmental changes. Ecosystem Health and Sustainability, **1**, art4.

Tian HQ, Lu CQ, Melillo J *et al.* (2012) Food benefit and climate warming potential of nitrogen fertilizer uses in China. Environmental Research Letters, **7**.

Tian HQ, Xu XF, Liu ML, Ren W, Zhang C, Chen GS, Lu CQ (2010b) Spatial and temporal patterns of CH4 and N2O fluxes in terrestrial ecosystems of North America during 1979-2008: application of a global biogeochemistry model. Biogeosciences, **7**, 2673-2694.

Tian HQ, Xu XF, Lu CQ *et al.* (2011) Net exchanges of CO2, CH4, and N2O between China's terrestrial ecosystems and the atmosphere and their contributions to global climate warming. Journal of Geophysical Research-Biogeosciences, **116**.

Tian HQ, Yang QC, Najjar RG, Ren W, Friedrichs MaM, Hopkinson CS, Pan SF (2015b) Anthropogenic and climatic influences on carbon fluxes from eastern North America to the Atlantic Ocean: A process-based modeling study. Journal of Geophysical Research: Biogeosciences, **120**, 757-772.

Vogelmann JE, Howard SM, Yang L, Larson CR, Wylie BK, Van Driel N (2001) Completion of the 1990s National Land Cover Data Set for the Conterminous United States from Landsat Thematic Mapper Data and Ancillary Data Sources, Photogrammetric Engineering and Remote Sensing, 67:650-652. http://landcover.usgs.gov.

Walter BP, Heimann M, Matthews E (2001) Modeling modern methane emissions from natural wetlands 1. Model description and results. Journal of Geophysical Research-Atmospheres, **106**, 34189-34206.

Wmo (2015) World Meteorlogical Organization Greenhouse Gas Bulletin. pp Page, Citeseer.

Worthy DE, Levin I, Hopper F, Ernst MK, Trivett N (2000) Evidence for a link between climate and northern wetland methane emissions. Journal of Geophysical Research: Atmospheres, **105**, 4031-4038.

Xu XF, Tian HQ (2012) Methane exchange between marshland and the atmosphere over China during 1949–2008. Global Biogeochemical Cycles, **26**.

Xu XF, Tian HQ, Zhang C *et al.* (2010) Attribution of spatial and temporal variations in terrestrial methane flux over North America. Biogeosciences, **7**, 3637-3655.

Zhu P, Gong P (2014) Suitability mapping of global wetland areas and validation with remotely sensed data. Science China Earth Sciences, **57**, 2283-2292.

Zhu X, Zhuang Q, Gao X, Sokolov A, Schlosser CA (2013) Pan-Arctic land–atmospheric fluxes of methane and carbon dioxide in response to climate change over the 21st century. Environmental Research Letters, **8**, 045003.

Zhuang Q, Zhu X, He Y *et al.* (2015) Influence of changes in wetland inundation extent on net fluxes of carbon dioxide and methane in northern high latitudes from 1993 to 2004. Environmental Research Letters, **10**, 095009.

Zona D, Gioli B, Commane R *et al.* (2016) Cold season emissions dominate the Arctic tundra methane budget. Proceedings of the National Academy of Sciences, **113**, 40-45.

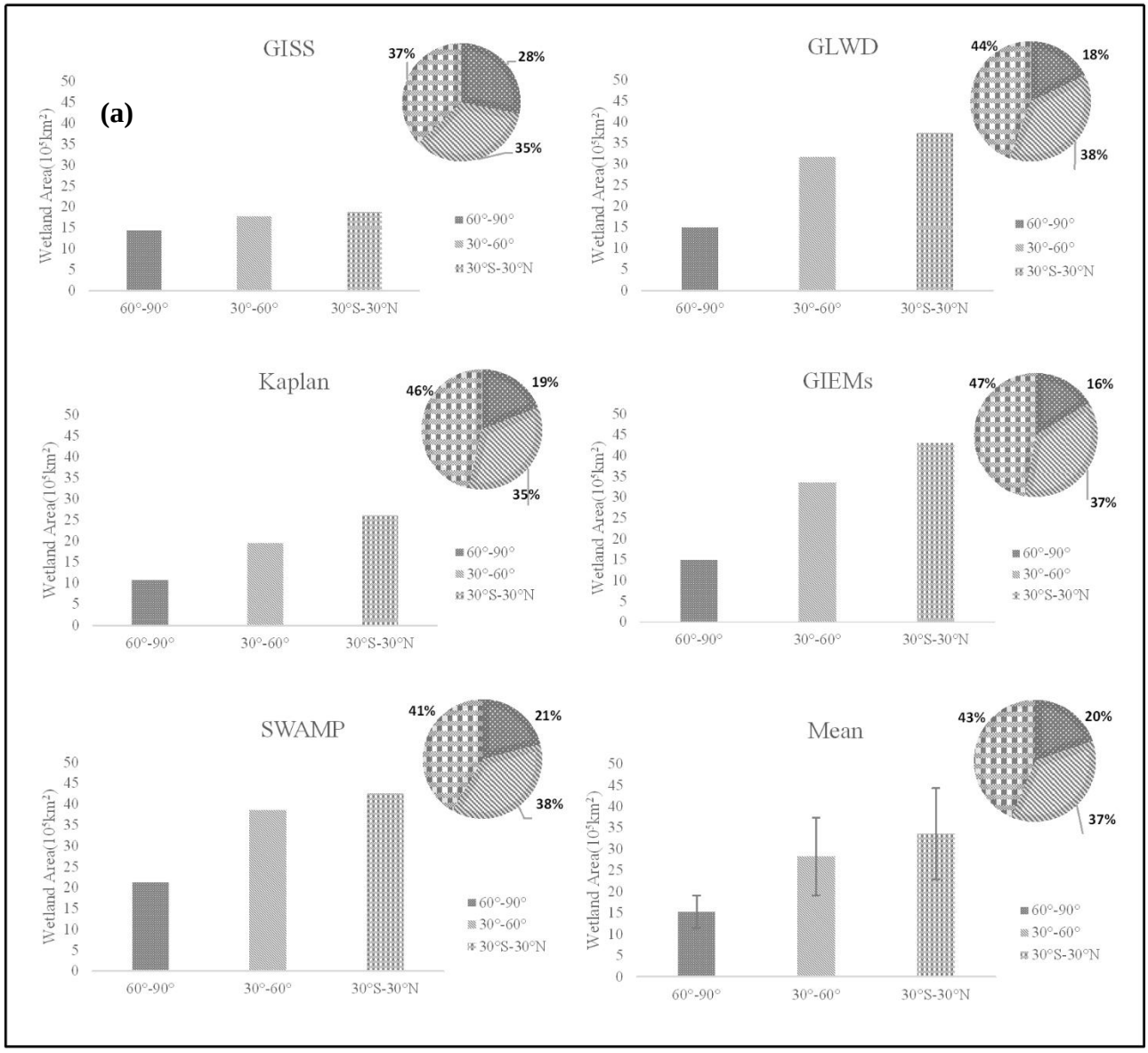
(a)
GISS
37%
28%
35%
GLWD
44%
18%
38%
Kaplan
46%
19%
35%
GIEMs
47%
16%
37%
SWAMP
41%
21%
38%
Mean
43%
20%
37%
Wetland Area(10^5km^2)
60°-90°
30°-60°
30°S-30°N

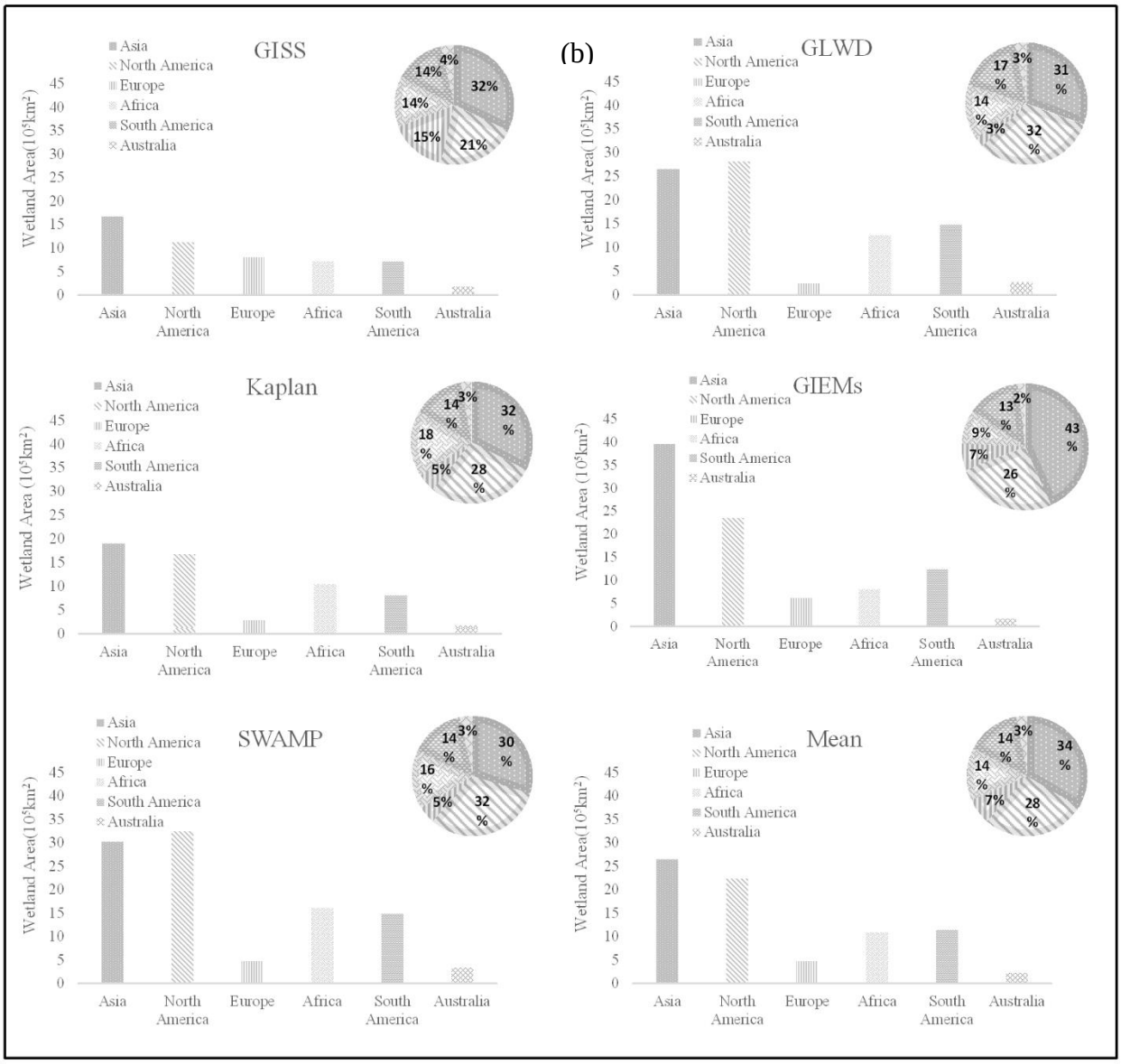

Figure 6.1 Wetland distribution at (a) high latitude region (HLR, 60° - 90° N and S), middle latitude region (MLR, 30° - 60° N and S) and low latitude region (LLR, 30°S -30°N), and (b) continental scale for different wetland datasets

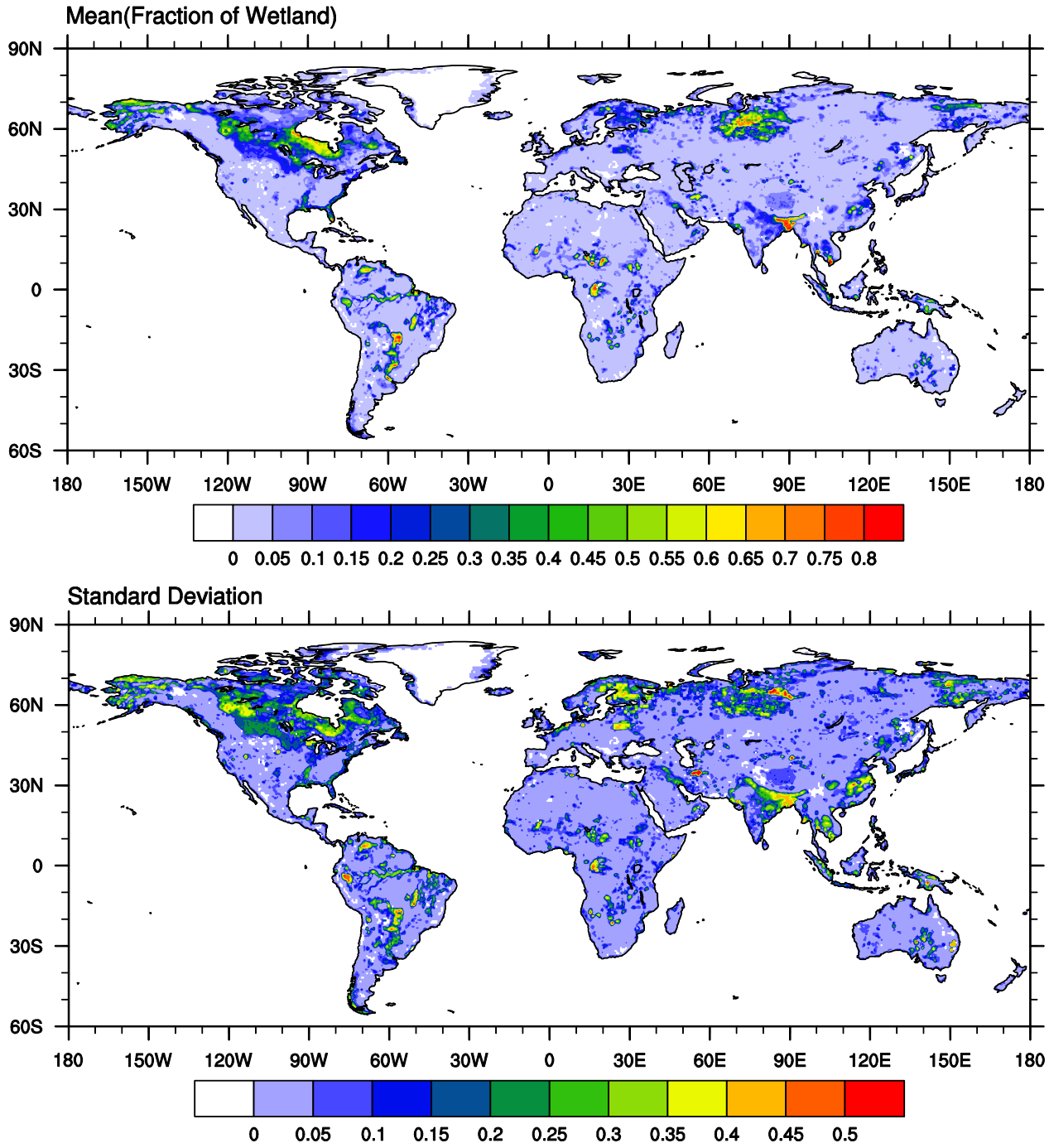

Figure 6.2 The spatial distribution of mean wetland fraction (top) and standard deviation (bottom) based on the 5 wetland datasets

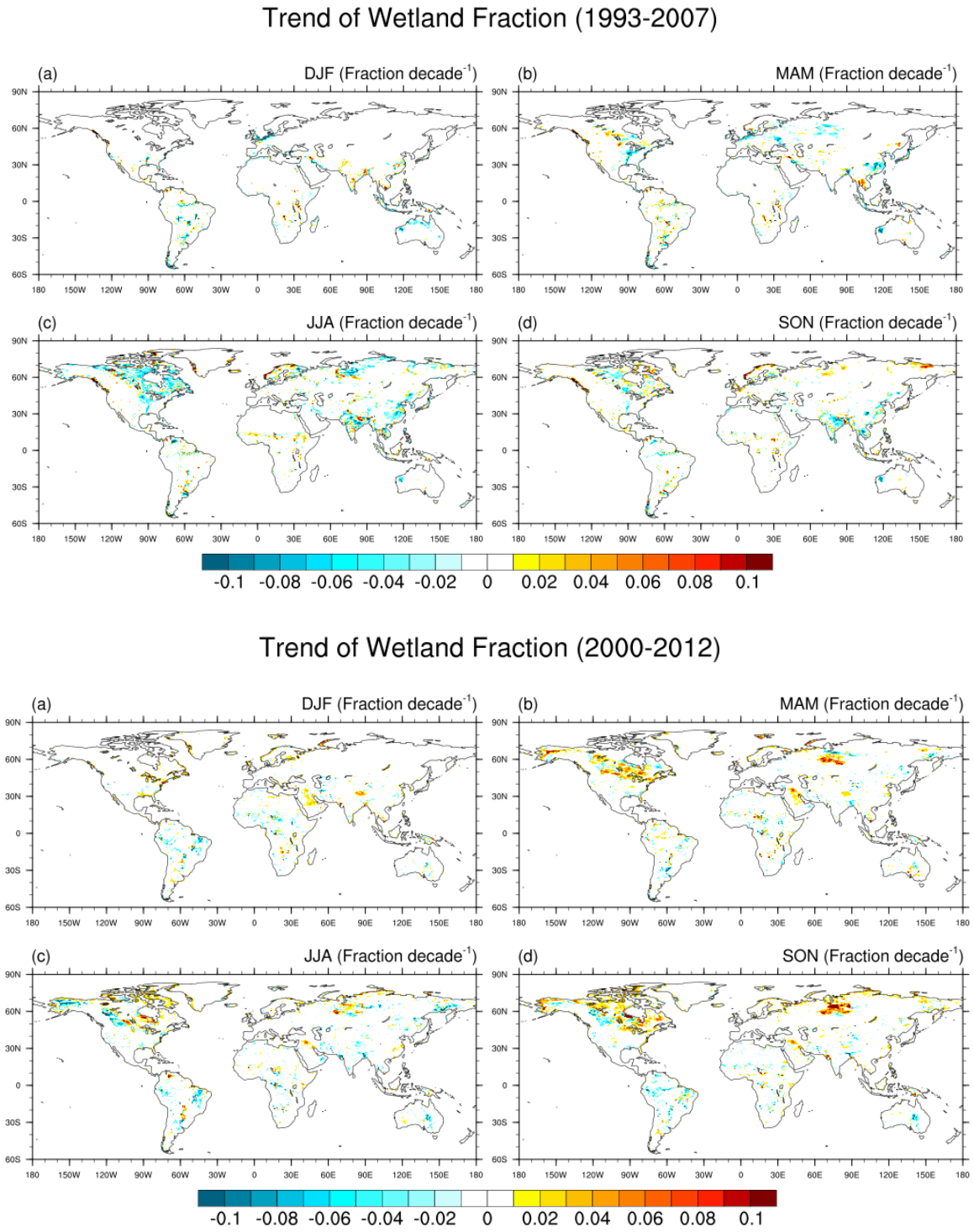

Figure 6.3 Seasonal trends of wetland fraction from GIEMS during 1993-2007 (top) and SWAMP during 2000-2012 (bottom)

Notes: The wetland fraction denotes the fraction of wetland area within a grid cell with 0.5° longitude/latitude, which is around 55.6 km at the equator.

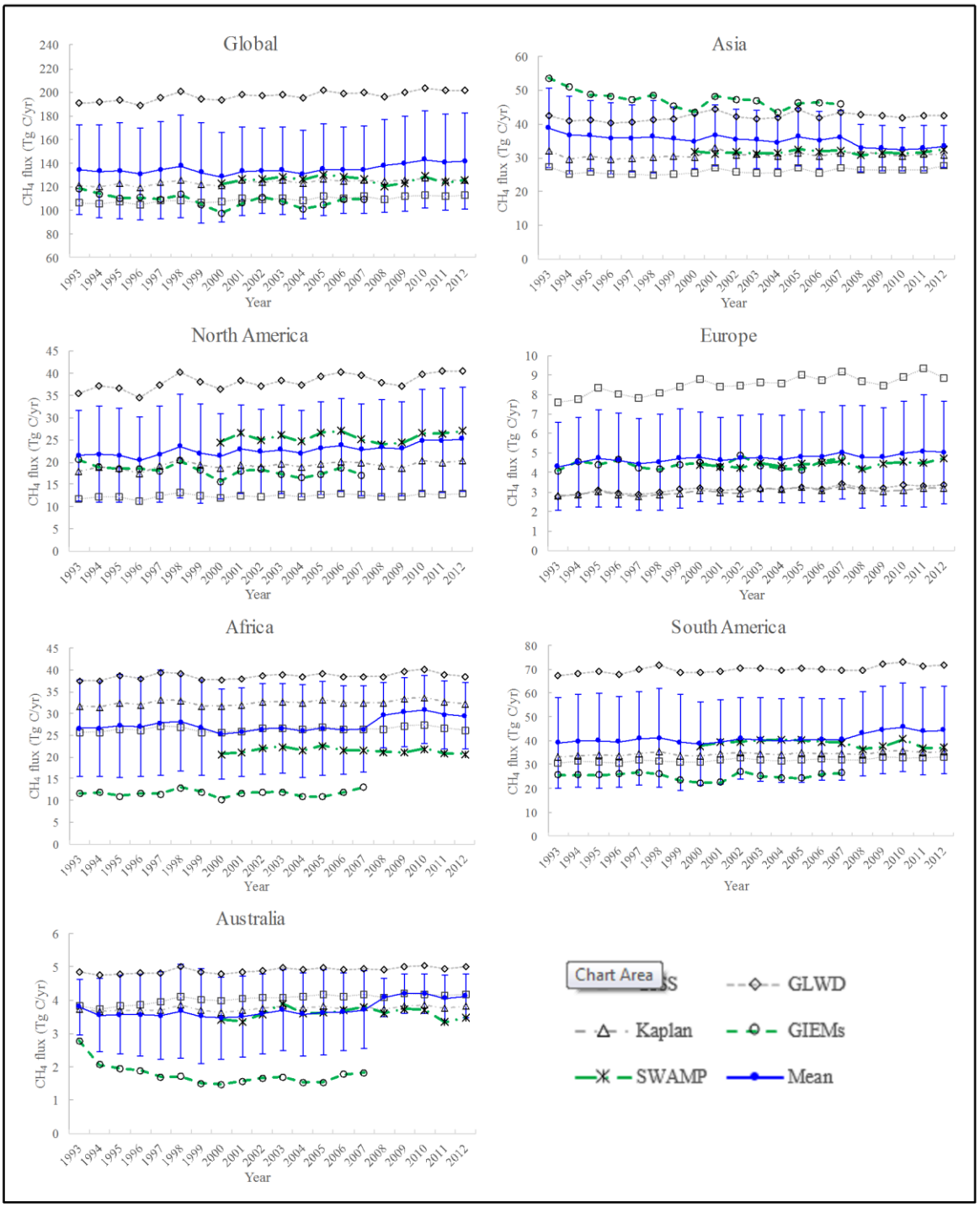

Figure 6.4 Wetland CH_4 emission at global and continental scales using different wetland datasets

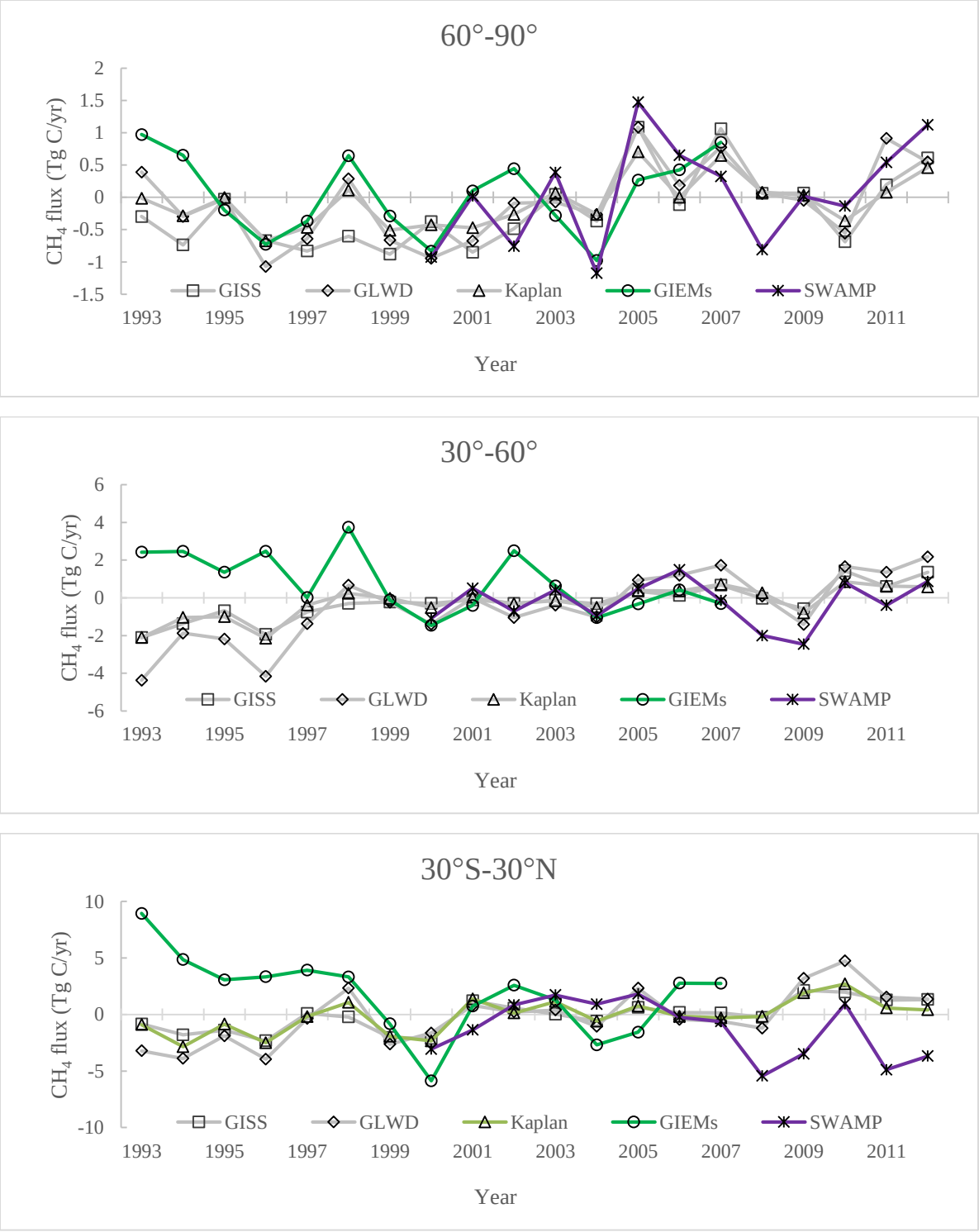

Figure 6.5 Modeled wetland CH_4 emission anomalies (i.e., annual number – mean value) using different wetland datasets at high latitude region (HLR, 60° - 90° N and S), middle latitude region (MLR, 30° - 60° N and S) and low latitude region (LLR, 30°S -30°N)

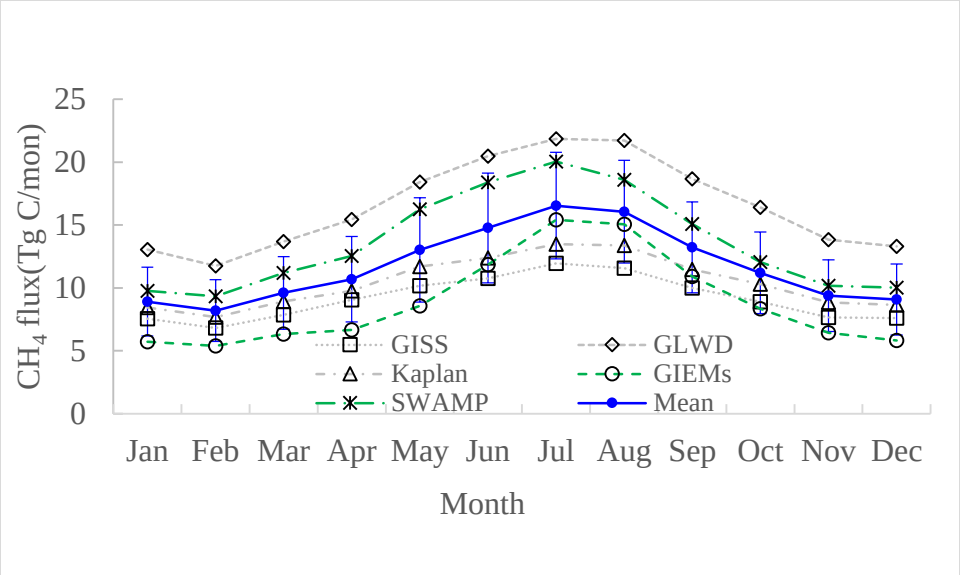

Figure 6.6 Intra-annual variation of estimated wetland CH_4 emission using different wetland datasets

Chapter 7

Conclusions and Future Research Needs

In this study, we examined the magnitude, spatial and temporal patterns of CH_4 flux from different biogenic and pyrogenic sources and sink (e.g., wetlands, rice field, ruminants, biomass burning and upland soil) by using a process-based biogeochemical model, the Dynamic Land Ecosystem Model and inventory approach and identified their relative contributions to changes in atmospheric CH_4 growth rate during the recent two decades. In addition, we quantified the magnitude of CH_4 fluxes from terrestrial ecosystems in the arctic and boreal region under the future scenarios. Finally, we assessed the estimation uncertainty from various wetland extent datasets.

The key conclusions are listed below:

1) The global net CH_4 flux from wetlands, rice field, ruminants, biomass burning and upland soil was 163.9±6.4 Tg C/yr and exhibited strong inter-annual variation. Among all the CH_4 sources, wetland contributed almost half (~49.2%) of the global total CH_4 emission, followed by ruminants (~36.8%), rice field (~7.5%) and biomass burning (~6.5%). The upland soil offset ~13.2% of the total emitted CH_4 from those four sources. Tropical region dominated the global total CH_4 fluxes. Among 6 continents, Asia accounted for over one-third of the global net CH_4 fluxes owing to the large rice-growing and ruminant-dense region. Methane emission from wetland dominated the atmospheric CH_4 variation during 1993-2014 and the contribution of CH_4 emission from ruminants became increasingly important, especially after 2006. Methane

emissions from biomass burning played a critical role in some specific years when huge peatland fire occurred. It can be anticipated that the future atmospheric CH_4 variation will be determined by the increasing demand of food production with the climate sensitive natural emissions.

2) The estimated CH_4 emissions from global rice fields varied from 18.3±0.1 to 38.8±1.0 Tg CH_4/yr in the 2000s depending on different water schemes, and CH_4 emissions under intermittent irrigation could be reduced by 50.6% comparing with continuous flooding. Over the past 110 years, the estimated CH_4 emissions from global rice cultivation increased 85%. The expansion of rice fields was the dominant factor for the increasing trends of CH_4 emissions, followed by elevated CO_2 concentration, and nitrogen fertilizer use. On the contrary, climate had the negative effect on the cumulative CH_4 emissions for most of the years over the study period. Our results imply that CH_4 emissions from global rice fields could be reduced by implementing optimized irrigation practices.

3) The estimated CH_4 emission from global wetland was around 92.9±4.2 Tg C/yr during 1993-2014, with ~ 64.3% originated from the tropical region. Among 6 continents, South America was the dominant contributor. The estimated CH_4 emission from wetland exhibited significant seasonal trend over the entire globe during 1993-2014, with the most apparent trend being found in autumn. The variation of wetland extent was important and needs to be considered for quantifying the inter-annual and intra-annual variation of estimated CH_4 emissions from wetland. 20% and 16% of the global inundation extent showed a significant correlation with precipitation and temperature, respectively. Inundation extent in most parts of the globe was found to have positive correlation with annual precipitation amount.

4) The magnitude of CH_4 emission from wetland in the arctic and boreal region is projected to increase 2%~65% by the end of 21st century compared with the contemporary level.

Seasonal analyses indicated that the change of CH_4 fluxes exhibits great spatial variability over time. The projected CH_4 emissions in summer account for the largest portion of annual emission and show the largest increase during the 21st century. The climate variation was the dominant factor for the projected increased CH_4 emission.

5) Large differences in the magnitude and spatial distribution of wetlands existed among different wetland datasets, ranging from 5.3 million km^2 (GISS) to 10.2 million km^2 (SWAMP), with the largest discrepancy in tropical region. By feeding these datasets into the dynamic land ecosystem model (DLEM), we further examined how different wetland datasets could bias model-estimated CH_4 emissions from global wetlands. The DLEM-estimated CH_4 emission from global wetland was 132.9 ± 37.2 Tg C/yr during 2000~2007, ranging from 106.0 Tg C/yr (GIEMS) to 197.6 Tg C/yr (GLWD). Tropical region accounted for the largest portion (~72 ± 7%) of the estimated CH_4 emission from wetlands and also had the largest uncertainty. Among 6 continents, the largest uncertainties were found in South America.

Several additional issues have been identified for advancing our research in the future, including (1) improving spatial resolution of input data and sub-grid heterogeneity for driving the model. Finer resolution data is needed for future model application at multiple spatial scales, which will serve to make more realistic assumptions based on conditions that are truly happening in the real world. (2) improving model representations of additional processes that regulate the CH_4 fluxes from the terrestrial ecosystem. Several important features are absent from the current DLEM. For example, the representation of sulfur deposition and iron reduction/oxidation are needed to better estimate CH_4 fluxes. However, due to the data scarcity and high spatial heterogeneity, it is very hard to incorporate into the model at this stage. Other critical factors, such as realistic representation of inundation, were missing in the current version of the DLEM.

These factors or local practices are very important in regulating the CH_4 fluxes, but have a large spatial and temporal variability, which are very difficult to collect at the large scale. Therefore, we call for the collection of such dataset in field study or regular census survey.